CANADIAN THESES

THÈSES CANADIENNES

NOTICE

The quality of this microfiche is heavily dependent upon the quality of the original thesis submitted for microfilming. Every effort has been made to ensure the highest quality of reproduction possible.

If pages are missing, contact the university which granted the degree.

Some pages may have indistinct print especially if the original pages were typed with a poor typewriter ribbon or if the university sent us an inferior photocopy.

Previously copyrighted materials (journal articles, published tests, etc.) are not filmed.

Reproduction in full or in part of this film is governed by the Canadian Copyright Act, R.S.C. 1970, c. C-30. Please read the authorization forms which accompany this thesis.

AVIS

La qualité de cette microfiche dépend grandement de la qualité de la thèse soumise au microfilmage. Nous avons tout fait pour assurer une qualité supérieure de reproduction.

S'il manque des pages, veuillez communiquer avec l'université qui a conféré le grade.

La qualité d'impression de certaines pages peut laisser à désirer, surtout si les pages originales ont été dactylographiées à l'aide d'un ruban usé ou si l'université nous a fait parvenir une photocopie de qualité inférieure.

Les documents qui font déjà l'objet d'un droit d'auteur (articles de revue, examens publiés, etc.) ne sont pas microfilmés.

La reproduction, même partielle, de ce microfilm est soumise à la Loi canadienne sur le droit d'auteur, SRC 1970, c. C-30. Veuillez prendre connaissance des formules d'autorisation qui accompagnent cette thèse.

THIS DISSERTATION HAS BEEN MICROFILMED EXACTLY AS RECEIVED

LA THÈSE A ÉTÉ MICROFILMÉE TELLE QUE NOUS L'AVONS REÇUE

Computer-Aided Analysis and Selection of Vehicle Cab Suspensions

Kalyanaraman Venkataraman

A Thesis

in

The Department

of

Mechanical Engineering

Presented in Partial Fulfillment of the Requirements
for the Degree of Master of Engineering at
Concordia University
Montréal, Québec, Canada

July 1985

ABSTRACT

Computer-Aided Analysis and Selection of Vehicle Cab Suspensions

Kalyanaraman Venkataraman

The main objective of this thesis is to develop a mathematical model of a cab suspension and to carry out free and forced vibration analyses of the model, so as to improve the ride characteristics of an off-road tracked vehicle. Due to certain inherent advantages, the cabs of such vehicles are disposed over their engines, and such configuration is known as "Cab Over Engine" or simply "COE". These types of cabs are provided with tilt mechanisms with frontal load bearing supports acting as pivots and single or dual support at the rear. A six degrees of freedom model developed for the lumped mass analysis is verified through a finite-element analysis carried out with ANSYS package. The equations of motion formulated for free vibration analysis is further extended with random excitations at the supports.

A practical problem of improving the ride in a Snow Pusher-cum-Tiller manufactured under the trade name of "BR-400" by Bombardier Inc., is chosen as a specific case study for this thesis. Field trials to record the input and response accelerations of the cab of "BR-400" were carried out. A computer program is developed to simulate the response Power Spectral densities from the discretised input PSDs. The results thus obtained are compared with that of the field trials. Finally, the parametric variations are carried out to arrive at a reduced acceleration reponse spectra in all the degrees of freedom and a solution for improved ride is recommended.

ACKNOWLEDGEMENT

The author is greatly indebted to Prof. S. Sankar, for suggesting a practial problem and also for providing continued guidance and support during this endeavour.

Thanks are also due to Dr. Subhash Rakheja, Mr. James Alanoly and other members of the faculty and staff of the Mechanical Engineering Department of Concordia University for their assistance and time during the course of this work.

Technical assistance provided by Bombardier Inc., particularly during the field trials and by way of furnishing the drawings and specifications is greatly appreciated.

Financial support provided by Natural Sciences and Engineering Research Council of Canada, vide their Grant Nos.A3685 and CRD 8406 is also acknowledged.

Further, the author wishes to acknowledge the support of his family members for their perseverance and endurance shown as an encouragement to his efforts.

Finally, thanks are due to Ms. Nancy Nicholson for typing the manuscript.

Table of Contents

	Page
ABSTRACT	iii
ACKNOWLEDGEMENT	iv
LIST OF FIGURES	viii
LIST OF TABLES	xi
NOMENCLATURE	xii
CHAPTER I	
INTRODUCTION	1
1.1 General	2
1.2 Literature Survey	3
1.3 Scope of the Present Research Work	7
CHAPTER II	
FORMULATION OF MATHEMATICAL MODEL FOR CAB SUSPENSIONS	10
2.1 Introduction	11
2.2 Overview of Cab Suspensions	11
2.3 Mathematical Model of Tilt-Cab Suspensions with Three Supports	12
2.3.1 Equations of Motion for Free Vibration	14
2.3.2 Equations of Motion for Terrain-Induced Vibrations	21
2.4 Summary	24
CHAPTER III	
DESCRIPTION AND EXTRACTION OF RELEVANT PARAMETERS OF A CANDIDATE OFF-ROAD VEHICLE	25
3.1 Introduction	26

Page

3.2 Description of "BR-400". 27

3.3 Cab Suspension of "BR-400" 32

3.4 Extraction of Relevant Parameters of the Vehicle 32

3.4.1 ANSYS Finite-Element Analysis. 36

3.4.2 Finite-Element Model of the Cab. 38

3.4.3 Stiffness Evaluation of the Front Bushing. . . . 51

3.4.4 Evaluation of the Damping coefficient of the Front Bushing. 51

3.4.5 Stiffness and Damping coefficient of the Rear Mount. 56

3.5 Summary. 59

CHAPTER IV

FREE VIBRATION ANALYSIS OF THE CAB 60

4.1 Introduction 61

4.2 Natural Frequencies and Mode Shapes of the Cab via Lumped Mass Model. 61

4.3 Natural Frequencies and Mode Shapes of the Cab via Finite-Element Model 64

4.4 Comparison of Free Vibration Results between Finite-Element and Lumped Mass Analyses 66

4.5 Summary. 77

CHAPTER V

FORCED VIBRATION ANALYSIS OF THE CAB 78

5.1 Introduction 79

5.2 Input and Response Acceleration Spectra of the Tilt-Cab of "BR-400" derived for the Field Tests. 80

Page

5.3 Computer Simulation for the determination of Random Response. 88

5.4 Comparison of Response Spectra between the Field Measured Data and the Simulation Results 93

5.5 Summary 98

CHAPTER VI

PARAMETRIC STUDIES AND RECOMMENDATIONS. 99

6.1 Introduction. 100

6.2 Parametric Study by varying the Stiffness of Rear and Frontal Isolators 101

6.3 Parametric Study by varying the Damping Coefficients of the Mount/Isolators. 101

6.4 Parametric Study with variations in the Frontal Support Distance. 103

6.5 Parametric Study with Dual Rear Supports instead of a Single Support. 103

6.6 Comparison of Results 109

6.7 Recommendations 111

6.8 Summary 113

CHAPTER VII

CONCLUSIONS AND RECOMMENDATIONS FOR FURTURE WORK. 114

7.1 Conclusions 115

7.2 Recommendations for Future Work 117

REFERENCES. 118

APPENDIX I

EQUATIONS OF MOTION OF A TILT-CAB WITH FOUR SUPPORTS 121

List of Figures

Figure		Page
2.1	Perspective View of a Cab having Three Supports	13
2.2	Mathematical Model of a Three-Point Cab Layout	15
2.3	Three-Point Cab Subjected to Terrain Excitations	22
3.1	Perspective View of "BR-400"	28
3.2	Arrangement of the Rear Support	31
3.3	Frontal Bracket of the Cab-"BR-400"	33
3.4	Bushing used in the Front Support-"BR-400"	34
3.5	Rear Mount and its Load-Deflection Characteristics-"BR-400"	35
3.6	Typical Phases of the "ANSYS" Analysis	37
3.7	Basic Flow Chart of the Pre-Processor PREP7	39
3.8	Isometric View of the F.E Model of the Cab	40
3.9	Top and Rear Panels of the F.E Model of the Cab	41
3.10	Bottom Panel of the F.E Model of the Cab	42
3.11	Front Panel of the F.E Model of the Cab	43
3.12	Isometric View of the Cab Model developed in "ANSYS"	45
3.13	Rear View of the Cab Model developed in "ANSYS"	46
3.14	Side View of the Cab Model developed in "ANSYS"	47
3.15	Top View of the Cab Model developed in "ANSYS"	48
3.16	F.E Model of the Front Bracket	49
3.17	"MTS" Equipment used for the determination of stiffness of the Bushing	52

		Page
3.18	Set-up prepared for the Evaluation of Stiffness of the Bushing	53
3.19	Load-Deflection Characteristics of the Bushing	54
3.20	Test Set-up prepared for the measurement of Damping-Coefficient of the Bushing	55
3.21	Damped Oscillations of the Front Bushing	57
4.1	Modal Analysis Solution Flow Chart	67
4.2	First Mode Shape of the Cab (at 2.5 Hz)-Top View	69
4.3	Second Mode Shape of the Cab (at 7.0 Hz)-Side View	70
4.4	Third Mode Shape of the Cab (at 7.6 Hz)-Front View	71
4.5	Fourth Mode Shape of the Cab (at 9.3 Hz)-Top View	72
4.6	Fifth Mode Shape of the Cab (at 12 Hz)-Side View	73
4.7	Sixth Mode Shape of the Cab (at 20 Hz)-Side View	74
5.1	Location of the Input and Response Accelerometers	81
5.2	Input Acceleration PSDs (Rough Track, Blade up)	82
5.3	Input Acceleration PSDs (Rough Track, Blade down)	83
5.4	Response Acceleration PSDs (Rough Track, Blade up)	84
5.5	Response Acceleration PSDs (Rough Track, Blade down)	85
5.6	Response Acceleration PSDs (Smooth Track, Blade up)	86
5.7	Response Acceleration PSDs (Rough Track, Blade down)	87
5.8	Transformation Matrix	94
5.9	Comparative Plots of Response Acceleration PSDs at the Accelerometer #2'	96
5.10	Comparative Plots of Response Acceleration PSDs at the Accelerometer #4'	97

		Page
6.1	Widened Rear Bracket with Dual Mounts.	107
6.2	Proposed Four Point Cab Layout	108
AI.1	Mathematical Model of a Four Point Cab Layout.	123
AI.2	Four Point Cab Subjected to Terrain Excitations.	124

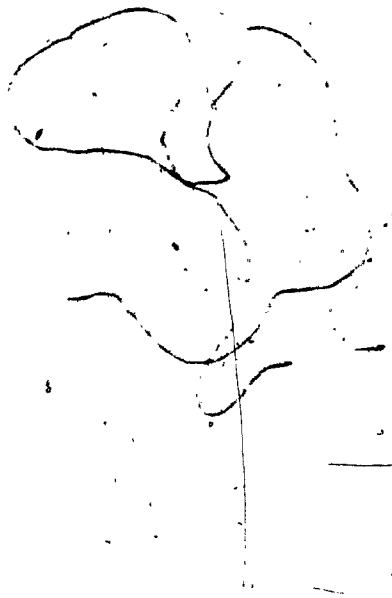

List of Tables

Table		Page
3.1	Specifications of "BR-400".	29
3.2	Specifications of "BR-400".	30
3.3	Analytical Results extracted through ANSYS.	50
3.4	Stiffness and Damping coefficients of the Isolators	58
4.1	Natural Frequencies and Eiegenvectors via the Lumped mass Model	63
4.2	Damped Eigenvalues and Complex Eigenvectors via the Lumped mass Model	65
4.3	Natural Frequencies of the F.E Model.	68
4.4	Comparison of Natural Frequencies between the Lumped mass Model and the F.E Analyses	68
5.1	Complex Fequency Response Function Matrix for 8.5 Hz frequancy.	91
6.1	Response of the cab at its centroid for various stiffnesses of the Front and Rear Isolators.	102
6.2	RMS values of the Cab Response at its centroid for various Damping Coefficients.	104
6.3	Response of the Cab at its Centroid for various Front Support Distance.	105
6.4	Response of the Cab at its centroid for a Four Point Cab Layout.	110
6.5	Response of the Cab at a Location beneath the Seat of the Driver	112

NOMENCLATURE

a	Distance between the front support and the centroid of the cab measured along the Z-axis.
b	Distance between the rear support and the centroid of the cab measured along the Z-axis.
c_{xi}	Damping coefficient of the isolator at support i (i=3 and 4), along the X-axis.
c_{yi}	Damping coefficient of the isolator at support i(i=1, 2, 3, and 4), along the Y- axis.
c_{zi}	Damping coefficient of the isolator at support i(i=1, 2, 3, and 4), along the Z- axis.
d	Distance between the cab floor and the rear support measured along the Y-axis.
e	Distance between the cab floor and the centroid measured along the Y-axis.
f	Distance between the cab floor and the front support measured along the Y-axis.
g	Distance between the centre line of the cab and one of the rear supports measured along the X-axis.
h	Distance between the centre line of the cab and one of the front supports measured along the X-axis.
$H(j\omega)$	Complex frequency response function of the cab model.
I_{xx}	Mass moment of inertia at the centroid about the X-axis.
I_{yy}	Mass moment of inertia at the centroid about the Y-axis.
I_{zz}	Mass moment of inertia at the centroid about the Z-axis.
k_{xi}	Stiffness of the isolator/mount at support i(i=3 and 4), along the X-axis representing shear stiffness.
k_{yi}	Stiffness of the isolator/mount at support i(i=1, 2, 3 and 4),

along the Y-axis representing tension/compressive stiffness.

k_{zi} Stiffness of the isolators/mounts at support i(i=1, 2, 3 and 4), along the Z-axis representing tension/compressive stiffness if i=1 or 2; and shear stiffness if i=3 or 4.

m Total mass of the cab.

MSP Main Spectral Peak Occurrence in Hz.

Peak Peak spectral density of the response.

RMS Root mean square value of the response.

$S_x(\omega)$ Input spectral density.

$S_y(\omega)$ Output spectral density.

x Displacement response of the cab along the X-axis.

$\dot{x}$ First derivative of 'x' with respect to time.

$\ddot{x}$ Second derivative of 'x' with respect to time.

x_{oi} Displacement input at support i(i=3 and 4) along the X-axis.

$\dot{x}_{oi}$ First derivative of 'x_{oi}' with respect to time.

$\ddot{x}_{oi}$ Second derivative of 'x_{oi}' with respect to time.

y Displacement response of the cab along the Y-axis.

$\dot{y}$ First derivative of 'y' with respect to time.

$\ddot{y}$ Second derviative of 'y' with respect to time.

y_{oi} Displacement input at support i(i=1, 2, 3, and 4) along the Y-axis

$\dot{y}_{oi}$ First derivative of 'y_{oi}' with respect to time at support i(i=1, 2, 3 and 4).

$\ddot{y}_{oi}$ Second derivative of 'y_{oi}' with respect to time at support i(i=1, 2, 3 and 4).

z Displacement response of the cab along the Z-axis.

$\dot{z}$ First derivative of 'z' with respect to time.

$\ddot{z}$ Second derivative of 'z' with respect to time.

z_{oi} Displacement input at support i(i=1, 2, 3, and 4) along the z-axis.

$\dot{z}_{oi}$ First derivative of 'z_{oi}' with respect to time at support i(i=1, 2, 3 and 4).

$\ddot{z}_{oi}$ Second derivative of 'z_{oi}' with respect to time at support i(i=1, 2, 3 and 4).

θ Generalised co-ordinate representing the rotational response of the cab about the Z-axis.

$\dot{\theta}$ First derivative of 'θ' with respect to time.

$\ddot{\theta}$ Second derivative of 'θ' with respect to time.

ϕ Generalised co-ordinate representing the rotational response of the cab about the X-axis.

$\dot{\phi}$ First derivative of 'ϕ' with respect to time.

$\ddot{\phi}$ Second derivative of 'ϕ' with respect to time.

Ψ Generalized co-ordinate representing the rotational response of the cab about the Y-axis.

$\dot{\Psi}$ First derivative of 'Ψ' with respect to time.

$\ddot{\Psi}$ Second derivative of 'Ψ' with respect to time.

ζ Damping factor.

λ Eigenvalue.

Φ Eigenvector.

ω Natural Frequency.

CHAPTER I

INTRODUCTION

CHAPTER I

INTRODUCTION

1.1 General

A prime requirement for any vehicle acceptance is the ride quality, since the driver as well as the passengers of the vehicle spend a number of hours in travel. Therefore, passenger cars and buses in mass transit stress considerable importance in the design and manufacture of their suspension systems. As the wheeled vehicles generally have tires and travel on smooth roads, their ride characteristics, particularly, the quality of ride is very much improved due to the primary suspension of these cushioned tires.

Vehicles such as bulldozers, snow-pushers, armoured military cars, etc., are categorised as "tracked vehicles" due to their running gear. Due to the absence of pnuematic tires in such vehicles, the torsion bars fitted at their wheels act as the only source of primary suspension. Therefore, the ride behaviour of these vehicles can be improved economically, only through the modification of secondary suspensions; namely, cab and/or seat suspensions.

The improvement of ride quality via cab suspension can be considered to be more logical, economical and practical due to the following reasons:

1. Unlike the seat, the cab attachment to the frame is a proprietory area of the vehicle and is seldom affected by the product

decisions of the buyer, such as in the case of buying seat with its suspension units.

2: The large pitching and fore-aft motion caused due to the high location of the cabin in such vehicles can be isolated successfully by a suitable cab suspension design; where as the seat suspension could provide a better ride in the bounce mode alone.

3. Relative motion between the control panel and the driver is greatly reduced by following this method.

The above cited points, are the principal reasons for the selection of cab suspensions as the best alternative to achieve a better ride, especially in a tracked vehicle.

1.2 Literature Survey

Heavy trucks and tracked vehicles normally have their cabs mounted over the engine. Such an arrangement is often preferred due to limited space requirement; and hence resulted in the "Cab-Over Engine" configuration in all these types of vehicles, with suitable design of cab tilt mechanisms. This concept gives rise to either four mount support or three mount support with two hinge type supports at the front which take care of the load bearing requirements while the cab is being tilted.

Over two decades ago, the first cab suspension was built at Ford for thier turbine powered truck with four leaf spring suspension units [1]. Subsequently in the year 1966, due to the recognition of the fact that better ride is a prime necessity, a ride improvement program began

which culminated in a fixed front pivot combined with rear spring mount [1]. In the year 1969, it was concluded that a low rate front and rear mounts would be required to achieve the ride improvement. The historical background and further details on the state-of-the-art of Cab suspension are presented in [1].

Flower [2] has compared the performance of the two types of Cab suspension systems; namely, the frontal pinned support with rear isolation and the rear pinned support with frontal suspension. A multi-degree of freedom computer model was developed and the simulated results were compared with the performance of both the types. The advantages of Front-Cab-Isolation System (FCIS) over the other systems are enumerated.

Selman and Pixton [3] have described the design and development of cab suspensions and the unique cab tilt system used in conjunction with the cab suspension. The recent trend towards the Four-Point Cab suspensions is highlighted in the concluding remarks.

Behaviour of passive, active and semi-active suspensions for a given acceleration input in an agricultural tractor cab was studied by Roley and Burkhardt [4]. A four degrees of freedom model was developed and the measured tractor accelerations were used in comparing the vibration attenuation performance [4]. Active and semi-active suspensions were found to achieve significant attenuation improvement over the passive suspension.

Suggs and Huang [5] have outlined an experimental procedure followed in testing a scale model of a tractor cab due to the limited capacity of available vibration platform. Actual ride problem of the cab and the optimization of design are carried out by the simulation of scale model. The advantage of improving the cab suspensions in minimizing the relative motion between the operator and the control panel is highlighted in this paper.

The relative advantages of using the fibre-reinforced plastic cab over the conventional aluminium cabs are presented by Cadman [6]. A finite-element structural analysis was carried out to assess the structural integrity of the cab. Finally the analytical results are verified experimentally to illustrate the validity of the analysis.

Young and Robideau [7] have developed a methodology which is capable of generating design criteria for truck-cab controls and display elements. This method combines the driver behaviour determined by a task analysis with the graphic theories of system interactions to analyse the influences of cab design features on safety-critical driver behaviour. Finally a complete safety oriented specification is generated

Practical approach to the Tilt-cab suspension to improve the ride quality is presented by Wild [8]. The main emphasis in this paper is to determine the Cab structural damage incurred through the cab suspension, and to determine by durabiltiy tests the projected vehicle mileage before any structural damage is caused to the cab.

Concept of a cab suspension system for improving the ride quality of off-road tractors in the bounce, longitudinal, lateral, pitch and roll modes was explored by Rakheja and Sankar [9]. By varying the suspension parameters, the ride performance was improved. The results corresponding to the optimal suspension were compared with the "fatigue decreased proficiency" curves specified by the International Standards Organisation.

Simons [10] has provided a general description of an approach used in the development of a uniquely configured COE class Eight highway truck. Various design aspects as related to driver comfort and associated component development are presented.

Crosby and Allen [11] have presented the analysis techniques, the test data, and the ride evaluation criteria which are used in the design of cab isolation systems. Computer simulations of improved cab ride are presented for conventional and COE tractors. The advantages of improving the cab suspension over the primary as well as seat suspensions are cited at the summary.

A three dimensional structural collapse analysis computer programme based on an incremental formulation of the conventional finite-element method is used by Miles and Wardill [12] to analyse and design safety vehicle structure. Satisfactory engineering solutions for failure loads of the real structure could be predicted with reasonable accuracy.

Rose [13] has examined the commercial and legislative background, the fundamental safety proposals, the detailed design and testing of the six-man safety cab of fire engines.

Leichtle [14] has described the improvements made on an assembly line to facilitate the production of a new line of fibreglass truck campers. The aspect of noise insulation of operator cabs for construction and agricultural equipment has been studied by Emme [15]. The paper presents a discussion on the noise control and design considerations for the basic structure, control levers, and effective sealing. Use of absorption and transmission loss materials is also described.

McAfee [16] outlines International Harvester's approach to total driver environment, Viz., physical room, control placement, visibility, interior noise level, occupant protection and temperature control.

1.3 Scope of the Present Research Work

Following paragraphs describe the approach followed in the present thesis, chapter wise, so as to give a fair idea of the research work carried out.

Chapter II exclusively presents a mathematical formulation of the problem and the equations of motion of a general six degrees of freedom cab suspension for both free and forced vibrations.

Chapter III deals with the description of a candidate off-road tracked vehicle; namely, "BR-400". "BR-400" is a snow-pusher cum-tiller manufactured by Bombardier Inc. The problem of ride quality improvement of this vehicle is chosen as a specific case study in the present thesis. The extraction of relevant geometrical parameters of the cab and the physical parameters of its isolators is also elaborated in this chapter.

The free vibration analysis of "BR-400" cab, for the calculation of natural frequencies and eigenvectors via lumped-mass analysis is presented in chapter IV. Modal analysis of the cab through the finite element ANSYS software package is also carried out. The natural frequencies and the mode shapes extracted are compared with that of the lumped-mass analysis, thus, validating the equations of motion formulated.

Chapter V is devoted to the random analysis of field measured vibration input and response accelerations of the candidate vehicle and the extraction of power-spectral density plots from the recorded signal. The response spectra is obtained analytically as well by using the system transfer function. Results of both the field trials and that of the computer simulation are compared finally.

The next chapter i.e., chapter VI is on "Parametric Studies and Recommendations". In this chapter the variables such as the stiffnesses of the rear and front mounts and the front support distance are progressively changed and the response is calculated each time. As a

next step of the "Parametric studies", a four point supported cab layout is considered. RMS values of the acceleration responses are tabulated for each case. Finally, the recommendations for improved ride characteristics are suggested.

The final chapter is devoted to the conclusions and recommendations for future work in the area of cab suspensions.

CHAPTER II

FORMULATION OF MATHEMATICAL MODEL FOR CAB SUSPENSIONS

CHAPTER II

FORMULATION OF MATHEMATICAL MODEL FOR CAB SUSPENSIONS

2.1 Introduction

Vehicular vibrations caused by uneven terrain-induced excitations posed an important problem in tracked vehicles, which do not possess any primary suspensions as in the case of passenger cars. Therefore, the problem of ride quality improvement of tracked vehicles can be achieved through proper design of cab and/or seat suspensions. Since majority of tracked vehicles have some form of cab suspension, in this chapter a detailed formulation of a mathematical model for cab suspensions is developed, for a complete analysis and parametric study.

2.2 Overview of Cab Suspensions

Before developing a mathematical model for cab suspensions, a brief review of the cab layout and configuration is presented in the following paragraphs. Unlike passenger cars; heavy trucks and tracked vehicles such as snow-pushers, bulldozers, etc. have their cabs mounted over their engines. This is primarily done to save space and secondly to improve the visibility of the operators.

This configuration is termed as "Cab-Over-Engine" or simply "COE" and this poses an intriguing dynamical problems due to the high C.G. location of the cab.

The "COE-Cabs" are normally provided with tilt mechanisms to allow for access to their engines for maintenance. Therefore, this leaves with the option of having the load bearing pivotal supports at the front with either a single or dual supports at the rear. Hence, a broad classification of "COE-Cabs" could be made on the basis of the number of rear supports and also based on the type of suspensions used in each of the front and rear supports; namely, passive active, and semi-active suspensions. With this brief introduction on the cab suspension of a "Cab Over Engine" configuration, a mathematical model is developed for a three point layout and subsequently for a four point layout. The model and the equations of motion become the basis for analysis and parametric study.

2.3 Mathematical Model of Tilt-Cab Suspensions with Three Supports

A three dimensional perspective view of a three point supported cab is shown in Figure 2.1. The model shown in the figure is applicable for a general purpose tilt-cab configuration. For developing a mathematical model, the following assumptions are taken into account:

- The frontal supports are pivoted in a tilt-cab and the pivots are provided with elastomer bushings. These bushes act as isolators for the terrain induced excitations. The front bush is assumed to behave similar to a bi-axial spring-damper arrangement, one along the vertical 'y' axis and the other along the horizontal 'z' axis (longitudinal).
- The rear mount is modelled as a combination of spring-damper, configured in parallel along the three orthogonal directions. While the vertical spring-damper represent the tension/compression properties of the mount, the rest; namely, the spring-

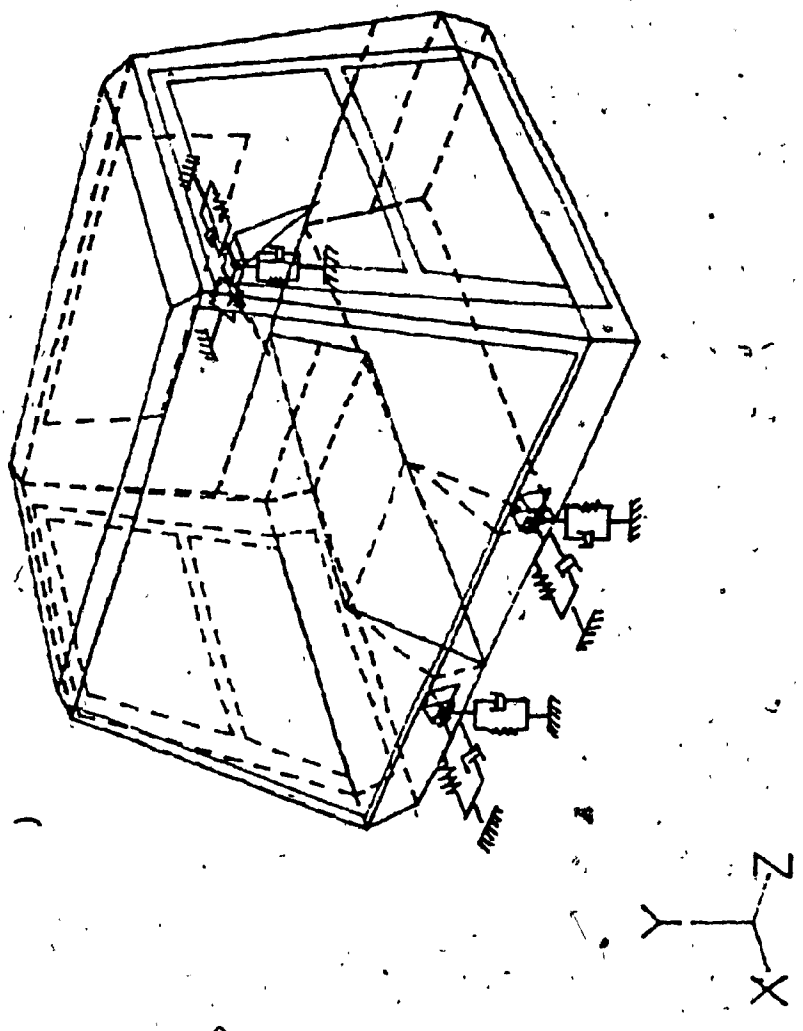

Fig 2.1: Perspective View of a Cab having Three Supports

damper along the lateral & longitudinal directions represent the shear properties of the mount.

Based on the assumptions the tilt-cab is modelled to have six degrees of freedom. These are:

-Translation along the x-axis or Lateral Motion

-Translation along the y-axis or Bounce Motion

-Translation along the z-axis or Longitudinal Motion

-Rotation about the x-axis or Pitch Motion (ϕ)

-Rotation about the y-axis or Yaw-Motion (Ψ)

-Rotation about the z-axis or Roll-Motion (θ)

2.3.1 Equations of Motion for Free Vibration

The cab suspension and the six degrees of freedom conceived for a tilt-cab is shown schematically in Figure 2.2. In order to estimate the natural frequencies and the mode shapes of the cab, the equations of motion for free oscillations of the system are formulated. The equations of motion are obtained by considering the following assumptions:

- The suspensions are mainly elastomers and hence they are assumed to be linear.
- The seat is assumed to be rigidly fixed to the cab floor. In other words, the seat, the seat suspensions and the mass of the passenger or operator are assumed to be rigid for the purpose of developing the model.
- Cross-coupled accelerations due to the three orthogonal rotational vectors are ignored.
- Normal component of the acceleration due to rotation is considered to be negligible.

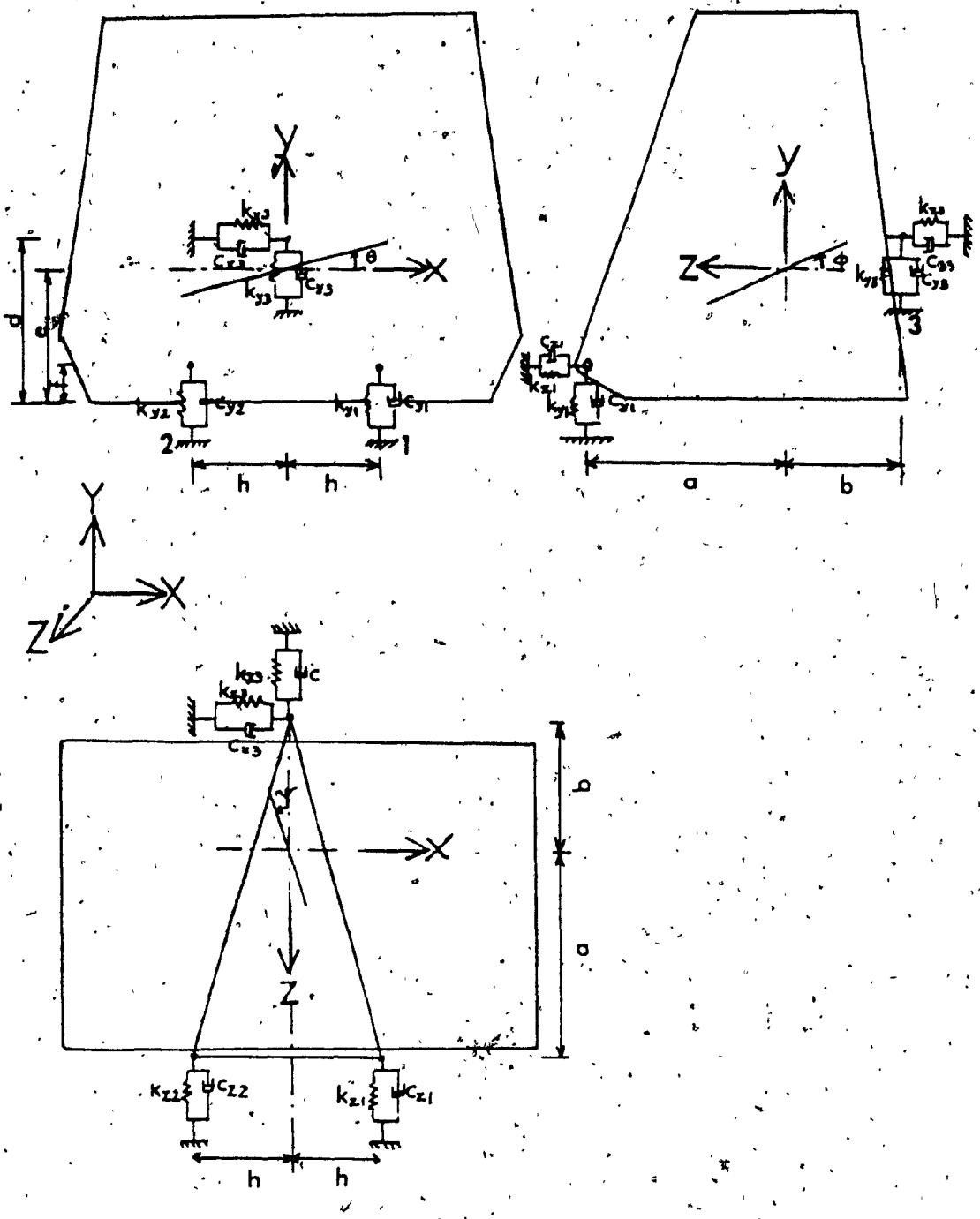

Fig 2.2: Mathematical Model of a Three-Point Cab Layout

The equations of motion are derived from the D'Alembert's principle which states that the sum of all the forces, real and inertial, acting on the system must vanish [17]. This can be written as

$$F_i + R_i - \ddot{mr}_i = 0 \ (i = 1,2 \ldots,N) \quad \ldots\ldots\ldots\ldots\ldots\ldots (2.1)$$

where,

F_i is the applied force and R_i is the constraint force applied on the i-th particle. $-\ddot{mr}_i$ has the dimensions of the force and is known as the inertial force acting on the i-th particle. m_i & r_i representing constant mass of the i-th particle and acceleration of the i-th particle relative to the inertial frame.

In the case of free vibration, the term F_i does not exist since there is no applied forces, resulting in the equation

$$R_i - \ddot{mr}_i = 0. \quad \ldots\ldots\ldots\ldots\ldots\ldots\ldots\ldots (2.2)$$

The detailed set of equations of motion is as follows:

Equation of Motion in the Vertical Direction or in the Bounce Mode:

$$\ddot{my} + K_{y1}(y-a\phi+h\theta) + K_{y2}(y-a\phi-h\theta) + C_{y1}(\dot{y}-a\dot{\phi}+h\dot{\theta})$$

$$+C_{y2}(y-a\dot{\phi}-h\dot{\theta}) + K_{y3}(y+b\phi) + C_{y3}(\dot{y}+b\dot{\phi}) = 0. \quad \ldots\ldots\ldots\ldots (2.3)$$

Equation of Motion in Rotation about the x-axis or in the Pitch Mode:

$$I_{xx}\ddot{\phi} + k_{z3}(z+(d-e)\phi)(d-e) + c_{z3}(\dot{z}+(d-e)\dot{\phi})(d-e)$$
$$-k_{z1}(z-(e-f)\phi-h\Psi)(e-f) - k_{z2}(z-(e-f)\phi+h\Psi)(e-f)$$
$$-c_{z1}(\dot{z}-(e-f)\dot{\phi}-h\dot{\Psi})(e-f) - c_{z2}(\dot{z}-(e-f)\dot{\phi}+h\dot{\Psi})(e-f)$$
$$+k_{y3}(y+b\phi)b + c_{y3}(\dot{y}+b\dot{\phi})b - k_{y1}(y-a\phi+h\theta)a$$
$$-c_{y1}(\dot{y}-a\dot{\phi}+h\dot{\theta})a - k_{y2}(y-a\phi-h\theta)a - c_{y2}(\dot{y}-a\dot{\phi}-h\dot{\theta})a=0. \quad (2.4)$$

Equation of Motion in Rotation about the z-axis or in the Roll Mode:

$$I_{zz}\ddot{\theta} + k_{y1}(y-a\phi+h\theta)h + c_{y1}(\dot{y}-a\dot{\phi}+h\dot{\theta})h$$
$$-k_{y2}(y-a\phi-h\theta)h - c_{y2}(\dot{y}-a\dot{\phi}-h\dot{\theta})h$$
$$-k_{x3}(x-(d-e)\theta-b\Psi)(d-e) - c_{x3}(\dot{x}-(d-e)\dot{\theta}-b\dot{\Psi})(d-e)=0. \quad (2.5)$$

Equation of Motion along the z-axis or in the Longitudinal Mode:

$$m\ddot{z} + k_{z1}(z-(e-f)\phi-h\Psi) + c_{z1}(\dot{z}-(e-f)\dot{\phi}-h\dot{\Psi})$$
$$+k_{z2}(z-(e-f)\phi+h\Psi) + c_{z2}(\dot{z}-(e-f)\dot{\phi}+h\dot{\Psi})$$
$$+k_{z3}(z+(d-e)\phi) + c_{z3}(\dot{z}+(d-e)\dot{\phi})=0. \quad (2.6)$$

Equation of Motion along the x-axis or in the Lateral Mode:

$$m\ddot{x} + k_{x3}(x-(d-e)\theta-b\Psi) + c_{x3}(\dot{x}-(d-e)\dot{\theta}-b\dot{\Psi})=0. \quad (2.7)$$

Equation of Motion in Rotation about the y-axis or in the Yaw Mode:

$$I_{yy}\ddot{\Psi}-k_{x3}\{x-(d-e)\theta-b\Psi\}b-c_{x3}\{\dot{x}-(d-e)\dot{\theta}-b\dot{\Psi}\}b$$
$$-k_{z1}\{z-(e-f)\phi-h\Psi\}h+k_{z2}\{z-(e-f)\phi+h\Psi\}h$$
$$-c_{z1}\{\dot{z}-(e-f)\dot{\phi}-h\dot{\Psi}\}h+c_{z2}\{\dot{z}-(e-f)\dot{\phi}+h\dot{\Psi}\}h=0. \quad \ldots\ldots\ldots\ldots (2.8)$$

The above equations can be written in the matrix form as follows:

$$[M]\{\ddot{\alpha}\}+[C]\{\dot{\alpha}\}+[K]\{\alpha\}=0. \quad \ldots\ldots\ldots\ldots\ldots\ldots (2.9)$$

Where,

$$[M]=\begin{bmatrix} m & 0 & 0 & 0 & 0 & 0 \\ 0 & I_{xx} & 0 & 0 & 0 & 0 \\ 0 & 0 & I_{zz} & 0 & 0 & 0 \\ 0 & 0 & 0 & m & 0 & 0 \\ 0 & 0 & 0 & 0 & m & 0 \\ 0 & 0 & 0 & 0 & 0 & I_{yy} \end{bmatrix}$$

$$
[C]=\begin{bmatrix}
c_{y1}+c_{y2}+c_{y3} & -a(c_{y1}+c_{y2})+bc_{y3} & h(c_{y1}-c_{y2}) & 0 & 0 & 0 \\
-a(c_{y1}+c_{y2})+bc_{y3} & (e-f)^2(c_{z1}+c_{z2})+(d-e)^2c_{z3}+b^2c_{y3}+a^2(c_{y1}+c_{y2}) & 0 & (d-e)c_{z3}-(e-f)(c_{z1}+c_{z2}) & 0 & 0 \\
h(c_{y1}-c_{y2}) & 0 & h^2(c_{y1}+c_{y2})+(d-e)^2c_{z3} & 0 & -(d-e)c_{x3} & b(d-e)c_{x3} \\
0 & (d-e)c_{z3}-(e-f)(c_{z1}+c_{z2}) & 0 & c_{z1}+c_{z2}+c_{z3} & 0 & 0 \\
0 & 0 & -(d-e)c_{x3} & 0 & c_{x3} & -bc_{x3} \\
0 & 0 & b(d-e)c_{x3} & 0 & -bc_{x3} & b^2c_{x3}+h^2(c_{z1}+c_{z2})
\end{bmatrix}
$$

$$
[K]=\begin{bmatrix}
k_{y1}+k_{y2}+k_{y3} & -a(k_{y1}+k_{y2})+bk_{y3} & h(k_{y1}-k_{y2}) & 0 & 0 & 0 \\
-a(k_{y1}+k_{y2})+bk_{y3} & (e-f)^2(k_{z1}+k_{z2})+(d-e)^2k_{z3}+b^2k_{y3}+a^2(k_{y1}+k_{y2}) & 0 & (d-e)k_{z3}-(e-f)(k_{z1}+k_{z2}) & 0 & 0 \\
h(k_{y1}-k_{y2}) & 0 & h^2(k_{y1}+k_{y2})+(d-e)^2k_{z3} & 0 & -(d-e)k_{x3} & -b(d-e)k_{x3} \\
0 & (d-e)k_{z3}-(e-f)(k_{z1}+k_{z2}) & 0 & k_{z1}+k_{z2}+k_{z3} & 0 & 0 \\
0 & 0 & -(d-e)k_{x3} & 0 & k_{x3} & -bk_{x3} \\
0 & 0 & b(d-e)k_{x3} & 0 & -bk_{x3} & b^2k_{x3}+h^2(k_{z1}+k_{z2})
\end{bmatrix}
$$

(α) is the state vector represented by $(y,\phi,\theta,z,x,\Psi)^T$; $(\dot{\alpha})$ and $(\ddot{\alpha})$ are the first and second derivatives with respect to time respectively.

2.3.2 Equations of Motion for Terrain-Induced Vibration:

In the case of tracked vehicles, the off-road terrian induced vibration is transmitted to the cab floor through the cab mounts and acts as the forcing function for the mathematical model. Figure 2.3 illustrates such an excitation being impressed upon the cab structure modelled in section 2.3.1.

Let y_{oi} represent the displacement due to the support excitation along the Y-direction at supports, i=1,2 and 3, and $\dot{y}_{oi}$ be the velocity and $\ddot{y}_{oi}$ be the acceleration inputs at the supports respectively.

Similarly, let z_{oi}, $\dot{z}_{oi}$ and $\ddot{z}_{oi}$ represent the displacement, velocity and acceleration respectively at the supports, i=1,2 and 3 along the z direction due to support excitations. Let χ_{03}, $\dot{\chi}_{03}$ and $\ddot{\chi}_{03}$ represent the displacement, velocity and acceleration repectively along the x-direction due to support excitations.

Following a similar procedure as in the equations of motion (2.9) formulated for free vibration, the equations of motion for terrain-induced vibration can be expressed in the matrix form thus:

$$[M](\ddot{\alpha}) + [C](\dot{\alpha}) + [K](\alpha) = [C'](\dot{\beta}) + [K'](\beta) \quad \ldots\ldots\ldots\ldots (2.10)$$

Where [M],[C] and [K] are the matrices represented under section 2.3.1.

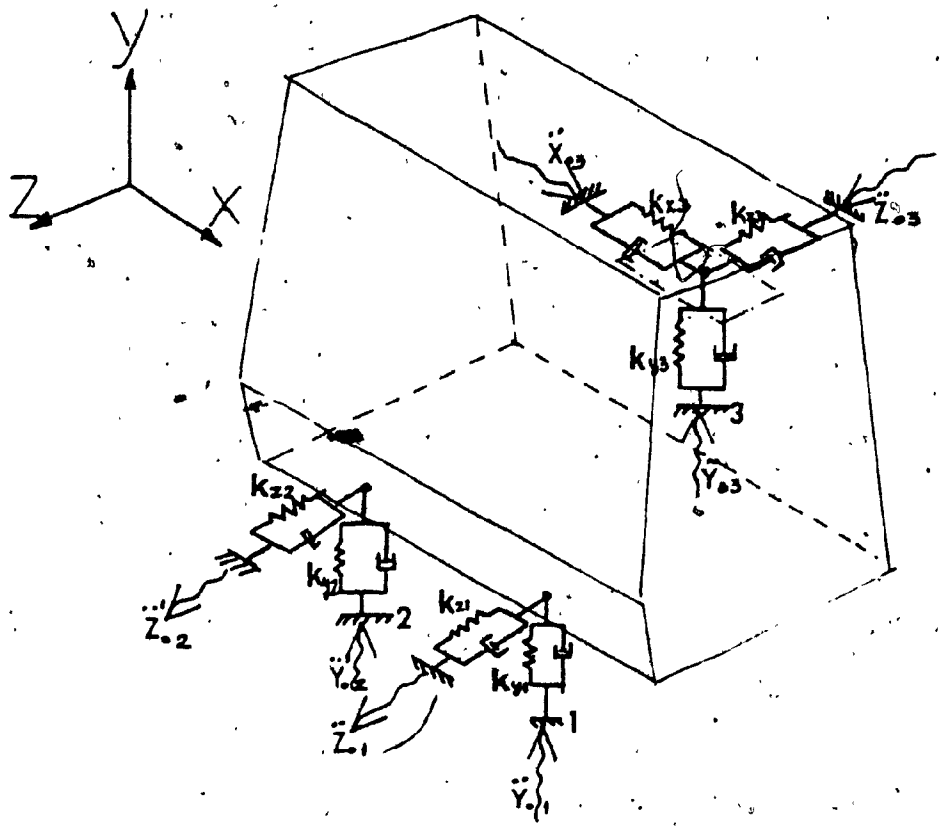

Fig 2.3: Three-Point Layout Cab Subjected to Terrain Excitations

The matrices [C'] and [K'] are given by:

$$[C'] = \begin{bmatrix} c_{y1} & c_{y2} & c_{y3} & 0 & 0 & 0 & 0 \\ -c_{y1}a & -c_{y2}a & c_{y3}b & -c_{z1}(e-f) & -c_{z2}(e-f) & c_{z3}(e-f) & 0 \\ c_{y1}h & -c_{y2}h & 0 & 0 & 0 & 0 & c_{x3}(d-e) \\ 0 & 0 & 0 & c_{z1} & c_{z2} & c_{z3} & 0 \\ 0 & 0 & 0 & 0 & 0 & 0 & c_{x3} \\ 0 & 0 & 0 & -c_{z1}h & c_{z2}h & 0 & -c_{x3}b \end{bmatrix}$$

$$[K'] = \begin{bmatrix} k_{y1} & k_{y2} & k_{y3} & 0 & 0 & 0 & 0 \\ -k_{y1}a & -k_{y2}a & k_{y3}b & -k_{z1}(e-f) & -k_{z2}(e-f) & k_{z3}(d-e) & 0 \\ k_{y1}h & -k_{y2}h & 0 & 0 & 0 & 0 & k_{x3}(d-e) \\ 0 & 0 & 0 & k_{z1} & k_{z2} & k_{z3} & 0 \\ 0 & 0 & 0 & 0 & 0 & 0 & k_{x3} \\ 0 & 0 & 0 & -k_{z1}h & k_{z2}h & 0 & -k_{x3}b \end{bmatrix}$$

(β) is the excitation vector represented by $(y_{01}, y_{02}, y_{03}, z_{01}, z_{02}, z_{03}, x_{03})^T$ and $(\dot{\beta})$ is the first derivative with respect to time.

Thus the equation (2.10) represents the forced vibration equations of motion for a general case of tilt-cab suspension with three supports.

Since some of the tilt-cabs have four supports, ie., two mounts at the rear instead of a single rear mount, the equations of motion are derived and presented in the matrix form under Appendix I.

2.5 Summary

In this chapter, the problem of ride quality improvement of a tracked vehicle is chosen as the topic of research with particular reference to tilt-cab suspensions having three supports. An overview of cab suspensions is presented. Subsequently, a mathematical six degrees of freedom model is developed and the equations of motion are formulated for both free and terrain-induced vibrations. The equations of motion for a tilt-cab suspension with four supports are presented in Appendix I, with accompanying figures for such an arrangement.

CHAPTER III

DESCRIPTION AND EXTRACTION OF RELEVANT PARAMETERS OF A CANDIDATE OFF-ROAD VEHICLE

CHAPTER III

Description and Extraction of Relevant Parameters of a Candidate Off-Road Vehicle

3.1 Introduction

Off-road vehicle designs vary dramatically with the type of use; agricultural, earthmoving, snow clearing, and military application. As mentioned in the earlier chapter, the main areas of interest in such vehicles are their dynamic behaviour, particularly the ride. Tracked vehicles in general, are low speed vehicles (5 miles/hr) with some exceptions. Majority of such vehicles do not possess any suspensions at their axles. Vibration isolation and thus ride quality improvement is mainly achieved by suspending their Cabs on vibration mounts.

One such vehicle is the snow pusher-cum-tiller used widely in the mountain ski-slopes for leveling snow. These vehicles vary widely in size and tractive power depending on the application. For the purpose of validating the computer simulation of the tilt-Cab suspension system, an off-road tracked vehicle - "BR-400", manufactured by the Industrial Equipment Division of Bombardier Inc. is selected as the candidate vehicle. In this chapter, the description of the vehicle and the methods used to extract the relevant physical and geometrial parameters of the vehicle are outlined. Some of these parameter values are available from the manufacturer. However, for few other parameters, finite element analysis and laboratory experiments were carried out and the results are outlined here.

3.2 Description of "BR-400"

BR-400 is a heavy-industrial-tracked vehicle. Figure 3.1 shows pictorially the perspective view of "BR-400". Its total shipping weight is about 5090 kg and it occupies an area of 4.06mx3.81m with an overall height of about 2.59m. It has totally 2 sets of 5 wheels on each side, mounted with hard rubber tires and when in operation runs with tracks made of rubber belts and steel cross links. The wheels are mounted on trailing arms and rubber torsion blocks. The chassis is fabricated out of heat-treated box sections over which is mounted the engine, the transmission, the heavy battery rack, and finally the tilt-cab. The front blade and the rear tiller with associated accessories are also attached to the rigid frame. Both the front blade and the rear tiller can be independently raised or lowered hydraulically. Table 3.1and 3.2 shows the specification of the vehicle.

The operator cabin (CAB), is mounted over the frame and occupies space just above the engine. Due to this configuration, the cab can be classified under the "Cab-Over-Engine" type. Similar to the earlier descriptions, this cab is supported on two frontal supports and a rear mount making it a three point layout.

Since the cab is positioned over the engine, a hydraulically operated piston mechanism is provided to tilt the cab about the frontal load bearing supports. Therefore, the rear mount has a positioning and locking mechanism when the Cab is brought to its normal position. Figure 3.2 illustrates this arrangement.

BOMBARDIER

BR-400

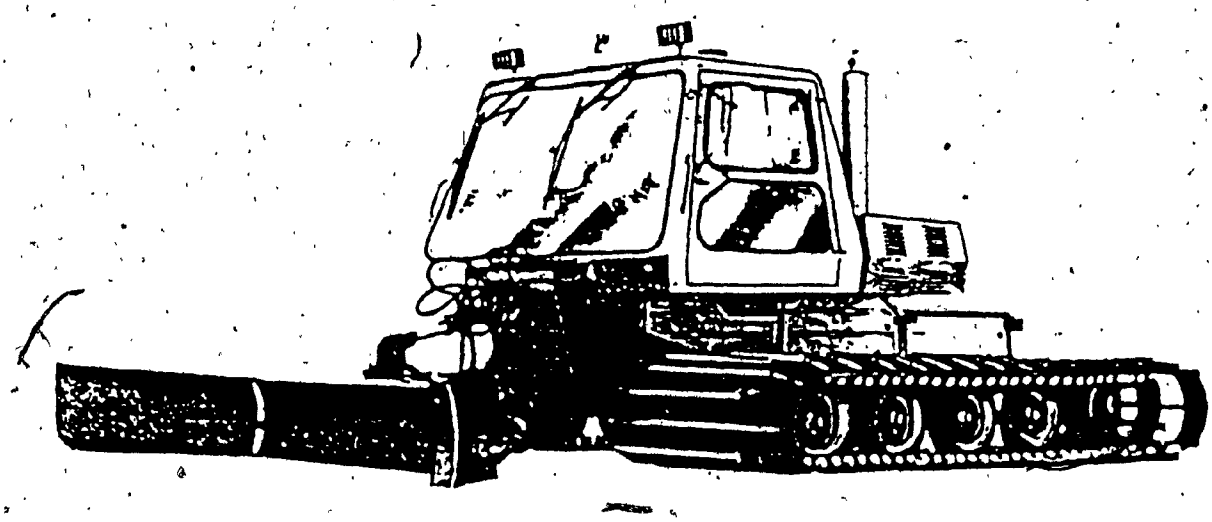

Fig.3.1 Perspective View of "BR-400"
(Courtesy Bombardier Inc.)

Table 3.1: Specifications of "BR-400"
(Courtesy Bombardier Inc.)

Specifications:

DIMENSIONS:	S.I.	
Overall Length	4.06 m	160"
Overall Width	3.81 m	150"
Overall Height	2.59 m	102"
Ground Clearance	29 cm.	11-1/2"
Shipping Weight (Basic Vehicle)	5090 kg	11,200 lbs

OPERATIONAL:		
Maximum Speed at governed RPM	18.5 km/h	11.5 MPH
Inside Turning Radius	0 m	0 ft
Basic Vehicle Ground Pressure at 0°	5.64 kPa	0.82 PSI
Maximum Gradeability Uphill	Up to 100%	
Sidehill	75% of Uphill	

ENGINE:		
Make	John Deere	
Model	6466 A	
No. of Cylinders	6	
Displacement	7.64 L	466 C.I.D.
Horsepower-Brake	224 HP @ 2100 RPM (SAE)	
Torque at 1400 RPM	901 N-m	665 ft lb

POWER TRAIN:	
Transmission - Type	Hydrostatic
- Model	Sundstrand serie 36
Final Drive Reduction	19.04 to 1
Drive Sprockets	
- Type	Polyurethane on aluminum hub
- Location	Rear
Brakes	
- Service	Positive deceleration through the hydrostatic transmission
- Parking	Dry multidisc spring applied pressure - released

STEERING:
Independent control for each track

ELECTRICAL:	
Voltage	24 volts
Battery Capacity	570 amps cranking capacity with 180 minutes reserve
Alternator Capacity	40 amps
Ground	Negative

Table 3.2: Specifications of "BR-400"

(Courtesy Bombardier Inc.)

Specifications: BR-400

Bombardier Inc.
Industrial Equipment Division

Valcourt, Que., Canada, J0E 2L0
Telephone (514) 532 2211
Cable Bombarsnow, Telex 05 832552

SUSPENSION:

2 front wheels mounted on cranking arms and rubber torsion blocks, 8 wheels on walking beams mounted on cranking arms and rubber torsion blocks

WHEELS:

Quantity	10
Type of Tire	2 solid rubber 8 inflated
Size	4.50 x 12
Ply Rating	8

TRACKS:

Type	Rubber belts and steel crosslinks
Width	147 cm 58"
Type of Belts	Rubber and fabric

CHASSIS:

Type	Heat treated heavy square tubes

CAPACITIES:	S.I.	IMP	U.S.
Cooling System	30 L	6.5 gal	7.8 gal
Fuel Tank	182 L	40 gal	48 gal
Engine Crankcase	21 L	4.6 gal	5.5 gal
Hydrostatic System	109 L	24 gal	29 gal
Hydraulic System	23 L	5 gal	6 gal

STANDARD EQUIPMENT:

2 man insulated power tilt cab
2 T-Bar seats
Tinted glass
Seat belts
Heavy-duty heater and defroster
Rear window wiper
Dome and instrument lights
4 front lights (flood halogen)
2 rear lights (flood halogen)
9 sections hydraulic system (6 front 3 rear)
Full instrumentation
Audio-visual warning system on major components
Rotating light
Hydrostatic oil tank heater
Rear view mirrors
Heated windshield
Grab bars
Pintle hook
Engine governor
Parking brake
Horn
Lighter
Ashtray
Electric-hydraulic joystick
Deluxe 5 way roof opening
2 adjustable intermittent front wipers
Door limiters
Master electric cut-off switch
Electric engine shut-down
Engine block-heater
Cold start aid
AM/FM stereo cassette radio
Directional halogen spotlight
Back up alarm
Ice calks
Fire extinguisher
Parts and operator's manuals

OPTIONAL EQUIPMENT:

All way front blade (Valley)
Rear lift frame and compaction bar
Rotary tiller
Electrically heated windows and mirrors

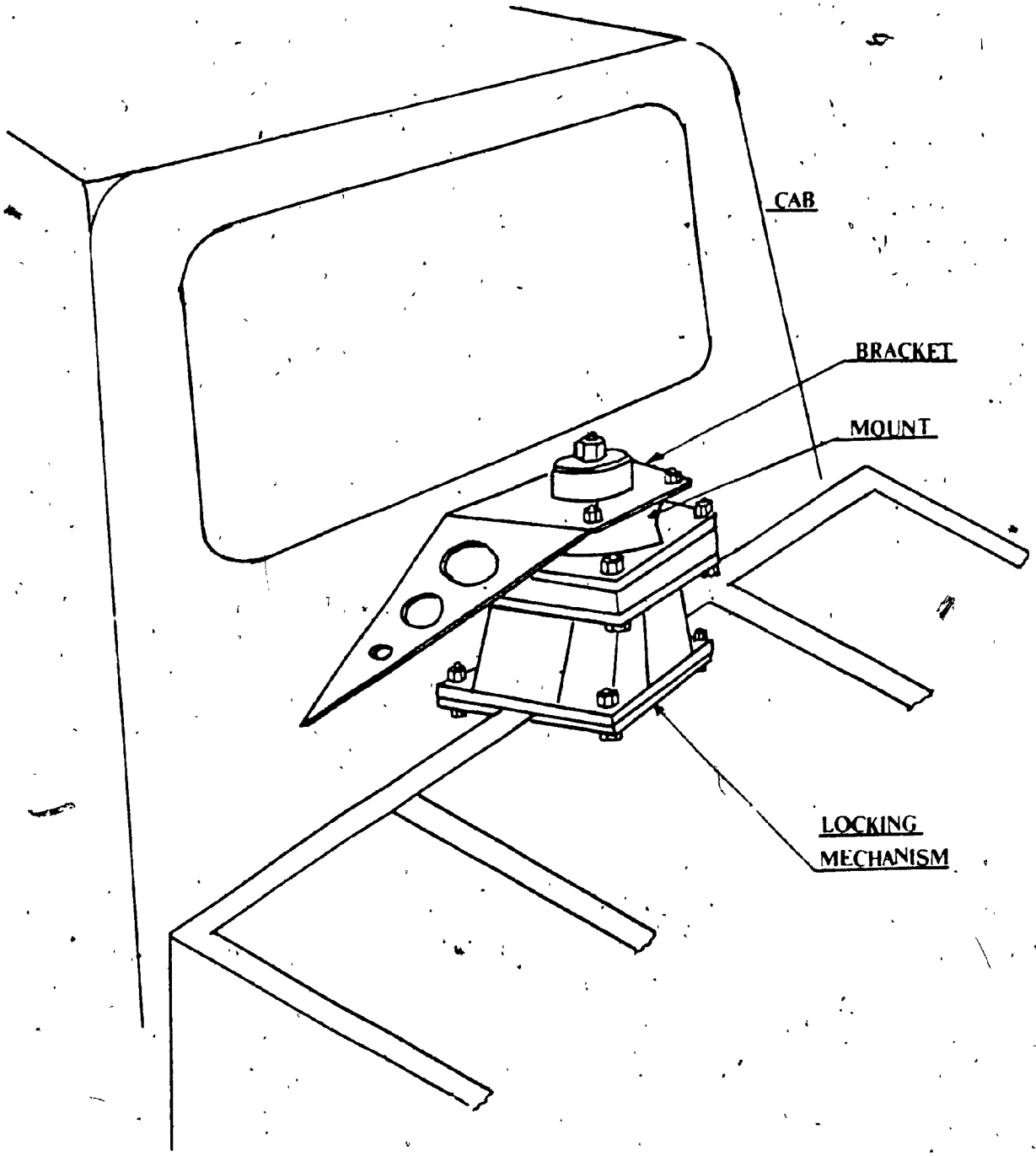

Fig 3.2: Arrangement of the Rear Support

3.3 Cab Suspension of "BR-400"

The cab of "BR-400" is basically a framed structure with a sheet metal covering all over leaving openings for front and rear wind shield glass and doors at the sides. It has two frontal brackets having the bushings, which are welded to the sheet metal body. Figure 3.3 shows the bracket and Figure 3.4 is the bushing presently in use. Once the bushes are assembled with the brackets, the assembly is pinned to the frame of "BR-400", suspending the cab as a whole.

The third support of the cab; namely, the rear mount arrangement consists of a sheet metal bracket to which is fitted the mount. Figure 3.5 shows the rear mount presently in use.

3.4 Extraction of Relevant Parameters of the Vehicle

As a first step towards achieving the goal of ride comfort in a cab of any vehicle, it is necessary to estimate the natural frequencies and mode shapes of the model developed. This is accomplished by solving the eigenvalue problem of the differential equations of motion formulated earlier in chapter II. In order to solve these equations, the following system parameters of the cab suspension are needed.

- Total mass of the cab
- Centroid of the cab
- Mass moment of inertias of the cab about the orthogonal co-ordinates

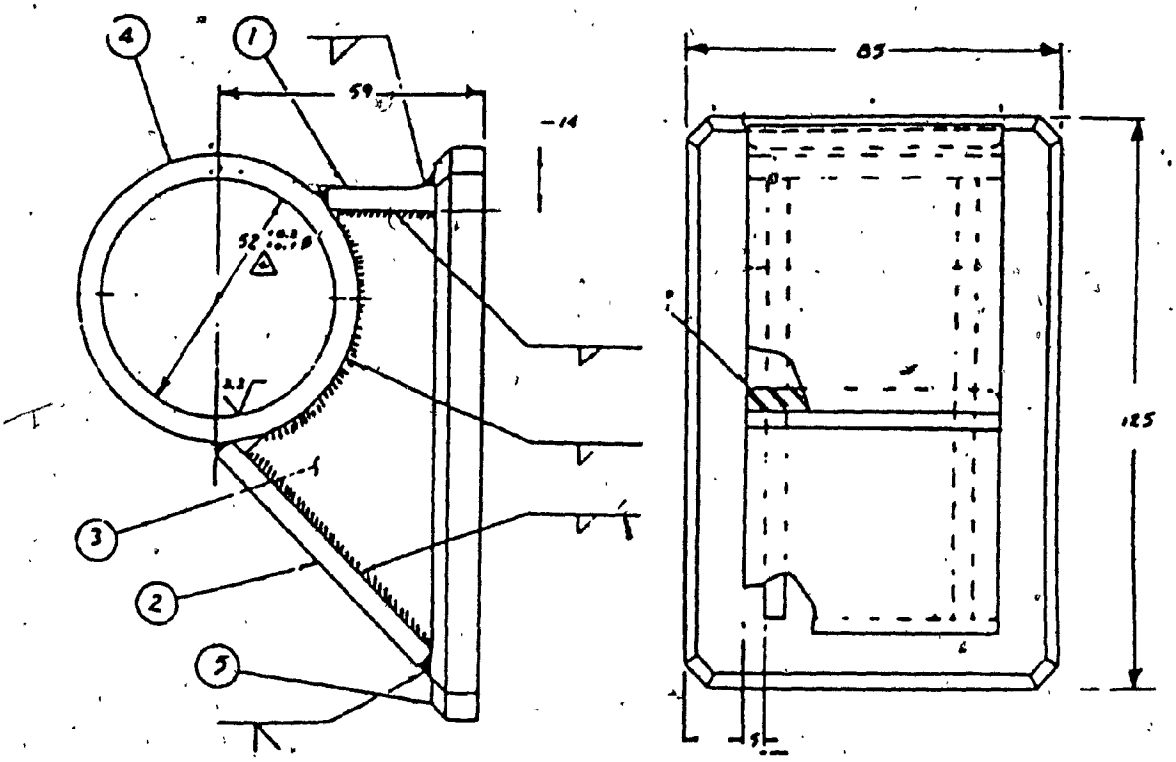

item No.	Description
1 & 2	Plate 3/16" thk
3	Side Plate
4	Tube
5	Base

Fig 3.3 Frontal Bracket of the Cab- "BR-400"
(Courtesy Bombardier Inc.)

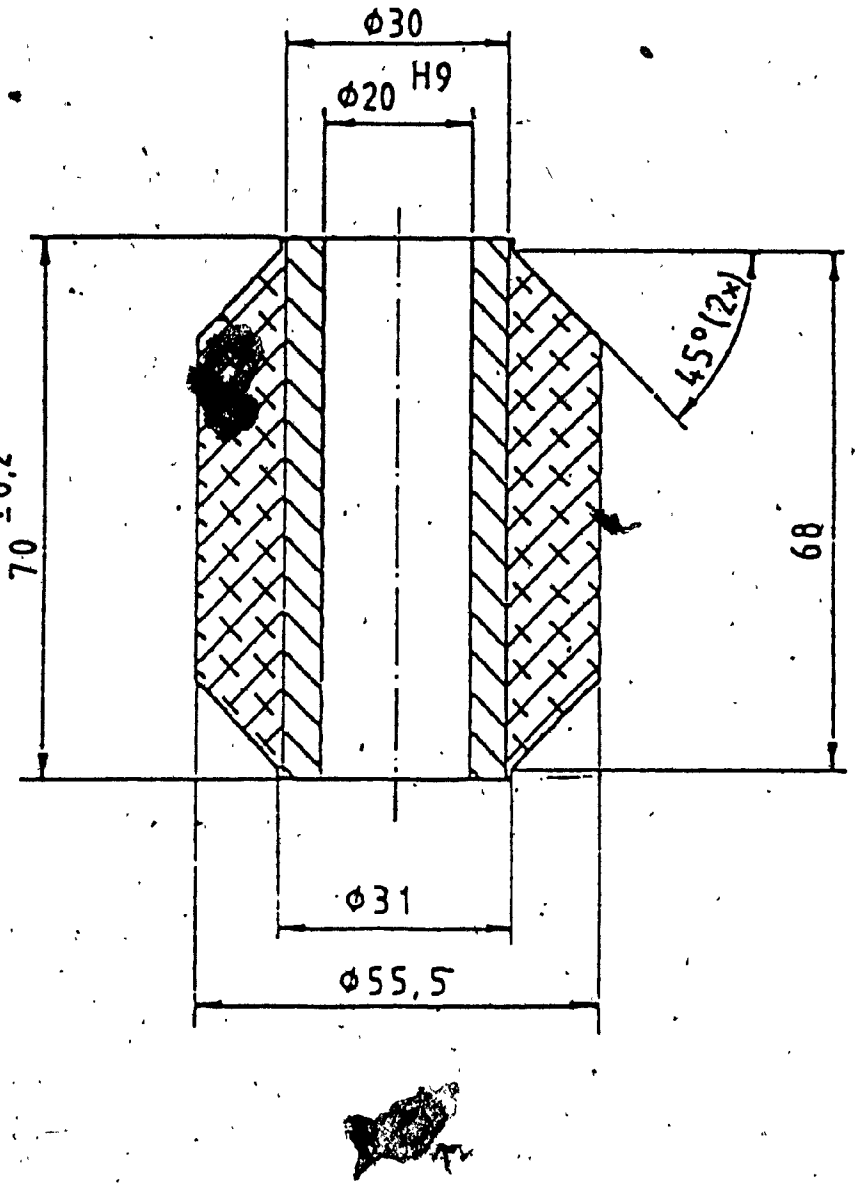

Fig 3.4: Bushing used in the Front Support- "BR-400"
(Courtesy Bombardier Inc.)

MODEL 512

(TYPE 2)

Load Range		
Min.	Nominal	Max.
230	460	690
280	560	840
340	680	1020
415	830	1245
500	1000	1500

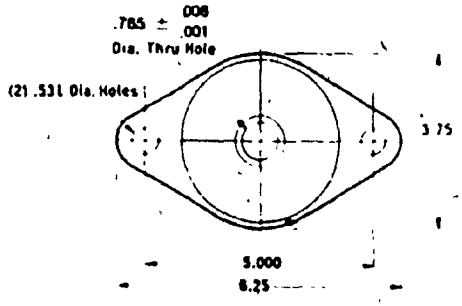

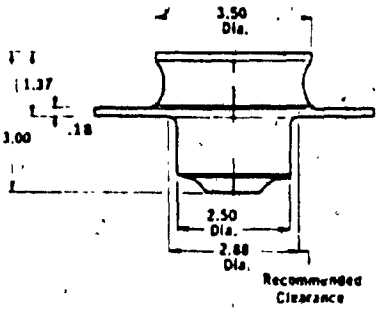

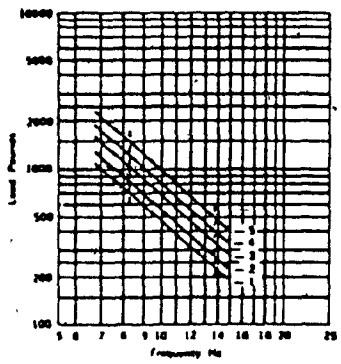

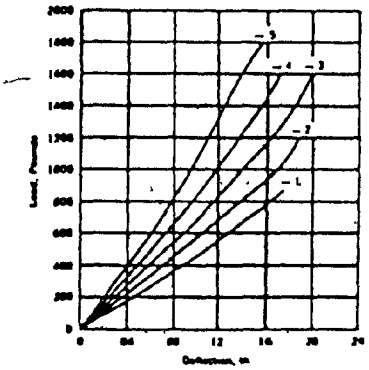

Characteristics of Model 500 Series.

Fig 3.5: Rear Mount and its Load-Deflection Charecteristics-"BR-400"
(Courtesy M/S Barry Controls)

- Stiffness and damping coefficients of the isolator/mounts.

Therefore, it can be seen that these data are the prime requisite to arrive at the solution for the specific case study undertaken. Hence, the following sections are devoted to the evaluation of the said data by means of both analytical and experimental methods. The first three parameters; namely, the mass, the C.G and the moment of inertias are evaluated by making use of the 'ANSYS' finite element software package. The cab of "BR-400" being a non-Symmetrial structure about the lateral 'X' axis and the the vertical 'Y' axis, it was felt necessary to use the finite element package to arrive at these parameters with reasonable accuracy. However, the isolator properties; namely, the stiffness and the damping coefficients are obtained by laboratory experiments.

3.4.1 ANSYS Finite-Element Analysis

The ANSYS computer program [18] is a large-scale, general purpose computer program for the solution of several classes of engineering analyses. Analysis capabilities include static and dynamic; elastic, plastic, creep and swelling; small and large deflections. Finite Element idealization is employed through out the program to analyze the model through the matrix displacement method. The library of finite elements available, numbers more than forty making it feasible to analyze two or three dimensional frame structures. Figure 3.6 gives the typical phases of the analysis and the main routines involved in them. The input data represented under the preprocessor stage, simply

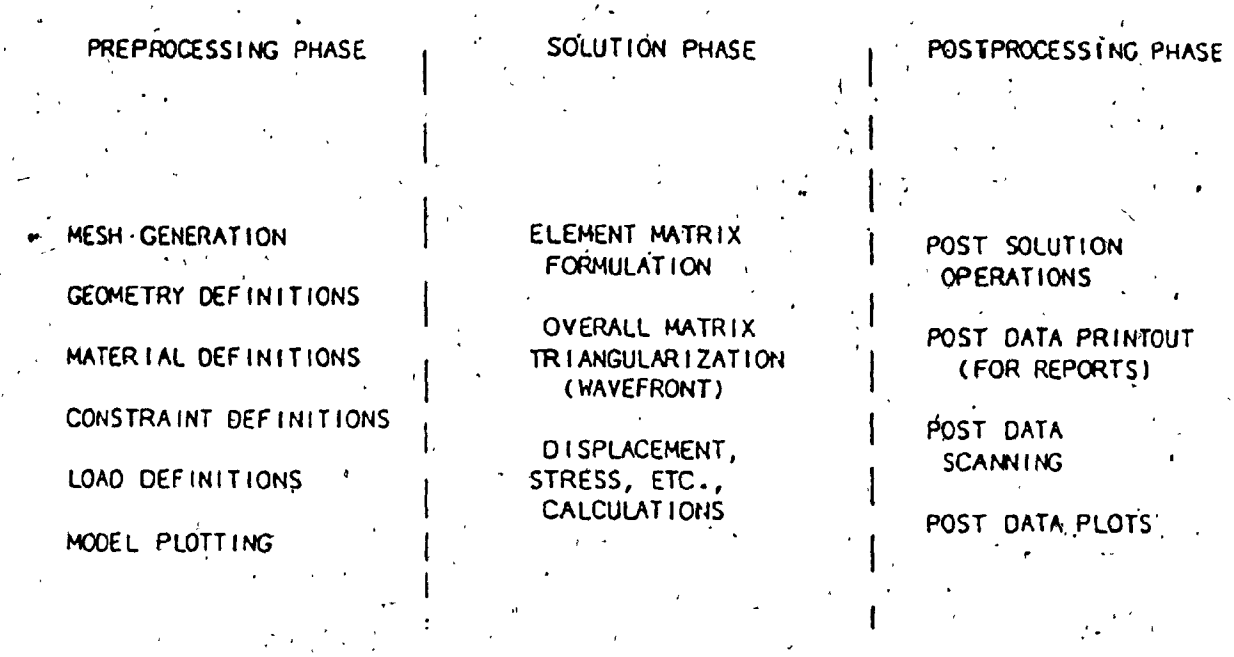

Fig 3.6: Typical Phases of the "ANSYS" Analysis(18)

mentioned as /PREPn defines the type of analysis. This stage provides the routines enough commands and data to generate the model and plot the geometry as well, apart from defining material properties, sizes and the loads.

PREP 7 is a common preprocessor used in the analysis of structures and has a number of modules. Each modules performs a different operation and contains a unique set of commands. Basic PREP 7 flow-chart is shown in Figure 3.7. Each file mentioned in the figure is intended to store the data whether it be for the solution phase, for plotting the geometry, or for the resumption of data. Based on this brief introduction, the next stage is to explain the finite element model of the cab developed.

3.4.2 Finite Element Model of the Cab

A coarse F.E model of the cab developed for the ANSYS program is shown in Figures 3.8, 3.9, 3.10 and 3.11. There are totally 110 modes constituting 229 elements. The major types of elements which are used to discritize the structure are listed as follows:

- Rectangular Elastic Shell
- Triangular Elastic Shell
- Quadrilateral Elastic Shell
- Symmetrical Elastic Beam
- Spring-Damper Element
- Mass Elements

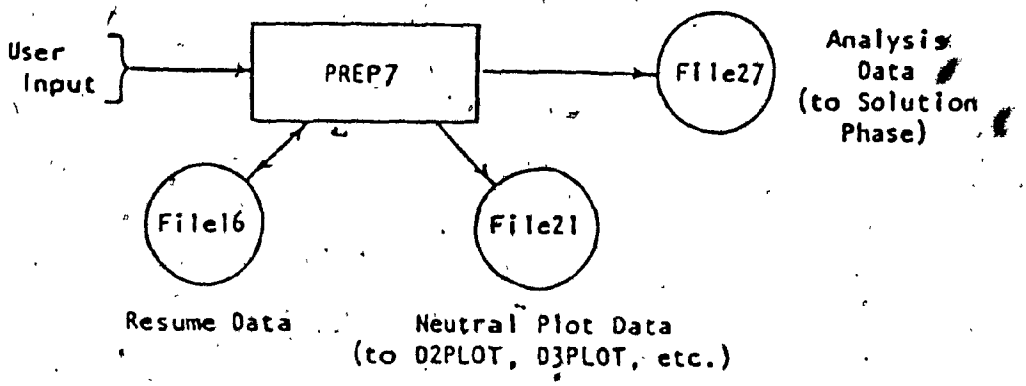

Fig 3.7: Basic Flow Chart of the Pre-Processor PREP7

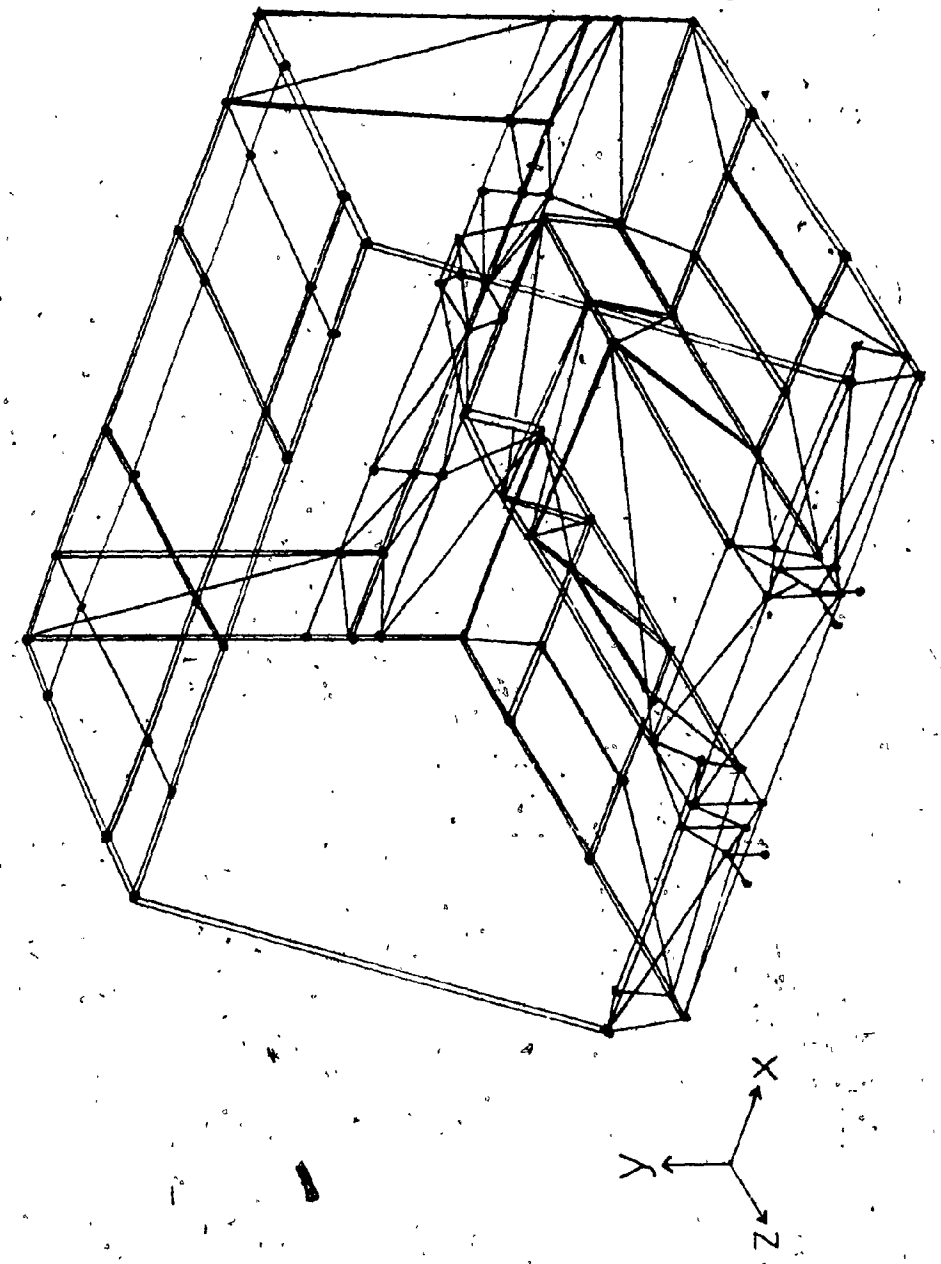

Fig 3.8: Isometric View of the F.E. Model of the Cab

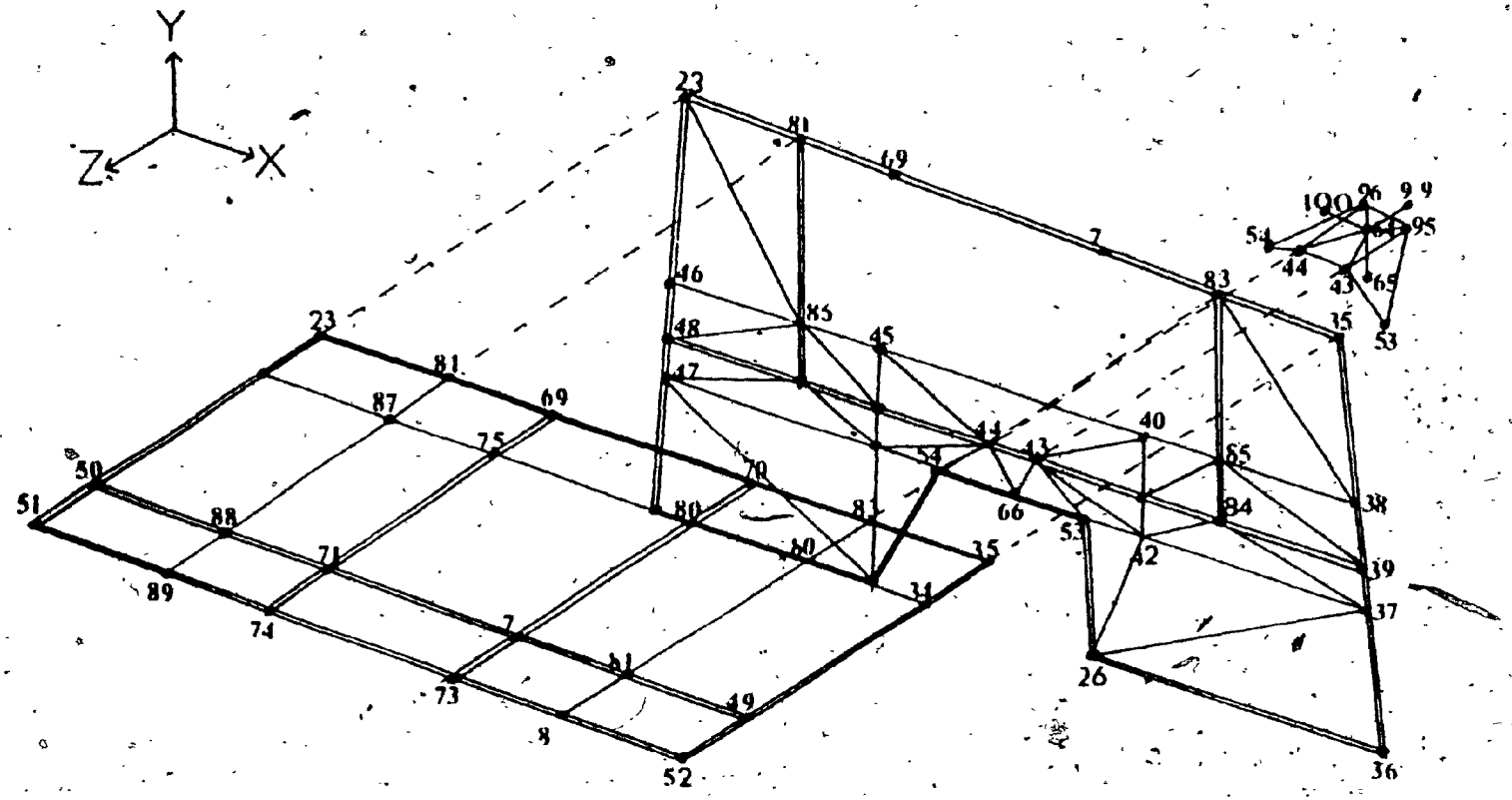

Fig 3.9: Top and Rear Panels of the F.E Model of the Cab

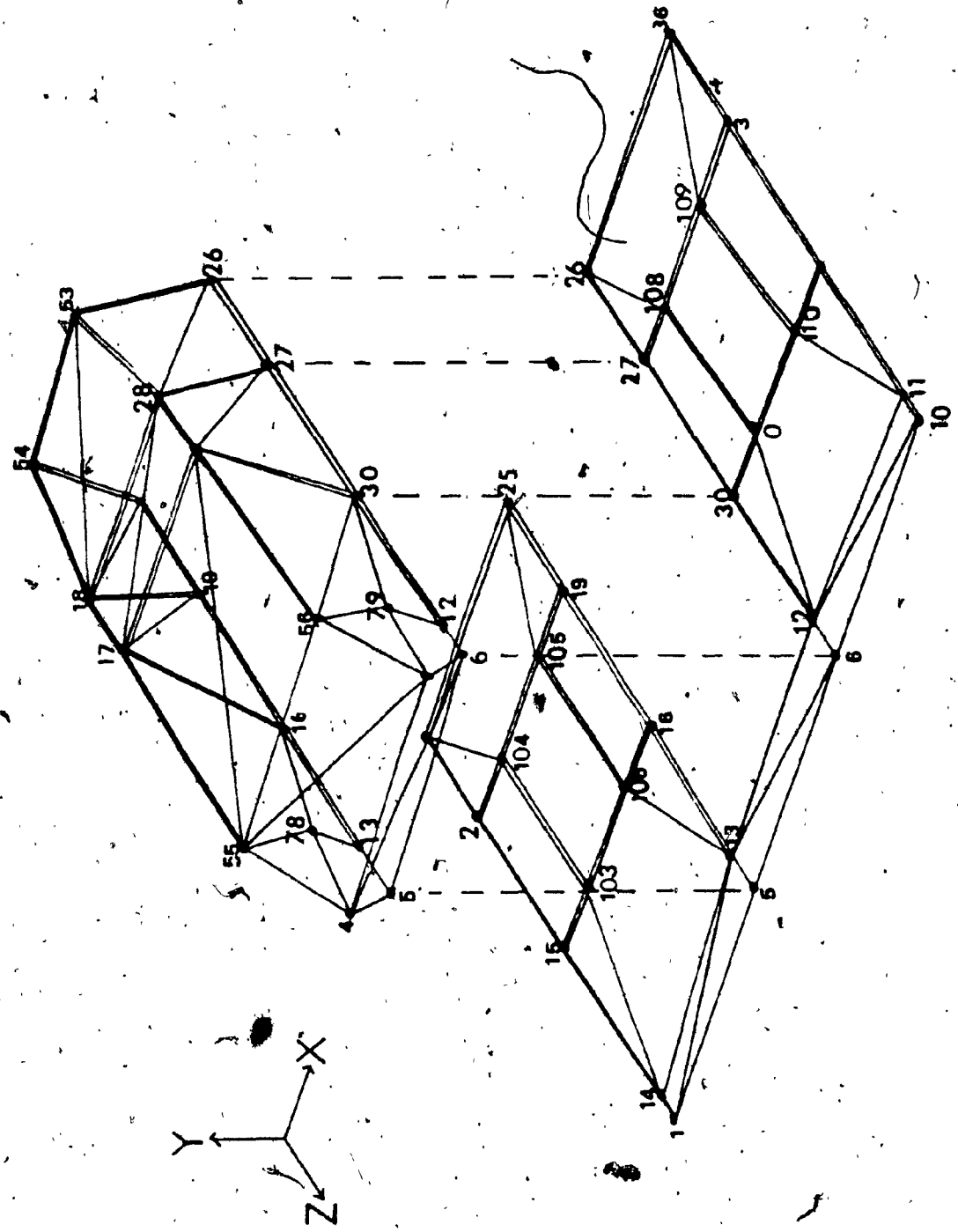

Fig 3.10: Bottom Panel of the F.E Model of the Cab

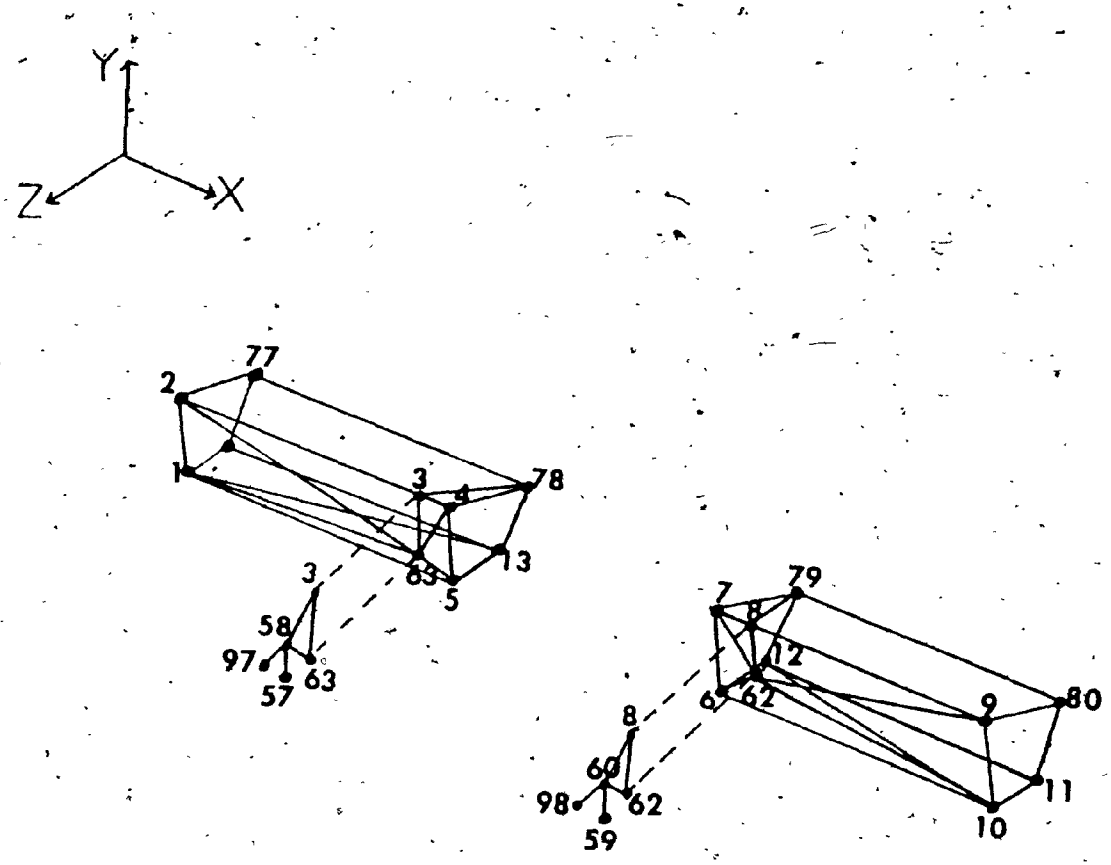

Fig 3.11: Front Panel of the F.E Model of the Cab

The beam elements are shown in double lines to distinguish them from the common boundary lines drawn between the flat elements. Figures 3.12, 3.13, 3.14 and 3.15 show the F.E model developed by the ANSYS Software package. As considered in the mathematical model developed in Chapter II, the supports at the front and rear are modelled as spring-damper elements arranged orthogonally at each location. The following paragraphs enumerate certain other assumptions made in developing the F.E model.

- The front brackets carrying the bushings are modelled as a triangular element of 30mm thickness. (A separate F.E program was developed to verify this assumption. A detailed F.E model of the bracket was developed as shown in Figure 3.16 and the static analysis was carried out. The stiffness figures were compared with that determined for a single traingular element. The results were found to be in agreement).

-The seat suspension and the operator are assumed to be rigid.

- The total mass of the seat-operator unit is assumed to act equally distributed at the four nodes of the cab floor on either side of the cab representing the driver as well as the passenger.

Table 3.3 gives the details of the parameters developed through the ANSYS pre-processor. The F.E model is then utilized to extract the natural frequencies and modeshapes of the cab. The finite

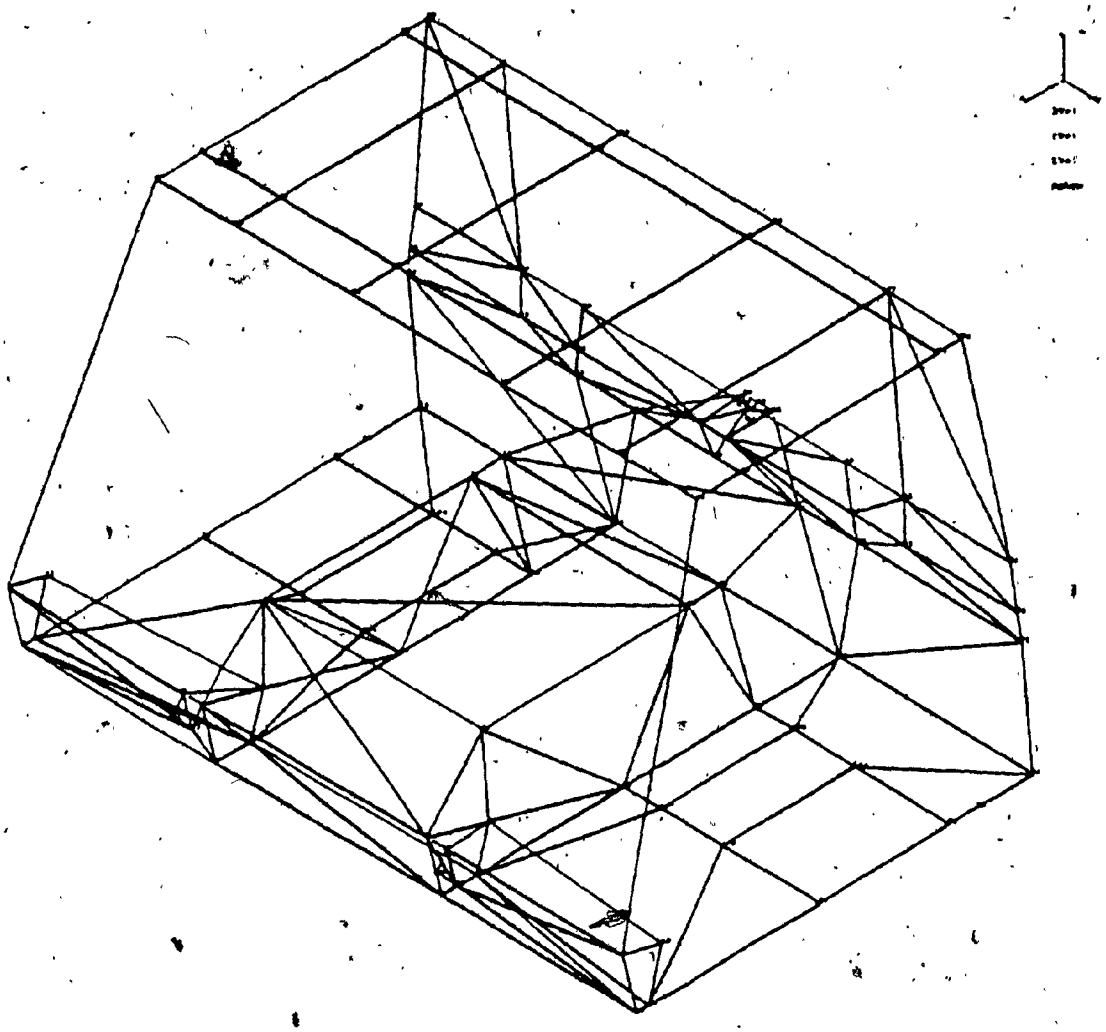

Fig 3.12: Isometric View of the Cab Model developed in "ANSYS"

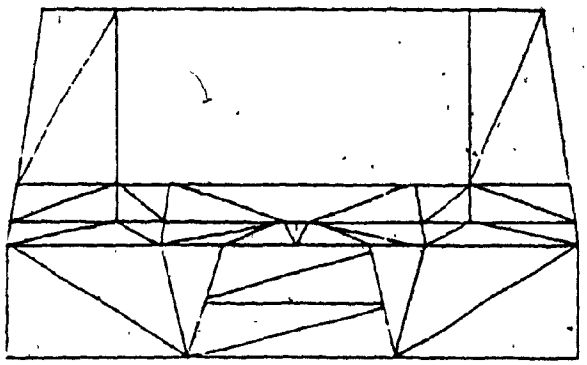

Fig 3.13: Rear View of the Cab Model developed in "ANSYS"

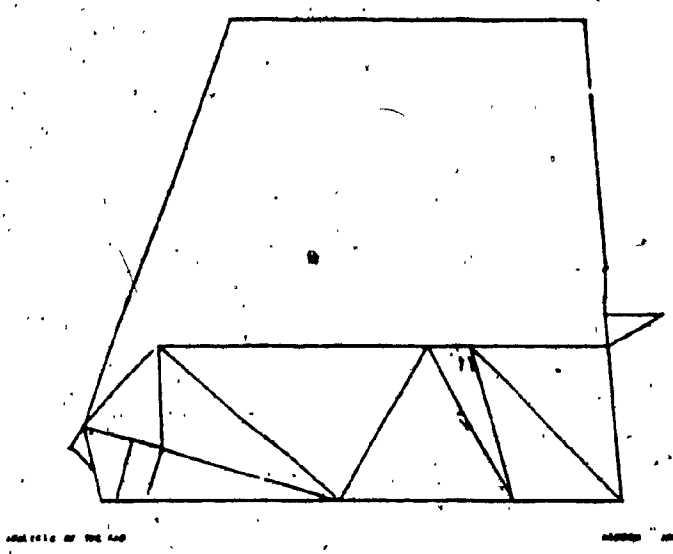

Fig 3.14: Side View of the Cab Model developed in "ANSYS"

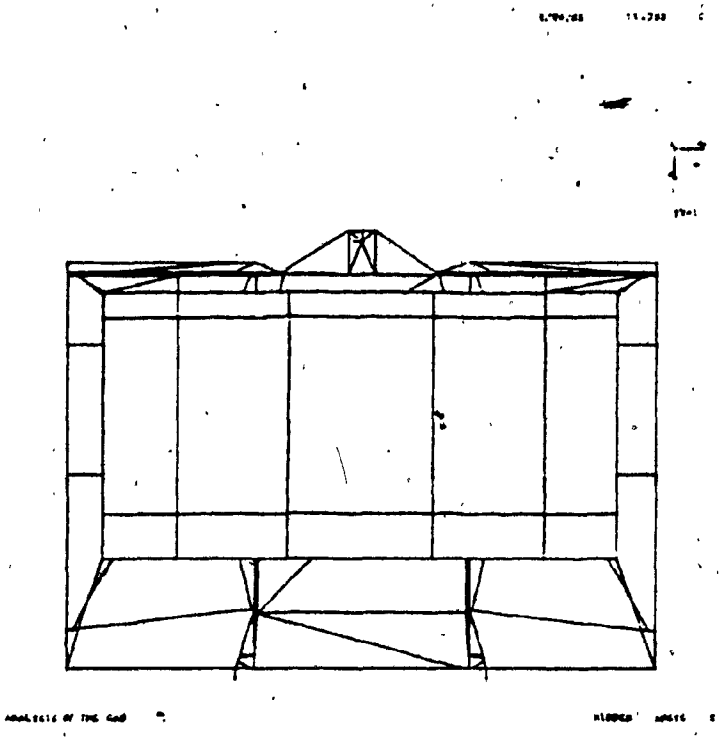

Fig 3.15: Top View of the Cab Model developed in "ANSYS"

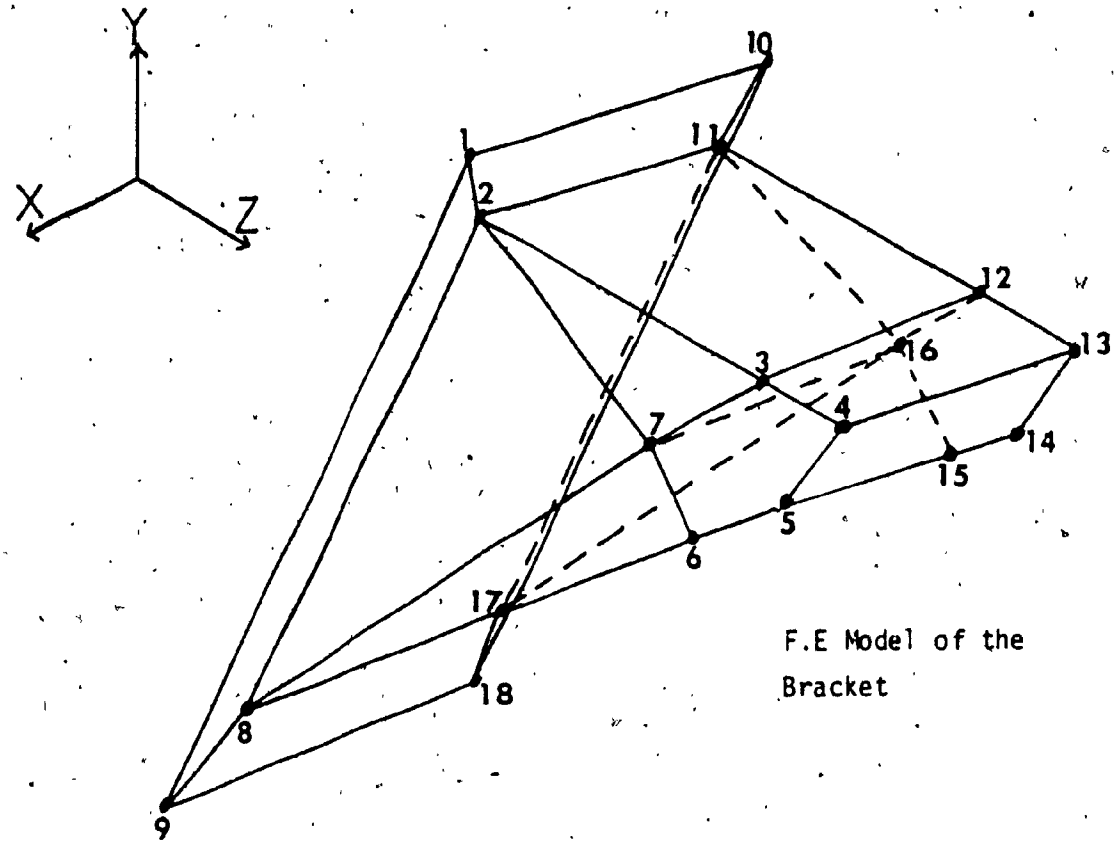

F.E Model of the Bracket

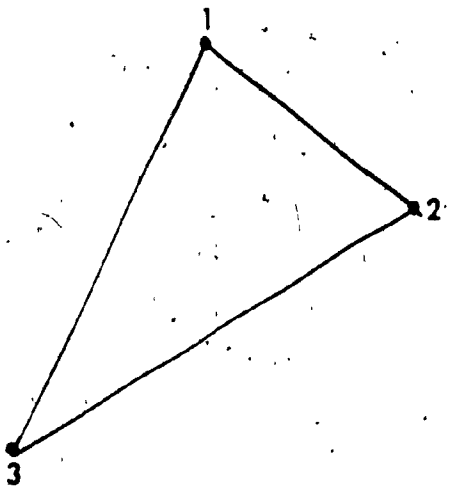

Equivalent triangular Element

Fig 3.16: F.E Model of the Front Bracket

Table 3.3 Analytical Results Extracted through "ANSYS"

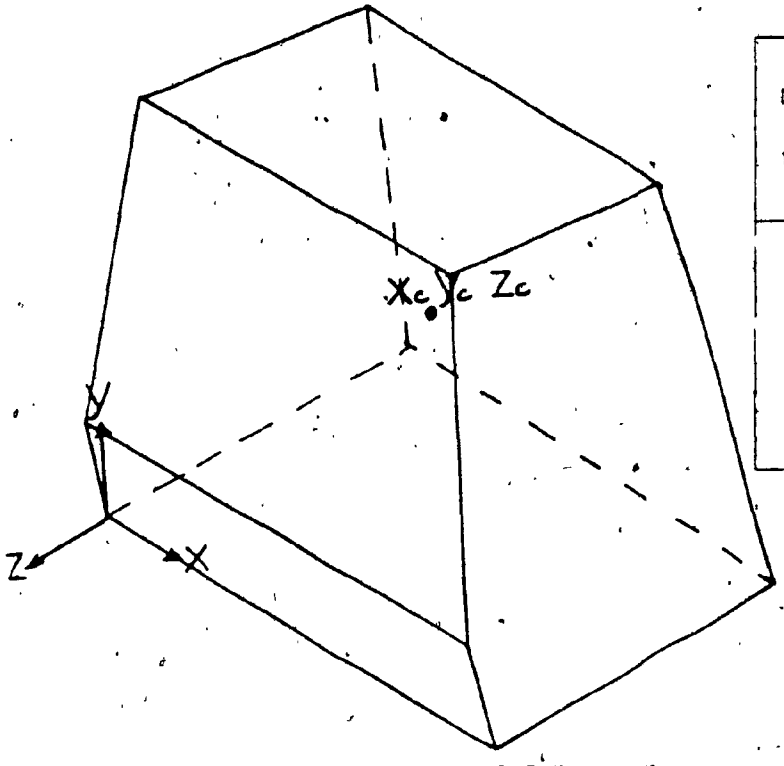

Moment of Inertia about the Centroid	
I_{xx}	256.6kg-m^2
I_{yy}	362.3kg-m^2
I_{zz}	414.6kg-m^2

X_c = 1.1040m
Y_c = 0.377m
Z_c = -0.8314m

Comparison of F.E and Experimental Results

Physical Data of Cab	Via F.E Analysis	Via Experimental*	% Error
Mass of the Cab	623.18kg	719kg	13.3
Centroidal Co-ordinates X_c	1.10m	1.10m	
Y_c	.377m	.40m	
Z_c	-.831m	-.838m	

(*Note: Information furnished by Bombardier Inc.)

element approach for the modal analysis is described in chapter IV.

3.4.3 Stiffness Evaluation of the Front Bushing

Figure 3.17 shows the equipment employed to determine the load-deflection characteristics of the elastomer bushing. Figure 3.18 explains the set up prepared to carry out the test so that the stiffness along the vertical axis is determined. (In this particular case the stiffness along the vertical and the longitudinal axes are considered to be identical; namely, $k_{y1}=k_{z1}=k_{y2}=k_{z2}$).

The testing equipment is a typical "MTS" System used for material testing. Basically, the machine is a closed loop hydraulic system which has a hydraulic power supply unit, a hydraulic actuator, a servo-valve to control the fluid flow and finally a pair of transducers to measure the load and deflection. The equipment is linked to an X-Y plotter. Figure 3.19 is the load-deflection plot obtained for the isolator. The y-axis represents the load in Newtons and the x-axis represents the defection in Centimeters. From this load-deflection curve, the value of stiffness is calculated as 26.67×10^5 N/M.

3.4.4 Evaluation of the Damping Coefficient of the Front Bushing

The damping factor of the bushing is experimentally determined by the "logarithmic decrement method". The test set up consists of an accelerometer mounted on the bush, with its output monitored by an oscilloscope. Figure 3.20 shows the block diagram of the test set up.

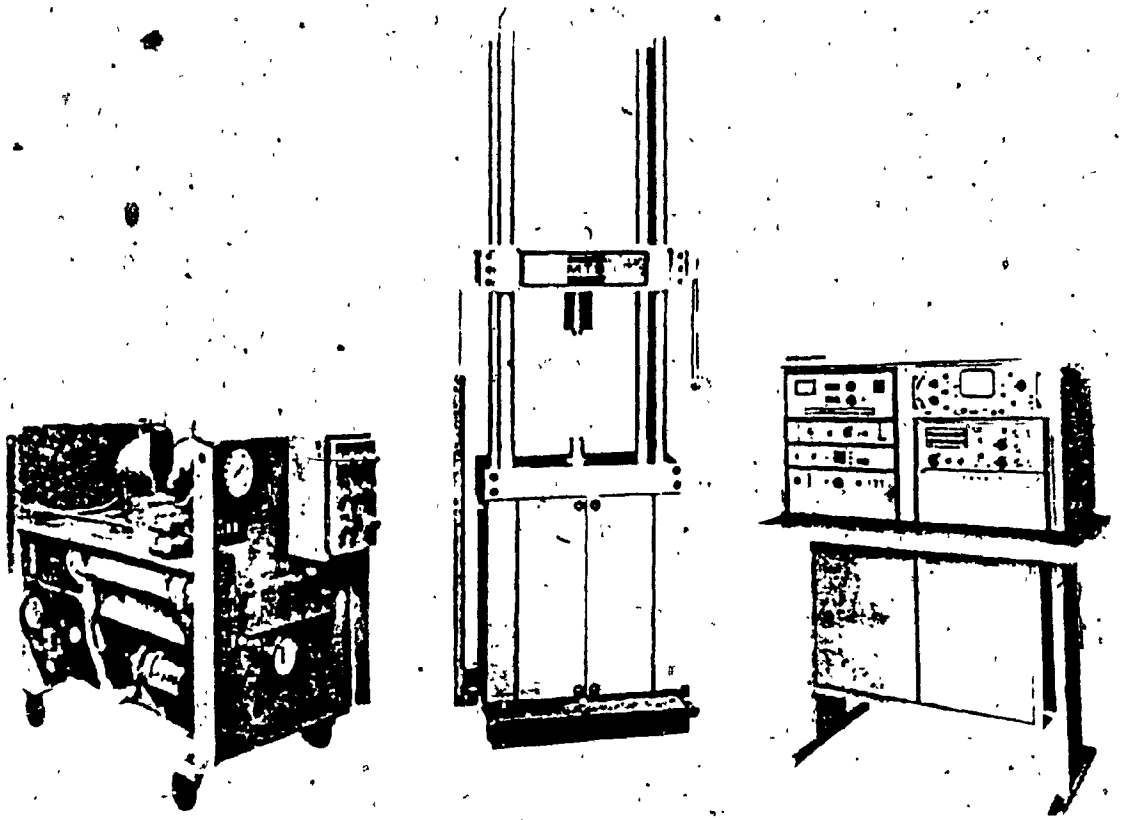

Fig 3.17: MTS Equipment used for the determination of Stiffness of the Bushing

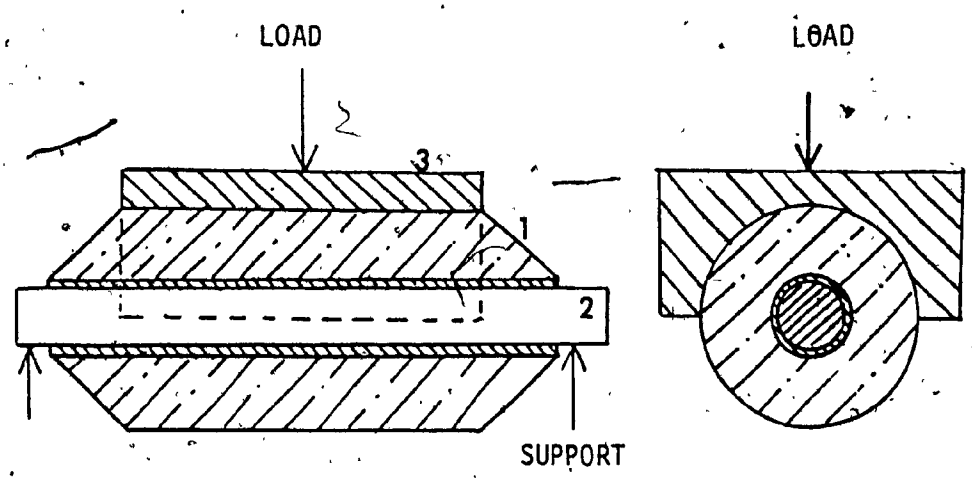

Item No.	Description
1	Elastomer Bush
2	Shaft
3	Circular Block to distribute the load

Fig 3.18: Set up prepared for the Evaluation of the Stffness of the Bushing

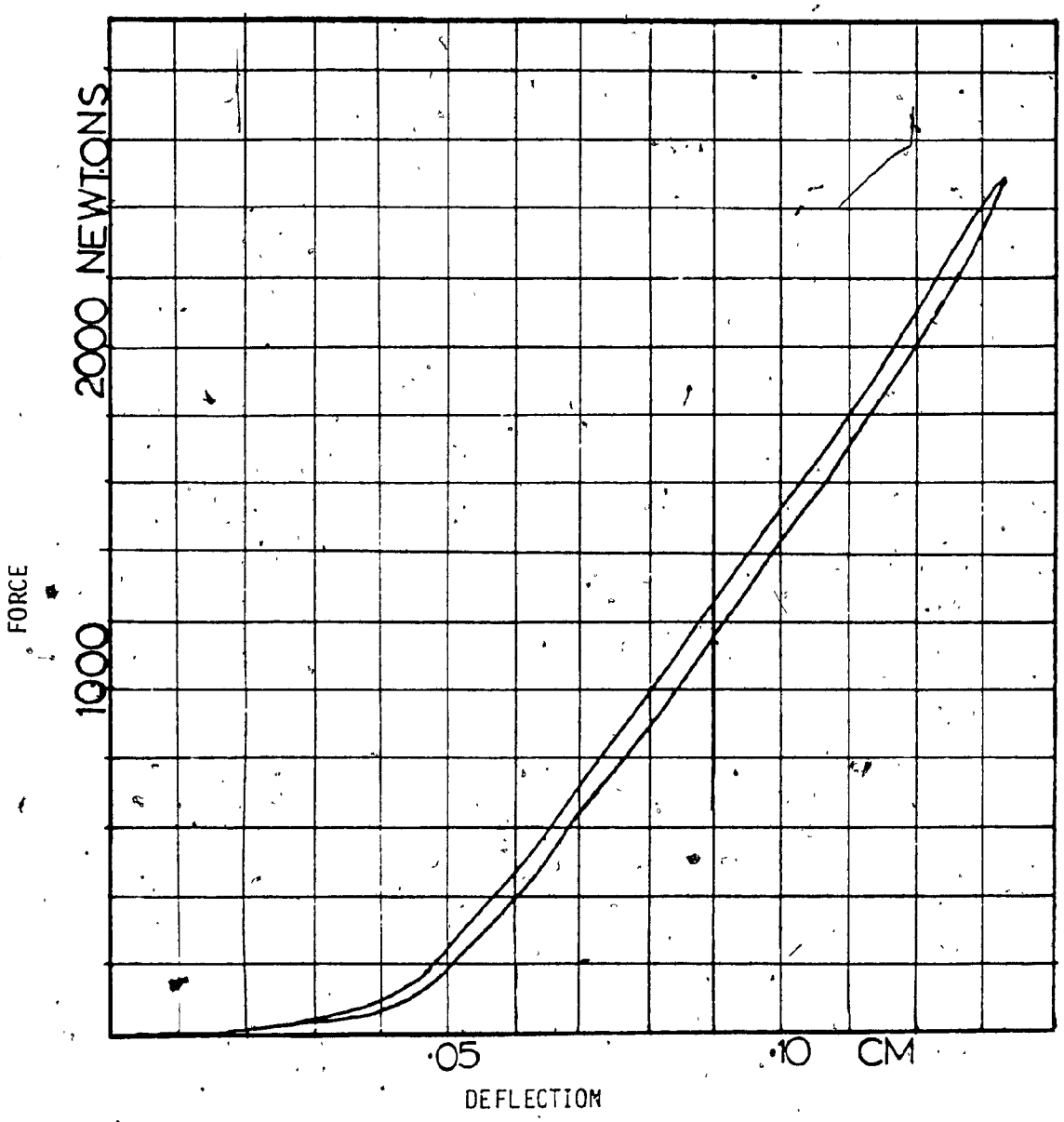

Fig 3.19: Load Deflection Charecteristics of the Bushing

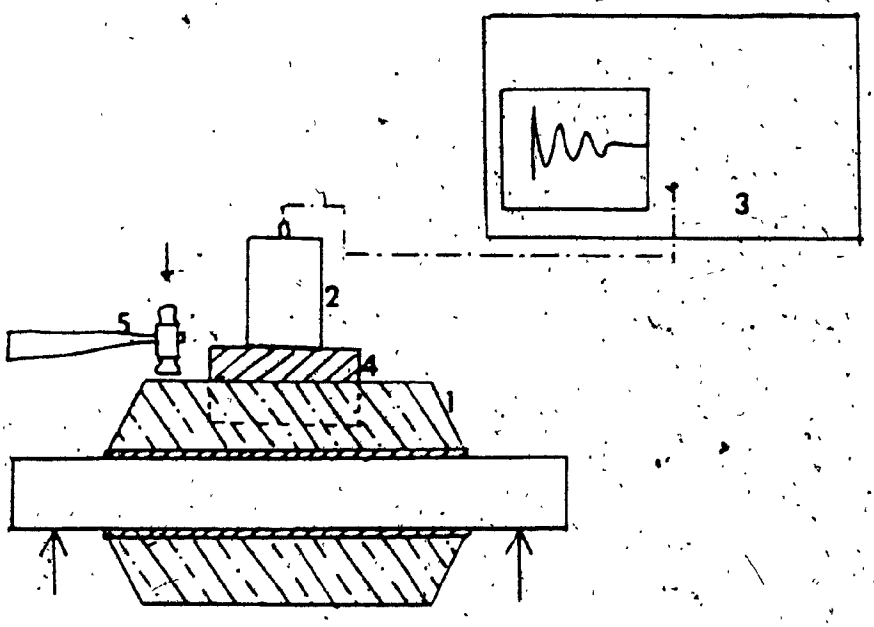

Item No.	Description
1	Elastomer Bush
2	Accelerometer
3	Oscilloscope
4	Circular Block glued to the Bush
5	Hammer

Fig 3.20: Test Set-Up prepared for measurement of Damping Coeffficient of the Bushing

Once the set up is ready, an impact is given on the bush and the oscillatory, decaying response is captured on the screen of the oscilloscope. Figure 3.21 shows the photograph of such a signal.

The damping ratio "ζ" of the bush is given by:

$$\ln(x_1/x_3) = \frac{2\pi\zeta}{\sqrt{1-\zeta^2}}$$

where x_1 and x_3 are the two successive amplitudes of the signal. From the experiment, the damping coefficient is calculated to be 61.25N sec/m.

3.4.5 Stiffness and Damping Coeficient of the Rear Mount

M/S Barry Controls supplier of the rear mount has furnished the load-deflection curve in tension/compression. Figure 3.5 furnishes the relevant data on the mount. However, the damping coefficient of the mount is calculated by assuming the damping factor "ζ" to be 4%. To calculate the stiffness and damping coefficient along the lateral directions, the shear stiffness of the mount is assumed to be one sixth of the compressive stiffness; the assumption is made based on the load-deflection curves furnished by the manufacturer for similar isolators. The complete information with regards to the stiffness and damping coefficients are tabulated in Table 3.4.

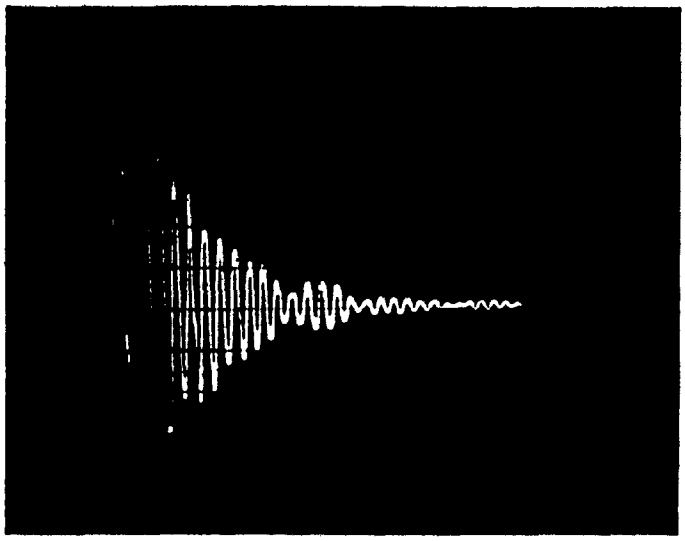

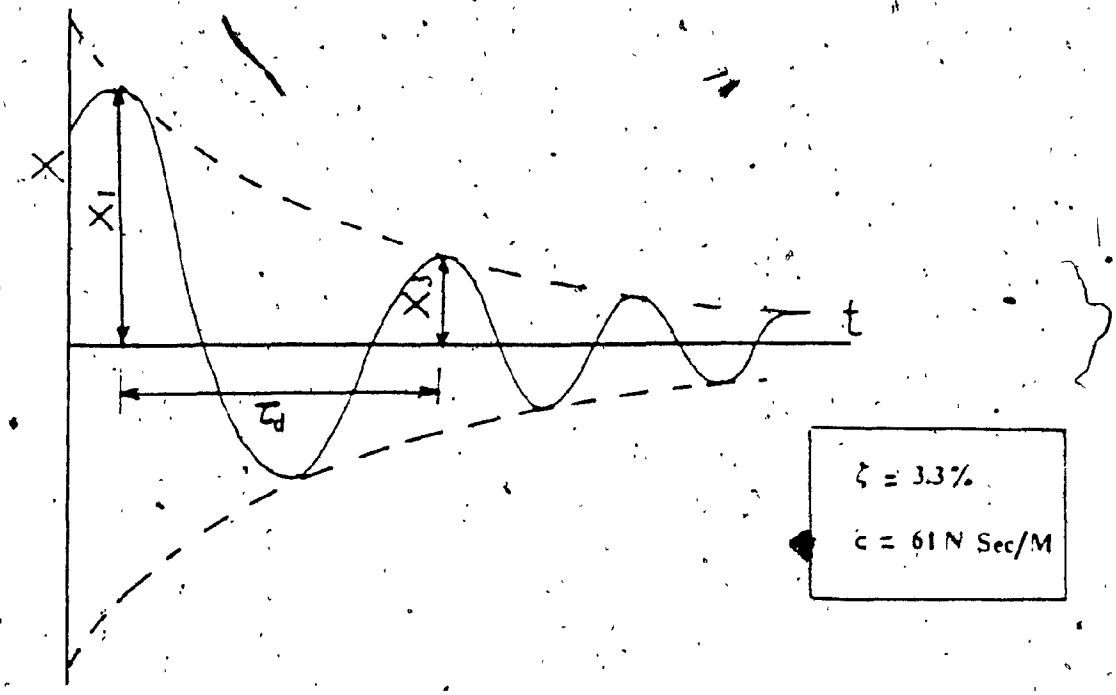

Fig 3.21: Damped Oscillations of the Front Bushing

Table 3.4 Stiffness and Damping Coefficients of the Isolator/Mount

a Front Bushing	
-Stiffness along 'Y' and 'Z' axes ($k_{y1}=K_{z1}=k_{z2}$)-Experimental	$26.6X10^5$ N/m
-Damping coefficient along 'Y' and 'Z' axes ($c_{y1}=c_{z1}=c_{y2}=c_{z2}$)-Experimental	61.25 $\frac{N\text{-}Sec}{m}$
b Rear Mount	
-Stiffness in Tension/compression obtained from the load-deflection curve provided by M/S Barry Controls-k_{y3}	$10.14x10^5$ $\frac{N}{m}$
-Stiffness of the rear mount in Shear ($k_{z3}=k_{x3}$)-Assumption	$1.69x10^5$ N/m
-Damping coefficient of the rear mount along the Y-axis (c_{y3})	76.8 $\frac{N\text{-}Sec}{m}$
-Damping coefficient of the rear mount along 'X' and 'Z' axes ($c_{x3}=c_{z3}$)	31.32 $\frac{N\text{-}Sec}{m}$

3.5 Summary

A description of the tracked vehicle "BR-400" and its cab suspension in particular are presented in this chapter. Further, the extraction of the physical parameters of the cab; namely, the mass, moment of inertias, the centroidal loction and finally the stiffness and damping coefficient of the mounts are discussed. The data evaluated for this candidate vehicle are utilized in the subsequent chapter for evaluating the natural frequencies and mode shapes.

CHAPTER IV

FREE VIBRATION ANALYSIS OF THE CAB

CHAPTER IV

Free Vibration Analysis of the Cab

4.1 Introducion

The first step towards improving the ride comfort is to carry out the free-vibration analysis, so as to determine the natural frequencies of the system in particular. Therefore, the present chapter deals with the calculation of natural frequencies and the corresponding modeshapes of the tilt-cab suspension of "BR-400" through analytical means.

The differential equations of motion formulated under section 2.3.1 is solved by making use of the parameters of the candidate off-road tracked vehcile. First, the damping is ignored in the isolators and the natural frequencies of the undamped system are determined. Subsequently, the natural frequencies and mode shapes of the damped system are determined. In order to verify the results determined through the lumped mass analysis, modal analysis of the cab via finite element modeling is carried out. Methods followed and the results obtained in both these analyses and their correlation of results are discussed in the following sections of this chapter.

4.2 Natural Frequencies and Mode Shapes of the Cab Via Lumped Mass Model

The parameters extracted and tabulated in Tables 3.3 and 3.4 are substituted in the equations of motion (2.9) formulated in chapter II. Initially, the natural frequencies and mode shapes of the model were determined assuming that there is no damping present in the isolators.

For this purpose, a subroutine "EIGZF" available in the IMSL library was used. Representing the standard matrix equations for eigenvalue problem form,

$$[A]=\lambda[B] \quad \ldots\ldots\ldots\ldots\ldots\ldots\ldots\ldots\ldots\ldots\ldots\ldots (4.1)$$

where, [A] and [B] represent the stiffness and mass matrices of the system and 'λ' represents the square of the natural frequency or just the eigenvalue.

Table 4.1 gives the undamped natural frequencies and the corresponding eigen vectors of the Cab model.

If damping is considered in the isolators, the eigenvalue problem is solved by introducing a set of auxiliary variables and converting the set of n second order ordinary differential equations into 2n first order ordinary differential equations [19]. The auxiliary set of variables are the momenta, represented by $[M]\{\dot{\alpha}\}$, where, [M] is the mass matrix and $\{\dot{\alpha}\}$ is the vector of velocity; thus resulting in a pair of differential equations:

$$-[M]\{\ddot{\alpha}\}-[M]\{\dot{\alpha}\}=0 \quad \ldots\ldots\ldots\ldots\ldots\ldots\ldots\ldots\ldots\ldots (4.2)$$

$$[M]\{\alpha\}+[C]\{\dot{\alpha}\}+[K]\{\alpha\}=0 \quad \ldots\ldots\ldots\ldots\ldots\ldots\ldots\ldots\ldots\ldots (4.3)$$

$$\text{if } \begin{Bmatrix}\dot{\alpha}\\ \alpha\end{Bmatrix} = \{\xi\} \quad \ldots\ldots\ldots\ldots\ldots\ldots\ldots\ldots\ldots\ldots (4.4)$$

$$\text{and } \begin{Bmatrix}\ddot{\alpha}\\ \dot{\alpha}\end{Bmatrix} = \dot{\xi} \quad \ldots\ldots\ldots\ldots\ldots\ldots\ldots\ldots\ldots\ldots (4.5)$$

Then the equations of motion can be put in the form:

$$[\mu]\{\dot{\xi}\}+[\nu]\{\xi\}=0 \quad \ldots\ldots\ldots\ldots\ldots\ldots\ldots\ldots\ldots\ldots (4.6)$$

Table 4.1 Natural Frequencies and Eigen Vectors Via the Lumped-Mass Model

Natural Frequency in Hz		2.5	8.32	8.42	9.38	15.02	26.62
Eigen -Vectors	"y"	0.00	.982	0.0	0.00	-.306	-0.386
	"ϕ"	0.00	1.00	0.0	0.00	-.042	1.00
	"θ"	.35	0.0	1.00	0.117	0.0	0.00
	"z"	0.00	0.32	0.00	0.00	1.00	-0.101
	"x"	1.00	0.0	-0.015	-0.065	0.0	0.00
	"Ψ"	.1074	0.0	0.136	1.00	0.0	0.00

where $$[\mu] = \begin{bmatrix} [0] & [M] \\ [M] & [C] \end{bmatrix} \quad \ldots\ldots\ldots\ldots\ldots\ldots (4.7)$$

and $$[\nu] = \begin{bmatrix} -[M] & [0] \\ [0] & [K] \end{bmatrix} \quad \ldots\ldots\ldots\ldots\ldots\ldots (4.8)$$

if $$\{\xi\} = \{\gamma\} e^{\lambda t} \quad \ldots\ldots\ldots\ldots\ldots\ldots (4.9)$$

The the equation (4.6) can be represented as

$$[\nu + \lambda\mu]\{\gamma\} = \{0\} \quad \ldots\ldots\ldots\ldots\ldots\ldots (4.10)$$

From the above equation, "λ" the complex eigenvalue is calculated by using the IMSL library routine. Table 4.2 shows the complex-conjugate pairs of the eigenvalues and the complex eigenvectors of the damped system.

4.3 Natural Frequencies and Mode Shapes of the Cab Via Finite-Element Model

In chapter III, a finite element model was presented for the extraction of various parameters, such as mass, centroid and moment of inertias. Even though the model was developed for the purpose of evaluation these parameters, it would be an added advantage if the same could be utilised for the determination of eigenvalues and mode shapes as well. By comparing the results of F.E analysis with those obtained from the lumped mass model, it helps to further validate the equations of motion formulated.

Table 4.2 Damped Eigenvalues and Complex Eigenvectors via Lumped Mass Model

Eigen Values	-.0033 +2.5i	-.026+ 8.32i	-.0052+ 8.42i	-.0104+ 9.37i	-.0202+ 15.02i	-.053 +26.62i
Eigen Vectors "y"	0+0i	0.982+0.0i	0+0i	0+0i	-0.306+0.0i	-0.38+0.0i
"ϕ"	0+0i	1.00+0.0i	0+0i	0+0i	-0.041+0.0i	1.00+0.0i
"θ"	.035+0i	0+0i	1.00+0i	0.117+00i	00+0i	0+0i
"z"	0+0i	0.32+0i	0+0i	0+0i	1.00+0.0i	-.10i+0.0i
"x"	1.0+0i	0+0i	-.015+0i	-0.065-.001i	0+0i	0+0i
"ψ"	.10+0i	0+0i	-.136-.001i	1.0+0i	0+0i	0+0i

For obtaining the natural frequencies and mode shapes, the Modal Analysis is carried out in the solution phase of the ANSYS program by evoking KAN=2 subroutine. Subsequent mode extraction is done by using the command KAY, 2, KEY, where KEY specifies the number of mode shapes to be extracted. Normally it is not more than one half of the eigenvalues evaluated. Since the number of degrees of freedom in a 110 node cab model could be about 660, it is not economial to conduct a modal analysis with so many degrees of freedom. Therefore, one of the features of the ANAYS program; namely, the dynamic matrix condensation is utilized by specifying the Master degrees of freedom. The purpose of specifying such a subset is to reduce the complexity of the analysis by including those degrees of freedom which are sufficient to characterize the behaviour of the structure. Commands are so chosen in the program such that only 10 master degrees of freedom are selected automatically by the program. Figure 4.1 shows the Model Analysis solution flow chart followed in the ANSYS.

Table 4.3 gives the results of the eigenvalues obtained from the ANAYS program. Figures 4.2, 4.3, 4.4, 4.5, 4.6 and 4.7 show the mode shapes corresponding to the first six lowest natural frequencies. These modes are plotted using the post processor which follows subsequent to the solution phase of the program.

4.4 Comparison of Free Vibration results between Finite Element and Lumped Mass Analyses

With the equations of motion being coupled, the resulting mode shapes are also coupled. Therefore, the dominant degree of freedom in each mode is considered while comparing the results between the two

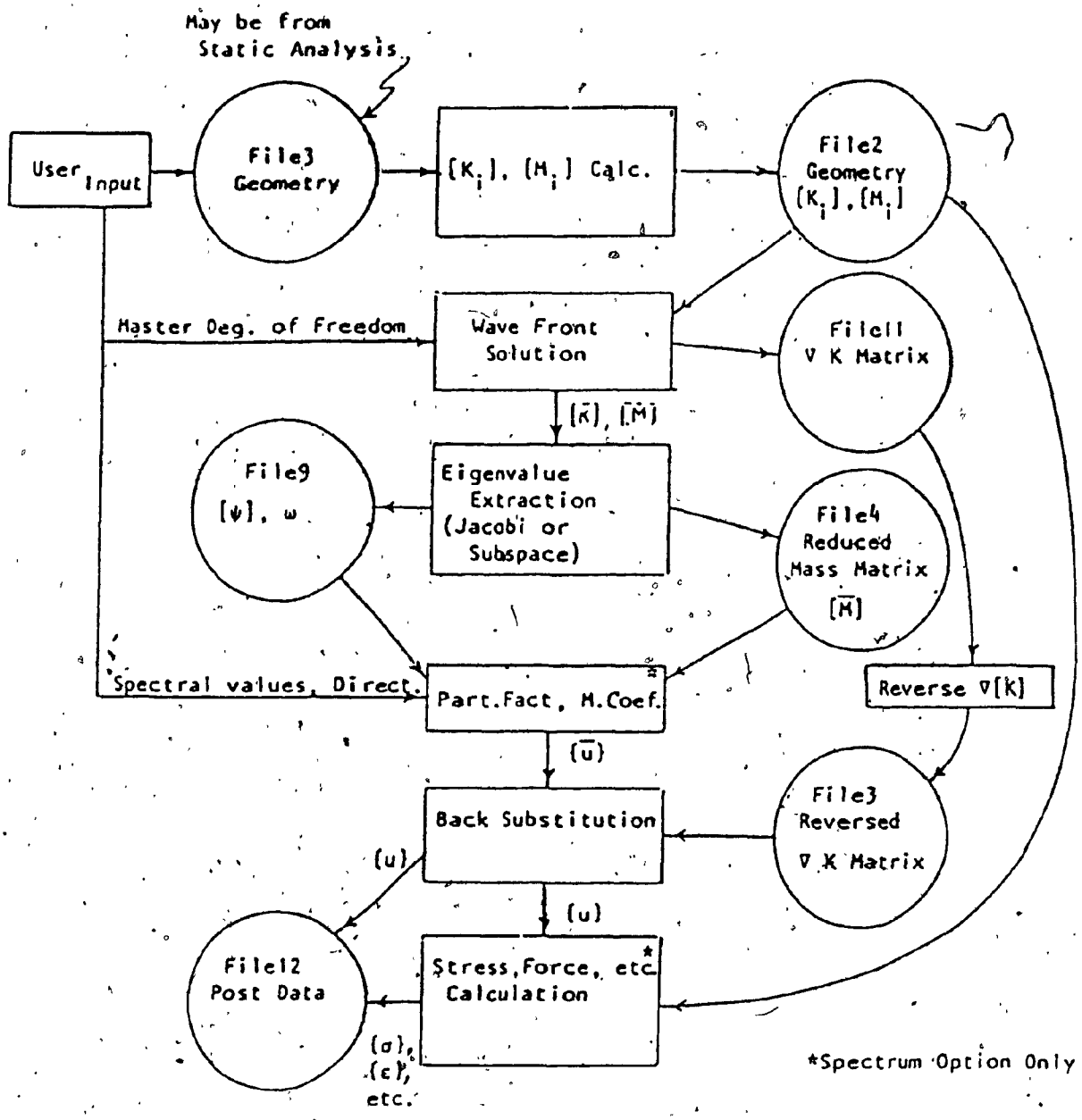

Fig. 4.1: Modal (KAN=2) Analysis Solution Flow Chart (18)

Table 4.3 Natural Frequencies of the F.E Model

No. of Natural Frequency	Natural Frequency, Hz	Dominant Mode
1	2.5	Lateral
2	7.00	Pitch and Bounce
3	7.60	Roll
4	9.30	Yaw
5	12.20	Longitudinal
6	20.17	Pitch and Longitudinal

Table 4.4 Comparison of Natural Frequencies between Lumped Mass and F.E. Analyses

Lumped Mass Results		F.E Results	
Natural Frequency, Hz	Dominant Mode	Natural Frequency, Hz	Dominant Mode
2.50	Lateral	2.50	Lateral
8.32	Pitch and Bounce	7.00	Pitch and Bounce
8.42	Roll	7.60	Roll
9.38	Yaw	9.30	Yaw
15.02	Longitudinal	12.20	Longitudinal
26.62	Pitch and Longitudinal	20.0	Pitch and Longitudinal

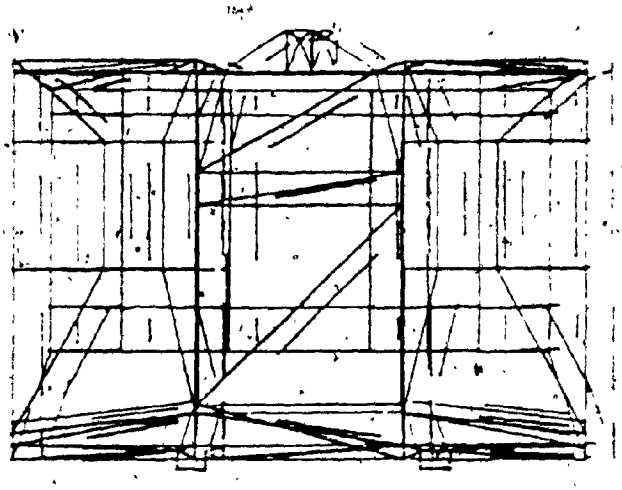

Fig. 4.2: First Mode Shape of the Cab (at 2.5Hz).
-Top View.

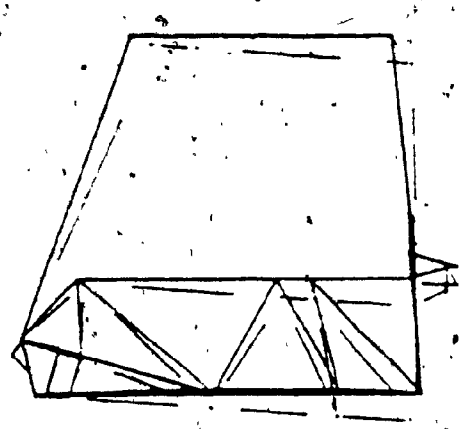

Fig. 4.3: Second Mode Shape of the Cab (at 7Hz)
- Side View.

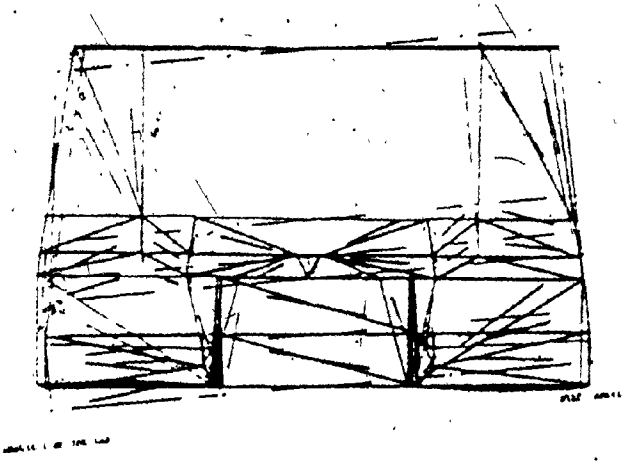

Fig. 4.4: Third Mode Shape of the Cab (at 7.6Hz).
-Front View.

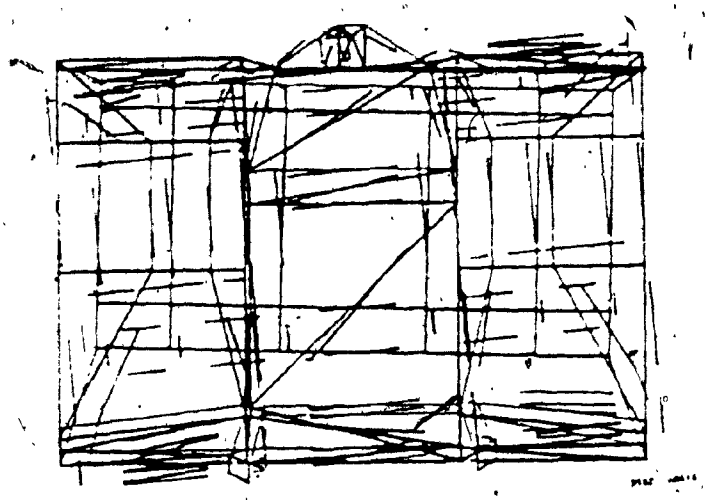

Fig. 4.5: Fourth Mode Shape of the Cab (at 9.3Hz).
-Top View.

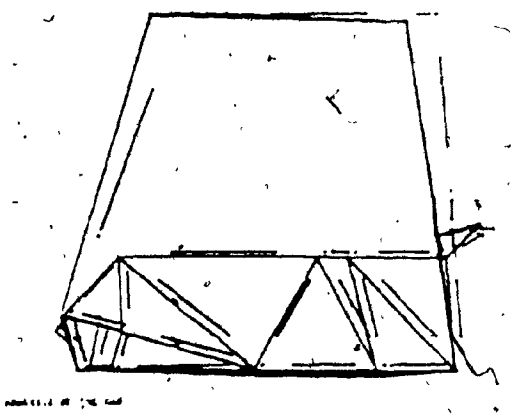

Fig. 4.6: Fifth Mode Shape of the Cab (at 12Hz).
-Side View.

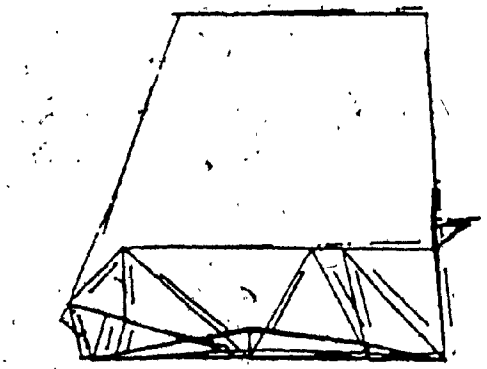

Fig. 4.7: Sixth Mode Shape of the Cab (at 20Hz).
-Side View.

methods. First considering the fundamental frequency of 2.5Hz in the lumped mass analysis, the following eigenvector show a dominant lateral motion.

$$(\Phi_1) = \begin{Bmatrix} 0.00 \\ 0.00 \\ 0.034 \\ 0.00 \\ 1.00 \\ 0.1074 \end{Bmatrix} \begin{matrix} \text{-Bounce} \\ \text{-Pitch} \\ \text{-Roll} \\ \text{-Longitudinal} \\ \text{-Lateral} \\ \text{-Yaw} \end{matrix}$$

The fundamental mode shape extracted through the ANSYS F.E. analysis show a dominant lateral motion at 2.5 Hz. Figure 4.2 show the top view of the cab having a large lateral mode shape.

The second lowest frequency is 8.32 Hz and the corresponding eigen vector shown below represent a dominant pitch motion, although the motion due to bounce also is quite considerable.

$$(\Phi_2) = \begin{Bmatrix} 0.98 \\ 1.00 \\ 0.00 \\ 0.32 \\ 0.00 \\ 0.00 \end{Bmatrix} \begin{matrix} \text{-Bounce} \\ \text{-Pitch} \\ \text{-Roll} \\ \text{-Longitudinal} \\ \text{-Lateral} \\ \text{-Yaw} \end{matrix}$$

The second lowest vibrational mode extracted using the F.E model is 7 Hz with a dominant pitch motion. For the purpose of illustration the side view of the cab with mode shape plotted is shown in Figure 4.3.

Similarly, the next lowest natural frequency found in the lumped mass model is compared with that of the F.E result and a close correlation is observed. The lumped mass model has a natural frequency of 8.42 Hz with the corresponding eigen vector as given below:

$$(\Phi_3) = \begin{Bmatrix} 0.00 \\ 0.00 \\ 1.00 \\ 0.00 \\ -0.015 \\ -0.14 \end{Bmatrix} \begin{matrix} \text{-Bounce} \\ \text{-Pitch} \\ \text{-Roll} \\ \text{-Longitudinal} \\ \text{-Lateral} \\ \text{-Yaw} \end{matrix}$$

The results show a dominance in roll mode. Whereas in the F.E analysis, the third natural frequency is found to be 7.6 Hz and shows the same modal pattern, i.e., dominance in roll displacement and is shown in Figure 4.4.

The forth natural frquency is 9.38 Hz in the lumped mass model and 9.30 Hz in the F.E model. Model displacements also show dominant Yaw mode in both cases. Figure 4.5 shows the mode shape of the F.E model corresponding to this natural frequency. The eigen vetor obtained in the lumped mass model is given below:

$$(\Phi)_4 = \begin{Bmatrix} 00.0 \\ 0.00 \\ 0.12 \\ 0.00 \\ -0.07 \\ 1.000 \end{Bmatrix} \begin{matrix} \text{-Bounce} \\ \text{-Pitch} \\ \text{-Roll} \\ \text{-Longitudinal} \\ \text{-Lateral} \\ \text{-Yaw} \end{matrix}$$

Analyzing the fifth mode, we arrive at similar correlation; namely, a dominant longitudinal displacement in both cases. Figure 4.6 shows the F.E. modal displacement.

The sixth mode also show correlation of both lumped mass and F.E analyses. Both of them show dominance in pitch with considerable longitudinal motion. Figure 4.7 shows the F.E modal displacement.

Table 4.4 displays a comparison of natural frequencies obtained through both the analyses.

Summing up, it is concluded that there is a close correlation between the natural frequencies and the mode shapes arrived in both the F.E and lumped mass analyses. Hence, the lumped mass model can be assumed to represent with fair degree of accuracy, the physical system and thus can be used for futher forced vibration analysis and parametric study.

4.5 Summary

This chapter presents the free vibration analysis of the cab model developed through the F.E as well as the lumped mass analysis. The results of the undamped natural frequencies and the corresponding normal modes are compared to find a close correlation between the two techniques, thus verifying the equations of motion formulated.

CHAPTER V

FORCED VIBRATION ANALYSIS OF THE CAB

CHAPTER V

Forced Vibration Analysis of the Cab

5.1 Introduction

In the previous chapters, the mathematical modelling and free vibration analysis of a suspended vehicle cab were presented. Such a study becomes a fundamental requirement for further study and analysis of the cab subjected to various types of terrain-induced excitations. Response due to deterministic excitations such as sinusoidal inputs can be theoretically evaluated either in time or frequency domain if we know the generalised matrices characterizing the system behaviour.

However, off-road vehicles, particularly the tracked vehicle such as snow-pusher-cum-tiller are subjected to random excitations which continually vary with time. Due to the randomness of the input variables, statistical representation of input and response characteristics are quite common and forms the nucleus of analysing such random data.

In this chapter, a description on the field trials carried out to record the random terrain excitations and response accelerations of "BR-400" and subsequent processing of the recorded signal using the Fast Fourier Analyser are presented. In addition, analytical determination of the response spectra of the cab, based on the measured input spectra is also discussed. Finally, analytical and experimental results are compared.

5.2 Input and Response Acceleration Spectra of the Tilt-Cab of "BR-400" derived from the Field Tests.

Figure 5.1 illustrates the locations of accelerometers for the measurement of both the input and response accelerations of the Tilt-Cab of "BR-400" in the field trials. 1, 2, 3 and 4 denote the accelerometer locations for the input excitations to the cab, whereas 1', 2', 3', and 4' denote the locations of the accelerometers where the cab response was measured. Accelerometers 1, 2, and 3 measured the vertical accelerations and the accelerameter 4 measured the lateral input. Similarly, in the case of response of the cab 1'and 2' measured the vertical accelerations at the locations beneath the driver and passenger seats respectively, whereas 4' measured the vertical acceleration at a location just above the rear mount. 3' measured the lateral acceleration beneath the seat. The random data were recorded for different input excitations, such as, blade down or up, rough or smooth track.

The next step is to transform the recorded signal in the frequency domain. This is carried out using a "NICOLET" dual channel Fast Fourier Analyser, type 660B. The instrument can accept two analog signals and the results of the analysis are presented on the built-in CRT. The detailed specification of the instrument and the opeating instructions are given in the manual of M/S Nicolet Scientific Corporation.

Spectral density plots for varied terrain excitations are obtained through the FFT analyzer for both the input and response accelerations of the cab and are shown in Figures 5.2, 5.3, 5.4, 5.5, 5.6, and 5.7.

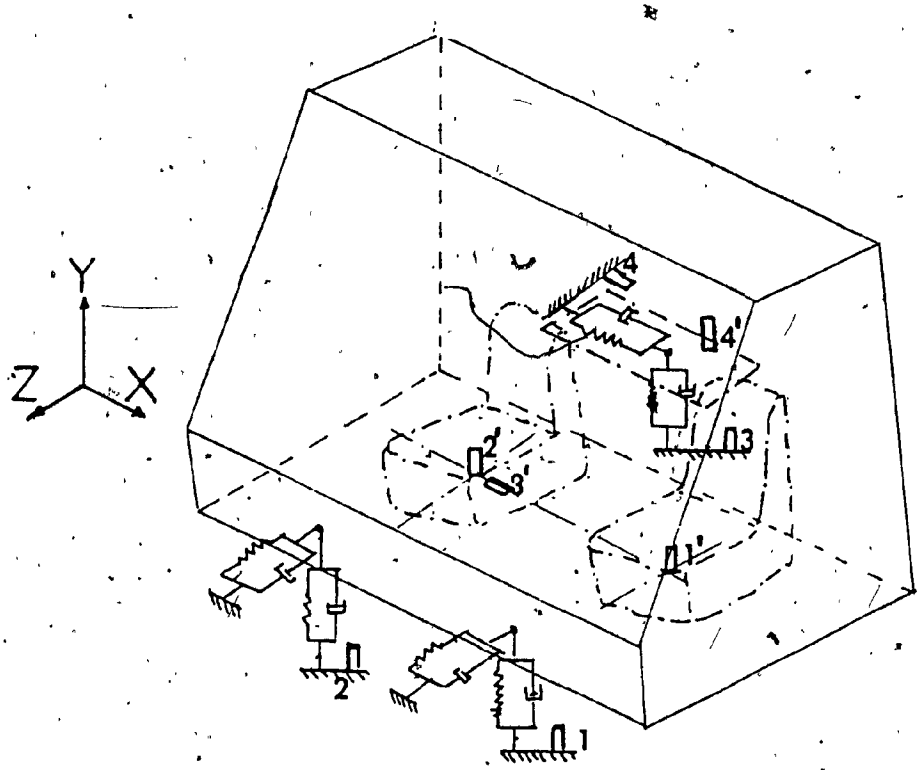

1,2,3 and 4 indicate the location of Input accelerometers

1',2',3' and 4' indicate the location of Response accelerometers

Fig 5.1: Location of Input and Response Accelerometers

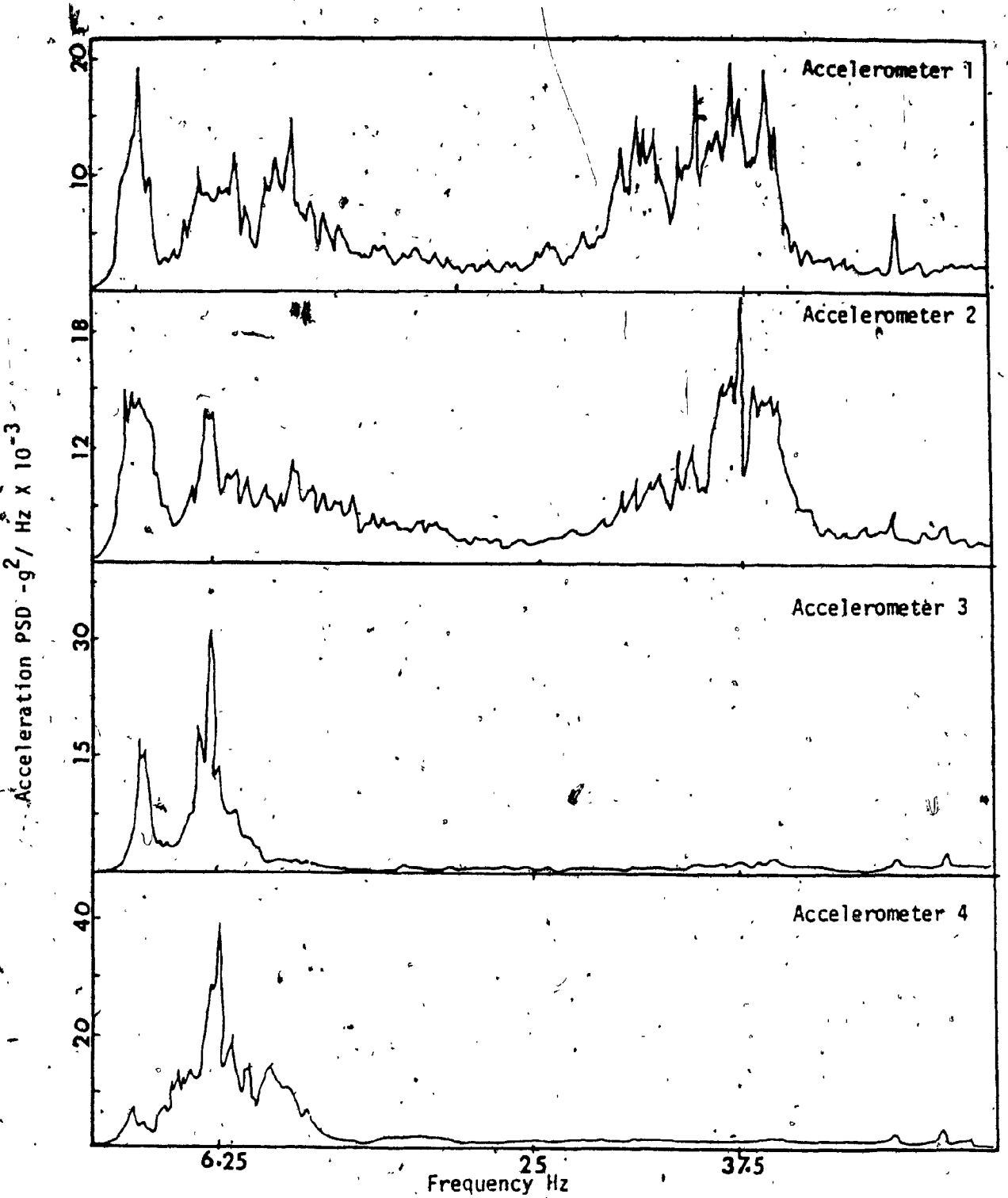

Fig 5.2: Input Acceleration PSDs (Rough Track, Blade Up)

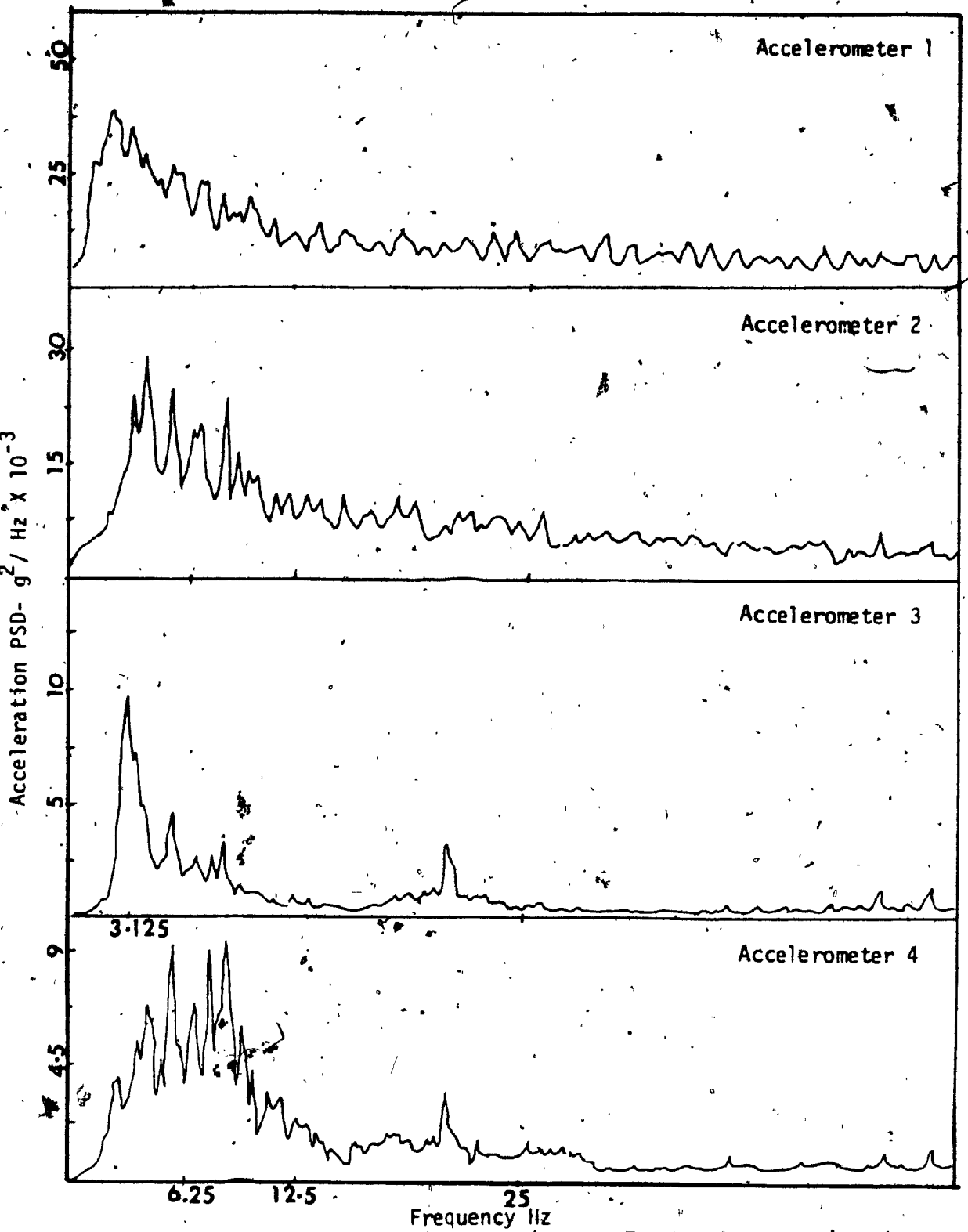

Fig.5.3: Input Acceleration PSDs (Rough Track, Blade Down)

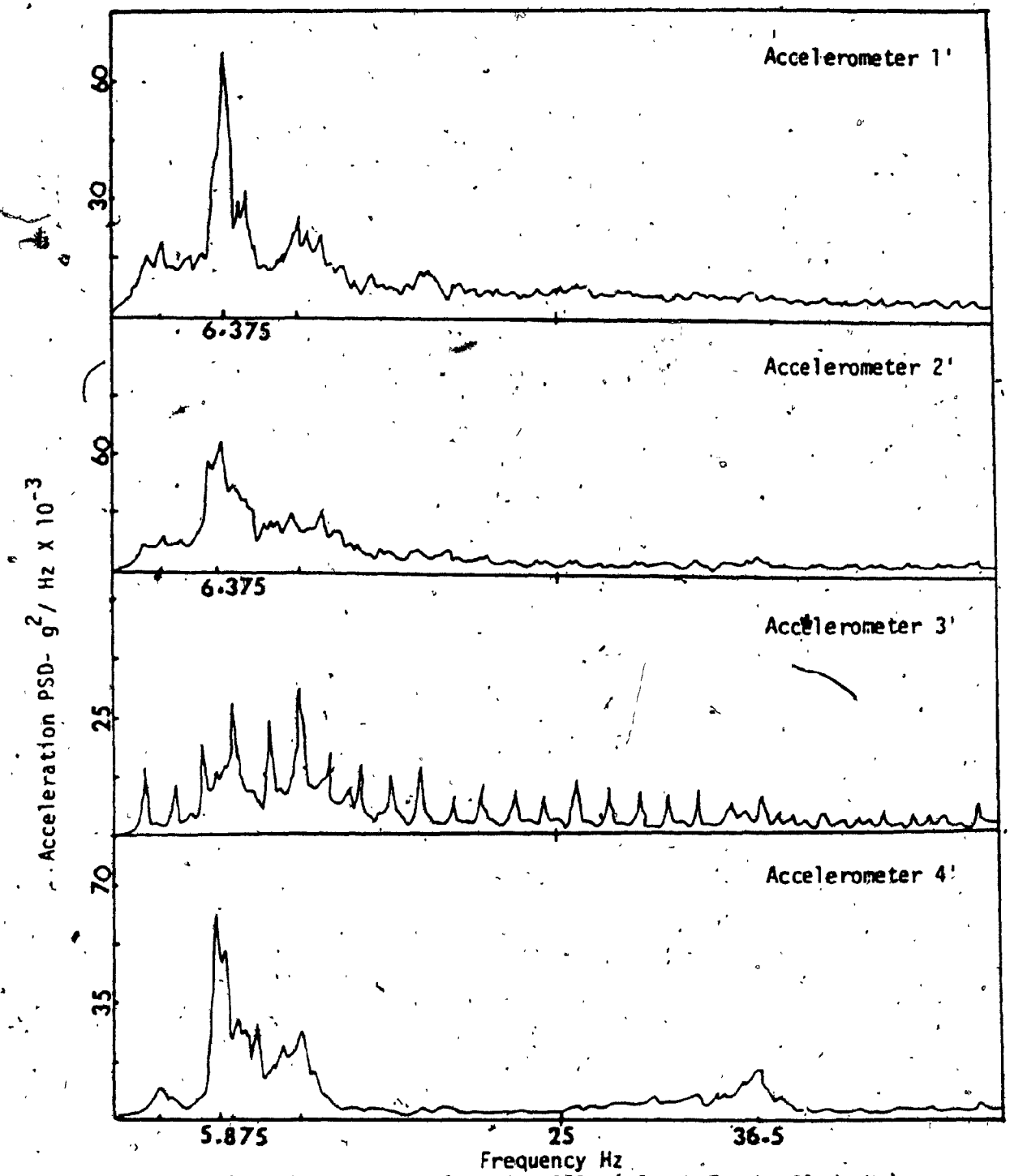

Fig 5.4: Response Acceleration PSDs (Rough Track, Blade Up)

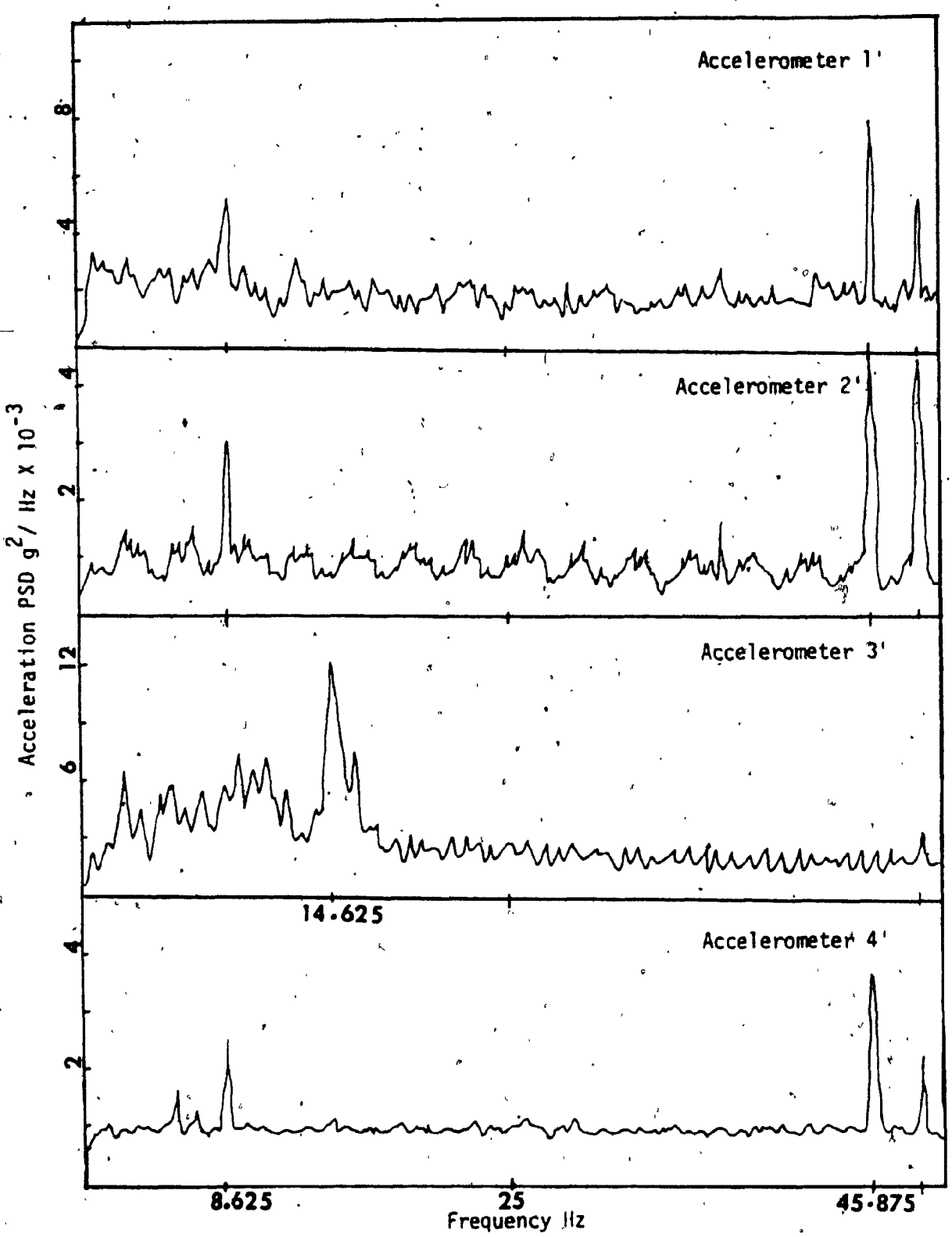

Fig 5.5: Response Acceleration PSDs(Rough Track, Blade Down, 1500 rpm Engine Speed)

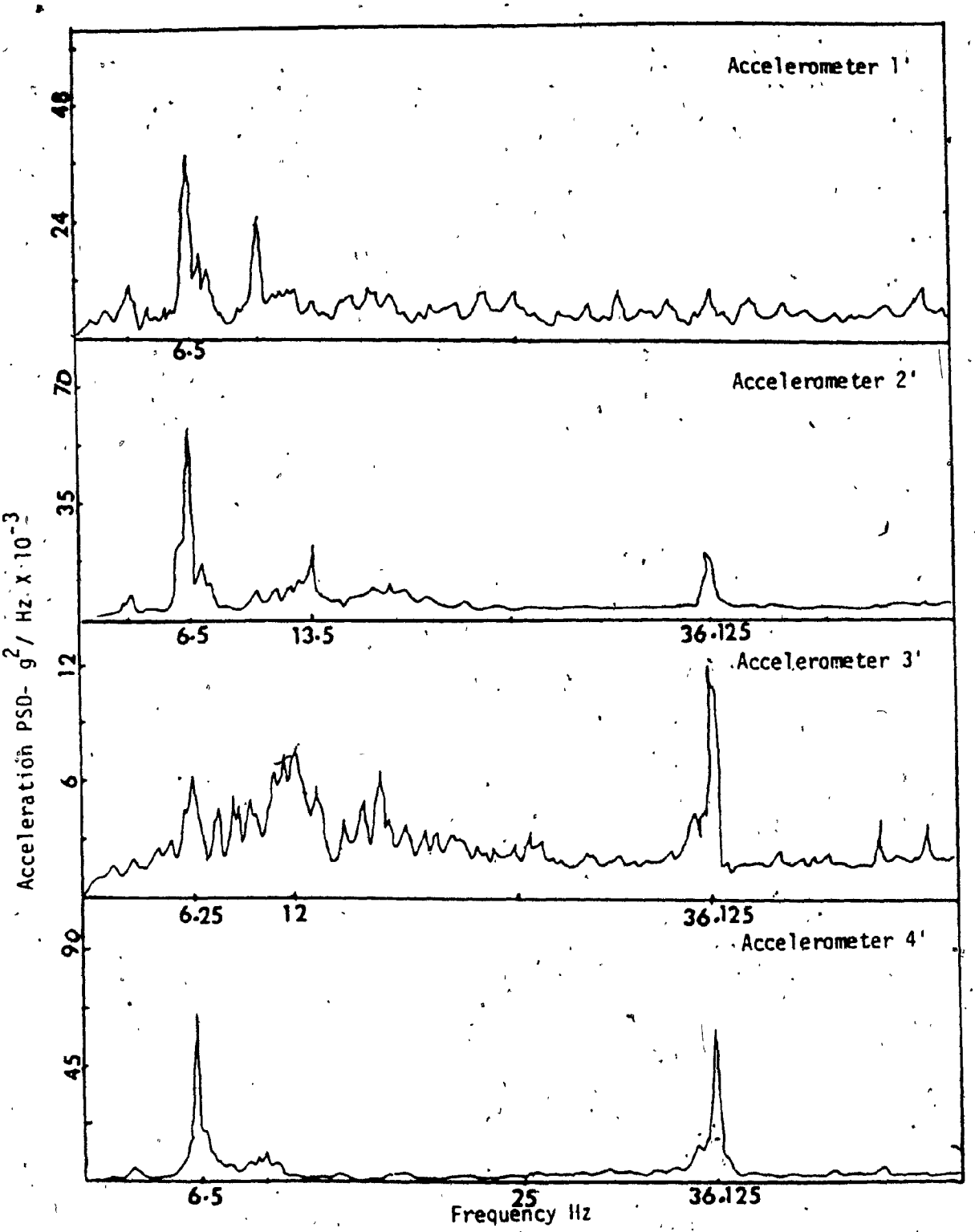

Fig 5.6 : Response Acceleration PSDs (Smooth Track, Blade Up)

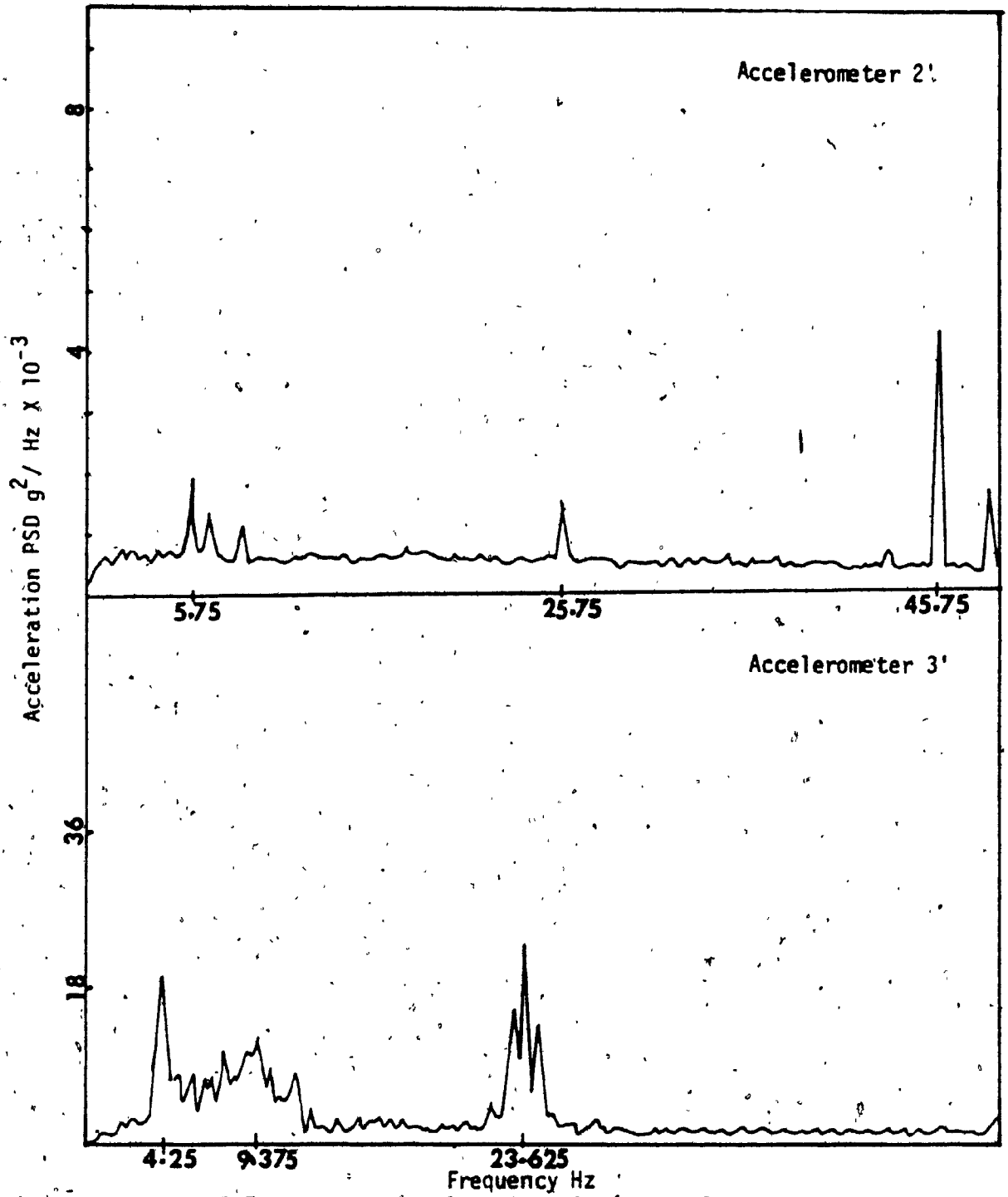

Fig 5.7: Response Acceleration PSDs(Rough Track, Blade Down 1700 rpm Engine Speed)

5.3 Computer Simulation for the Determination of Random Response

The random physical phenomenon being unique at every observation of the phenomena, it cannot be described by an explicit mathematical relationship. Therefore, they are represented by their statistical properties; viz, mean square value, probability density functions, power spectral density functions and auto and cross-correlation functions. Based on the nature of application, the random data are represented accordingly. For the purpose of representing the random response of the cab, power spectral density function is found to be the most convenient way of presentation, because it describes both the amplitude and frequency composition of the data.

For a linear differential equation such as equation 2.9, the data in the time domain can be converted to frequency domain by a fourier transformation of input and output variable and can be related thus [20]

$$(z(j\omega)) = [H(j\omega)](z_0(j\omega)) \quad \ldots\ldots\ldots\ldots\ldots\ldots\ldots\ldots \quad (5.7)$$

where,

$(z(j\omega))$ = Fourier transform of the vector containing the output variables.

$(z_0(j\omega))$ = Fourier transform of the vector containing the input variables.

$(H(j\omega))$ = Complex Matrix representing the frequency response function.

The equation 2.10 represent the equations of motion for a general case of Tilt-cab suspension subjected to terrain excitations. However, in the specific case of "BR-400", the recorded power spectral densities

along the z-direction are found to be far lower than the PSDs in the other modes. Hence, the matrices [C'] and [K'] representing the damping and stiffnesses of the forcing functions can be reduced in size, since the accelerations at the supports along the z-directions are ignored. In otherwords, $\ddot{z}_{o1}$, $\ddot{z}_{o2}$ and $\ddot{z}_{o3}$ are assumed to be absent while formulating the equations.

Based on this assumption, [C'] and [K'] matrices result thus:

$$[C'] = \begin{bmatrix} c_{y1} & c_{y2} & c_{y3} & 0 \\ -c_{y1}a & -c_{y2}a & +c_{y3}b & 0 \\ c_{y1}h & -c_{y2}h & 0 & c_{x3}(d-e) \\ 0 & 0 & 0 & 0 \\ 0 & 0 & 0 & c_{x3} \\ 0 & 0 & 0 & -c_{x3}b \end{bmatrix}$$

$$[K'] = \begin{bmatrix} k_{y1} & k_{y2} & k_{y3} & 0 \\ -k_{y1}a & -k_{y2}a & k_{y3}b & 0 \\ k_{y1}a & -k_{y2}h & 0 & k_{x3}(d-e) \\ 0 & 0 & 0 & 0 \\ 0 & 0 & 0 & k_{x3} \\ 0 & 0 & 0 & -k_{x3}b \end{bmatrix}$$

For the forced vibration analysis of the cab the matrix of complex frequency response function is given by:

$$[H(j\omega)] = \frac{([K']+j\omega[C'])}{([K]-\omega^2[M]+j\omega[C])} \quad \ldots\ldots\ldots\ldots\ldots\ldots\ldots (5.8)$$

Table 5.1 gives the complex frequency response function for the three point supported cab of "BR-400", at 8.5 Hz frequency.

In the frequency domain anlysis, which supplies the basic characteristics of the physical system involved; the output and input power spectral densites are related by:

$$S_y(\omega) = |H(\omega)|^2 S_x(\omega) \quad \ldots\ldots\ldots\ldots\ldots\ldots\ldots\ldots (5.9)$$

Table 5.1 Complex Frequency Response Function Matrix at 8.5 Hz Frequency

$$[H(j\omega)]_{@8.5\ Hz} = \begin{bmatrix} -.96-.14j & -.96-.14j & -11.95-1.4j & 0+0j \\ -1.5-.14j & -1.57-.14j & -12.14-1.42j & 0+0j \\ -52.2-3.3j & 52.2+3.3j & 0+0j & -2.3+.17j \\ -.5-.05j & -.5-.05j & -3.93-.45j & 0+0j \\ .7+.05j & -.7-.05j & 0+0j & -.02-.002j \\ 7.7+.5j & -7.7-.5j & 0+0j & -.27+.02j \end{bmatrix}$$

where,

$S_y(\omega)$= Output power spectral density.

$S_x(\omega)$= Input power spectral density.

$H(\omega)$= Frequency response function.

However, the above relationship holds good for a stationary random signal only [21].

If we represent the input and output spectral densities in the form of matrices, then they are related as follows [20].

$$(S_o(\omega)) = (H(j\omega))(S_i(\omega))(H(j\omega)^*)^T \quad \ldots\ldots\ldots\ldots\ldots\ldots (5.10)$$

where,

$(S_o(\omega))$= Spectral density matrix of the response variables.

$(S_i(\omega))$= Spectral density matrix of the input variables.

$(H(j\omega)^*)^T$= Transpose of the complex conjugate of $(H(j\omega))$

If we have to determine the spectral matrix at the location below the seat of the passenger or the driver, since this location is of prime factor for the purpose of ride quality of the cab; then the output matrix arrived in (5.10) has to be modified using a transformation matrix (T) as follows.

$$(S^r(\omega)) = (T)(S_o(\omega))(T)^T \quad \ldots\ldots\ldots\ldots\ldots\ldots\ldots\ldots (5.11)$$

where,

$(S^r(\omega))$= Spectral density matrix at a location on the cab floor just below the centre of the seat.

(T_i) = Transformation matrix.

For our specific case of "BR-400" the transformation matrix is given in Figure 5.8.

Procedure followed in the analytical determination of the response power spectral densities of the cab is furnished below:

-The input spectra representing the four input accelerations are discretized at equal intervals of 0.25 Hz.

-The data representing the power-spectral densities forms the diagnol elements of the matrix $S_i(\omega)$ (equation 5.10).

-Having generated the data, a computer program is developed to carry out the matrix manipulation upto 28 Hz, to determine the response spectral matrices as given in equations 5.10 and 5.11

-Power spectal densities of the response spectra arrived from the output matrix are printed out at an interval of 0.25 Hz.

5.4 Comparison of Response Spectra between the Field Measured Data and the Simulation Results

From the Figure 5.1 it can be seen that the accelerometers 1', 2', and 3' were located just beneath the driver and the passenger seats. Accelerometer 4' was located just above the rear mount. Accelerometers 2', and 4' measured the acceleration in the vertical direction. Therefore, in order to arrive at the theoretical response spectra at the locations 2' and 4'of the accelerometers the output spectral density matrix has to be manipulated as per the equation 5.11.

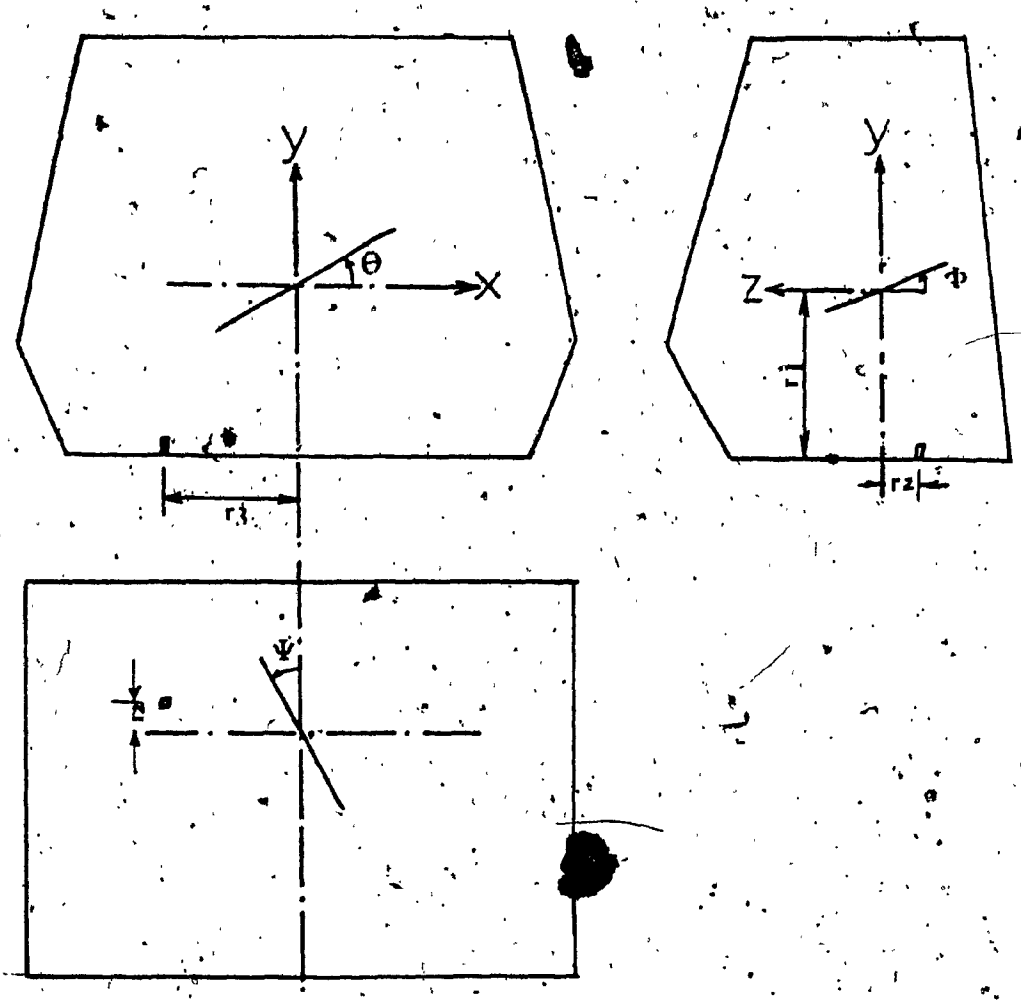

$$T = \begin{bmatrix} 1 & r_2 & -r_3 & 0 & 0 & 0 \\ 0 & 1 & 0 & 0 & 0 & 0 \\ 0 & 0 & 1 & 0 & 0 & 0 \\ 0 & -r_1 & 0 & 1 & 0 & r_3 \\ 0 & 0 & r_1 & 0 & 1 & -r_2 \\ 0 & 0 & 0 & 0 & 0 & 1 \end{bmatrix}$$

Fig 5.8: Transformation Matrix

The acceleration response spectrum thus obtained are superimposed over the acceleration response spectra measured in the field trials for similar rough-track, blade-up conditions. Figure 5.9 and 5.10 show the superimposed plots of PSDs and it is observed that the frequencies at which the peaks are observed for both the theoretical and field test results exibit correlation thus:

-For the bounce spectra shown the field trials show a peak at 6.38 Hz for accelerometer #2', where as the reponse due to analytical determination shows a peak at 8.50 Hz mainly due to the bounce and roll motions.

-Secondary peaks are observed at 10.25 Hz and at 2.75 Hz for the bounce accelerometers 1' and 2'. Secondary peak is observed in 6.375 Hz for the accelerometer 4' resulting due to the pitch mode; whereas secondary peaks are observed at 15 Hz and at 26.5 Hz in the analytical method, mainly due to the coupled longitudinal and pitch modes respectively.

However, the amplitudes of resonant peaks derived from the anaytical method is markedly higher than the actual experimental values. This may be due to anyone of the following reasons.

-In the actual case there may be constraints in the system resisting the motion, particulary the roll motion. But, such constraints being unknown they are not considered in the model.

-The cross-spectra which is ignored in the input spectral matrix may be high.

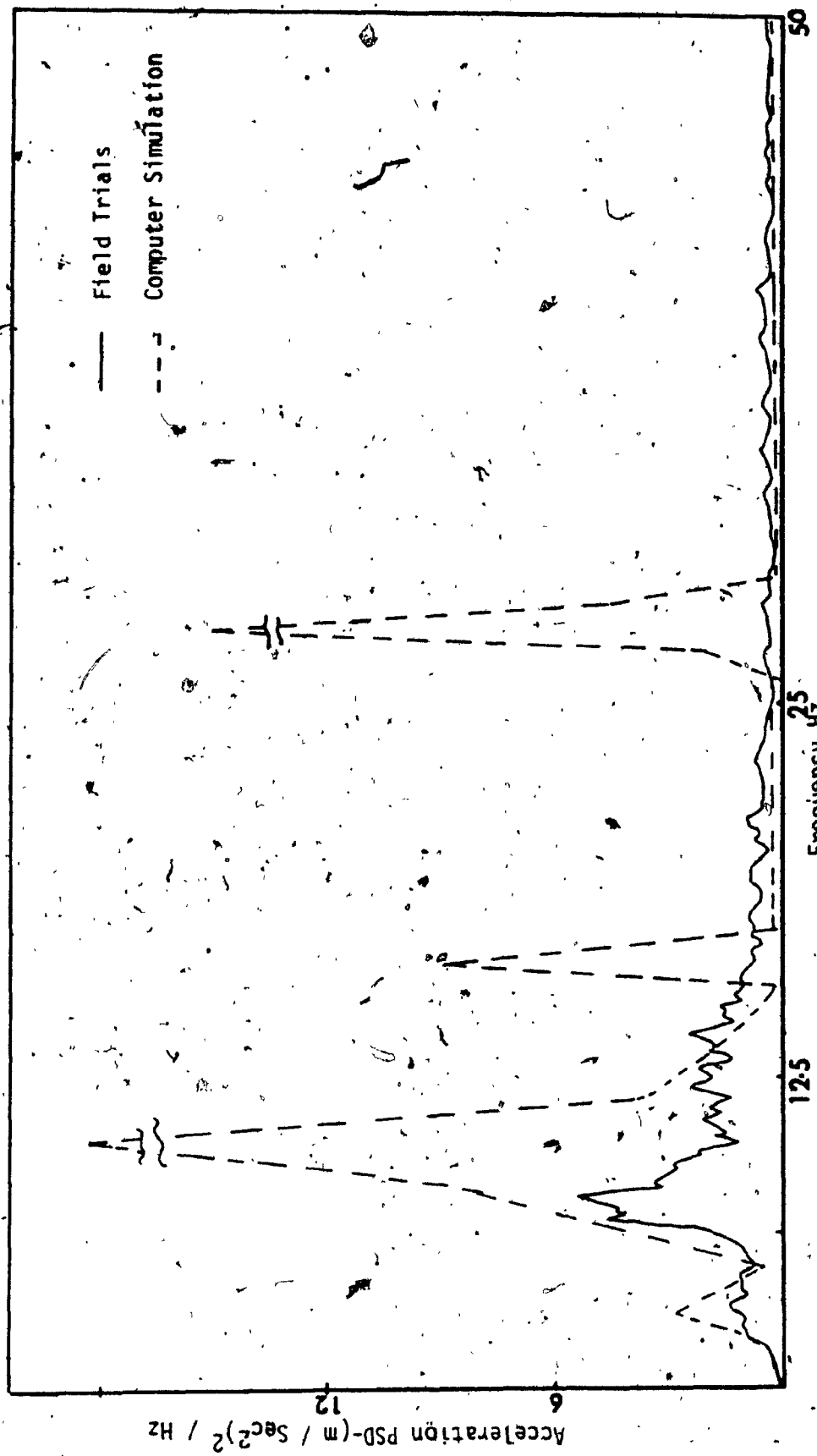

Fig 5.9: Comparative Plots of Response Acceleration PSDs at the Accelerometer 2'

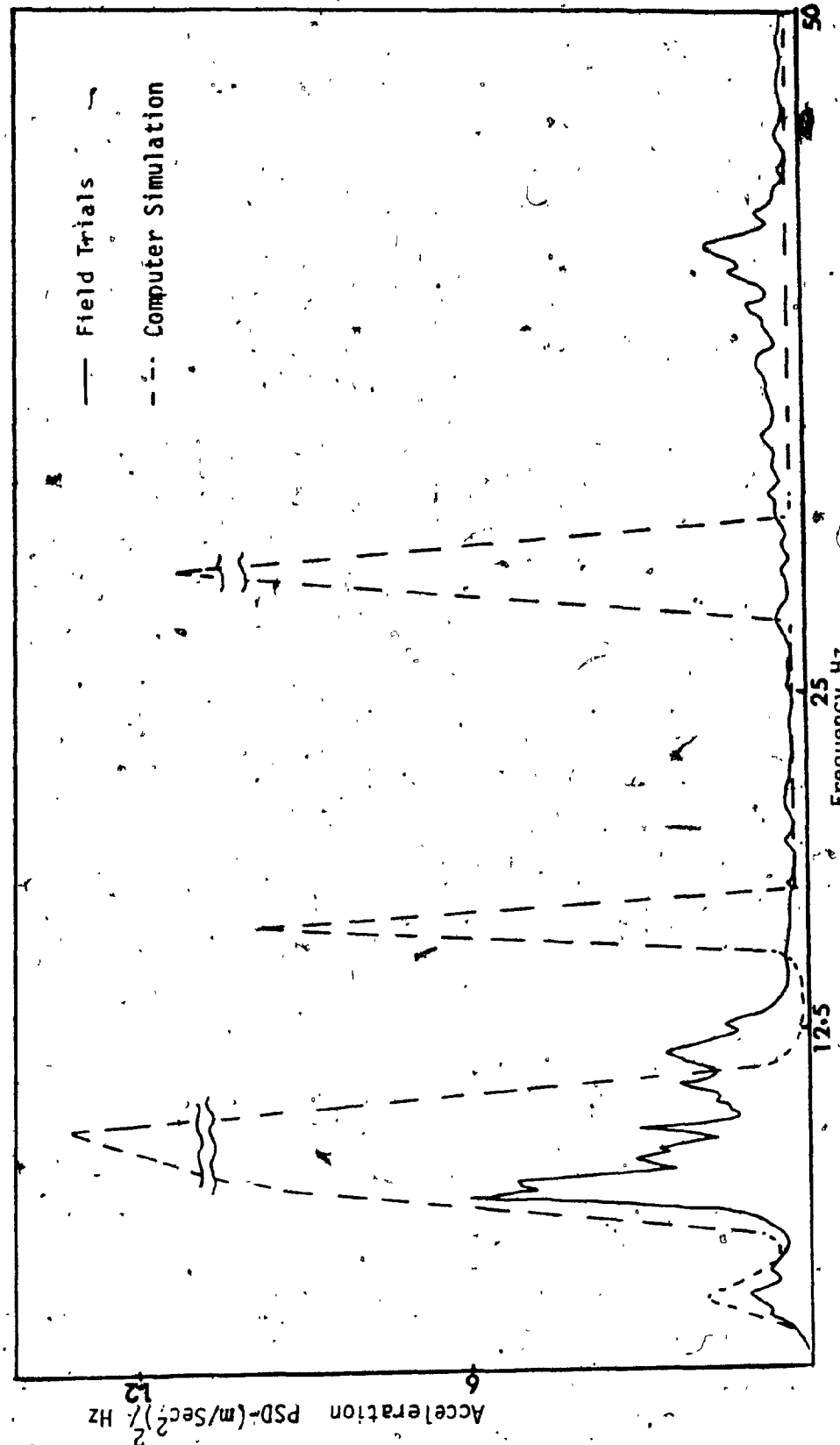

Fig 5.10: Comparative Plots of Response Acceleration PSDs at the Accelerometer 4'

-Each support in reality should have six input accelerations, three in translation and three in rotation; therefore, if all of them are considered it is likely that high resonant responses could be nullified.

5.5 Summary

Field measurements of input and response accelerations of the cab of the candidate tracked vehicle and the processing of the signal in a Fast Fourier Analyser are discussed in this chapter. Subsequently, the random response of the cab is analytically determined by making use of the equations of motion formulated earlier in chapter II. Results of both field measurements and theoretical analysis are compared and the conclusions are drawn.

CHAPTER VI

PARAMETRIC STUDIES AND RECOMMENDATIONS

CHAPTER VI

Parametric Studies and Recommendations

6.1 Introduction

In chapters III, IV, and V the description and extraction of relevant parameters, free and forced vibration analyses were presented respectively for a condidate off-road tracked vehicle. The next phase is to study the effect of various alternatives to improve the ride quality of "BR-400". Hence, the present chapter is devoted to the critical examination of the cab response for various parameters. Basically, the studies are carried out under four headings; and are listed below:

- -Parametric study by varying the stiffness of rear and frontal isolators.
- -Parametric study by varying the damping coefficients of isolator /mount.
- -Parametric study by varying the frontal support distance.
- -Parametric study by providing dual rear supports inlieu of the present single support.

Finally, the results of the response spectral densities and the RMS value of the responses in each case are compared. Based on the comparative table, and the prevailing design of the "Cab-Over-Engine", the recommendations are suggested.

6.2 Parametric Study by varying the Stiffness of Rear and Frontal Isolators

From the Table 3.4, it can be seen that the stiffness of the front isolator is nearly 2.5 times the rear isolator. Keeping in view of this fact of uneven stiffness distribution in the present set up, the parametric variations and analyses are carried out by progressively increasing the rear mount stiffness while decreasing the stiffnesses of the frontal supports.

Table 6.1 presents reponse of the cab at the centroid for various stiffness values of the front and rear mounts. It should be noted that for this parametric study the damping coeffiecients for the mounts, are assumed to be constant.

Parametric results show improvement in bounce, lateral and longitudinal modes of vibration when the stiffness of the rear mount is increased upto 1.25 times the present stiffness while the stiffness of the front mount is retained the same. However, in other modes; namely, roll and pitch the RMS values of the acceleration response show a slight increase. Yaw motion, however shows a definite increase. Therefore the present parametric variation has not shown any definite improvement with regard to the acceleration response at the C.G of the cab.

6.3 Parametric Study by Varying the Damping Coefficients of the Mount/Isolator

In this study the damping coefficients of both the front isolator and the rear mount are varied in steps of 20% upto twice the present

Table 6.1 Response of the Cab at its Centroid for various Stiffnesses of the Front and Rear Mounts

(Let $k_{y1}=k_{y2}=k_{z1}=k_{z2}=K1$, k_{y3}, k_{x3} and k_{z3} represented as K2)

MSP-Main spectral peak occurrence-Hz

Peak'-Peak PSD-$(m/s^2)^2/Hz$ $Peak^2$-$(rad/s^2)^2/Hz$

RMS'-Root mean square value (m/s^2) RMS^2-(rad/s^2)

Mode of vibration	Response data	K1				0.75K1				0.5K1			
		K2	1.25K2	1.5K2	1.75K2	K2	1.25K2	1.5K2	1.75K2	K2	1.25K2	1.5K2	1.75K2
Bounce	MSP	8.25	9.0	9.75	10.25	8.25	9.0	9.25	9.75	8.25	8.75	9.5	9.75
	Peak'	431	275	232	757	1226	1616	77	66	654	79	144	55
	RMS'	14.66	12.71	12.79	18.6	19.46	21.67	10.23	10.58	15.6	15.3	11.5	9.4
Longitudinal	MSP	15.0	15.0	15.25	15.25	13	13.25	13.25	13.5	11	11	11.25	11.25
	Peak'	456	44	64	940	527	183	361.1	43	67.2	1640	169	133
	RMS'	11.82	5.93	6.35	16.7	8.43	11.10	10.53	6.4	9.18	21.06	9.6	8.7
Pitch	MSP	26.5	26.75	26.75	26.75	23	23	23.25	23.25	19	19	19	19
	$Peak^2$	738	974	1518	2423	6.28	448	756	1360	995	2313	1755	728
	RMS^2	24.0	23.57	25.5	31.4	24.93	26.10	19.0	22.34	23.1	26.9	24.2	18.1
Roll	MSP	8.5	8.5	8.5	8.5	7.25	7.25	7.25	7.25	6	6	6	6
	$Peak^2$	2628	2784	2924	3048	11881	10479	9570	8802	10865	11721	12450	13079
	RMS^2	327	32.27	32.6	33.0	57.10	51.90	51.62	50.2	54	56.6	57.6	59.7
Yaw	MSP	9.5	9.5	9.55	9.75	8.25	8.25	8.5	8.75	7	7	7.25	7.5
	$Peak^2$	286	2108	97	571	3680	301	3140	74	234	62	486	778
	RMS^2	14.26	24.3	14.8	14.2	31	10.8	29.85	11.8	14.5	14.7	20	22
Lateral	MSP	2.5	2.75	3.00	3.25	2.5	2.75	3.0	3.0	2.5	2.5	2.75	3.0
	Peak'	5800	6307	23251	486	940	1044	215	152	101	176	2124	410
	RMS'	110	40	76	12	16	16.8	10.0	8.75	7.5	8.8	23.7	12.4

value. Table 6.2 furnishes the RMS value of the acceleration responses extracted for different damping values. It can be seen that the responses do not show marked improvement even for 100% increase in damping. Therefore, this alternative is not considered for further comparison and recommendations.

6.4 Parametric Study with Variations in the Frontal Support Distance

The front pivots supporting the cab being closely spaced, it was thought worthwhile to study the effect of cab response by increasing the distance between them.

Similar to the earlier parametric study, the present study also employs the variation in stiffness and damping matrices by progressively increasing the distance "h" upto 0.765m from the present 0.465m.

The RMS values of the acceleration response obtained for h=0.765m shows marked improvement in lateral and yaw modes, where as in the other modes, the response remained the same. However, if the results of the earlier parametric study is utilised; viz., by increasing the rear stiffness to 1.25 times the present stiffness, the response figures show improvement in all the modes, except the roll mode. These results are presented in table 6.3.

6.5 Parametric Study with Dual Rear Supports instead of a Single Support

Although the earlier study of increasing the front support distance decreases the RMS values of the response, due to the fact that

Table 6.2 RMS Values of the Cab Response at its Centroid for various Damping Coefficients

Vibrational Mode	C	1.2C	1.4C	1.6C	1.8C	2C
Bounce	14.7	14.3	14.0	13.7	13.3	12.9
Longitudinal	11.8	11.0	10.2	9.6	8.9	8.5
Pitch	24.0	23.5	22.9	22.2	21.6	21.0
Roll	32.7	32.2	32.1	32	32	31.9
Yaw	14.3	12.3	11.4	10.7	10.	9.6
Lateral	110	99	89.6	81.4	74.4	68.3

Note 1. "C" represents the present damping coefficient of the isolator as well as the mount.

2. The unit of RMS value is m/S^2 for Bounce, Longitudinal and Lateral Co-ordinates; and for the rest it is rad/S^2.

Table 6.3 Response of the Cab at its Centroid for variations in the Front-Support Distance

(k_{x3}, k_{z3} and k_{y3} are represented as K2)

(The units of MSP, Peak', RMS', Peak^2, and RMS^2 are the same as the previous table)

Mode of Vibration	Response Data	Existing Layout	K2		1.25 K2	
			h=0.615	h=0.765	h=0.615	h=0.765
Bounce	MSP	8.25	8.25	8.25	9.0	9.0
	Peak'	431	431	431	275	275
	RMS'	14.66	14.66	14.66	12.71	12.71
Longi-tudinal	MSP	15	15.0	15.0	15.0	15.0
	Peak'	456	456	456	44	44
	RMS'	11.82	11.82	11.82	5.93	5.93
Pitch	MSP	26.5	26.5	26.5	26.50	26.75
	Peak^2	738	738	738	974	974
	RMS^2	24	24	24	23.57	23.57
Roll	MSP	8.5	11.0	14	11.0	13.75
	Peak^2	2628	3379	3334	2959	3107
	RMS^2	32.7	42.5	33.7	42.34	32.77
Yaw	MSP	9.5	12.25	15.00	12.25	15.0
	Peak^2	286	28	113	1274	17.2
	RMS^2	14.2	5.5	5.8	18.56	3.35
Lateral	MSP	2.5	2.5	2.5	2.75	2.75
	Peak'	5800	336	143	169	77
	RMS'	120	9.82	6.9	7.6	6.05

the four point support to any rigid body system gives a better stability, the present study is undertaken. Appendix I furnishes the details of the equations of motion formulated for a four point cab layout subjected to random excitations.

Basically, the study was conducted with the following assumptions:

-The input acceleration spectral densities measured at the existing cab support 3. (Refer Figure 6.2) remains the same at support 3 and 4 or 3' and 4' as the case may be. (for both vertical and lateral accelerations).

-As in the case of a three point cab layout, the longitudinal input spectra are ignored at the supports.

With these assumptions, the study was carried out under two categories. The first one is carried out with the idea of widening the existing bracket to accomodate two mounts. Figure 6.1 illustrates such an arrangement. In this case the front support distance remains unaltered.

In the cab of "BR-400" the seats are located farther apart as shown in figure 6.2. Therefore, if there is an uneven distribution of masses in the two seats or if the vehicle is having only a driver as in most of the cases, then there is a likelyhood of a rocking motion caused by the unbalanced masses in the system.

Eventhough, our present study treats the whole cab along with the driver/passenger mass as a rigid body with centroid falling on the

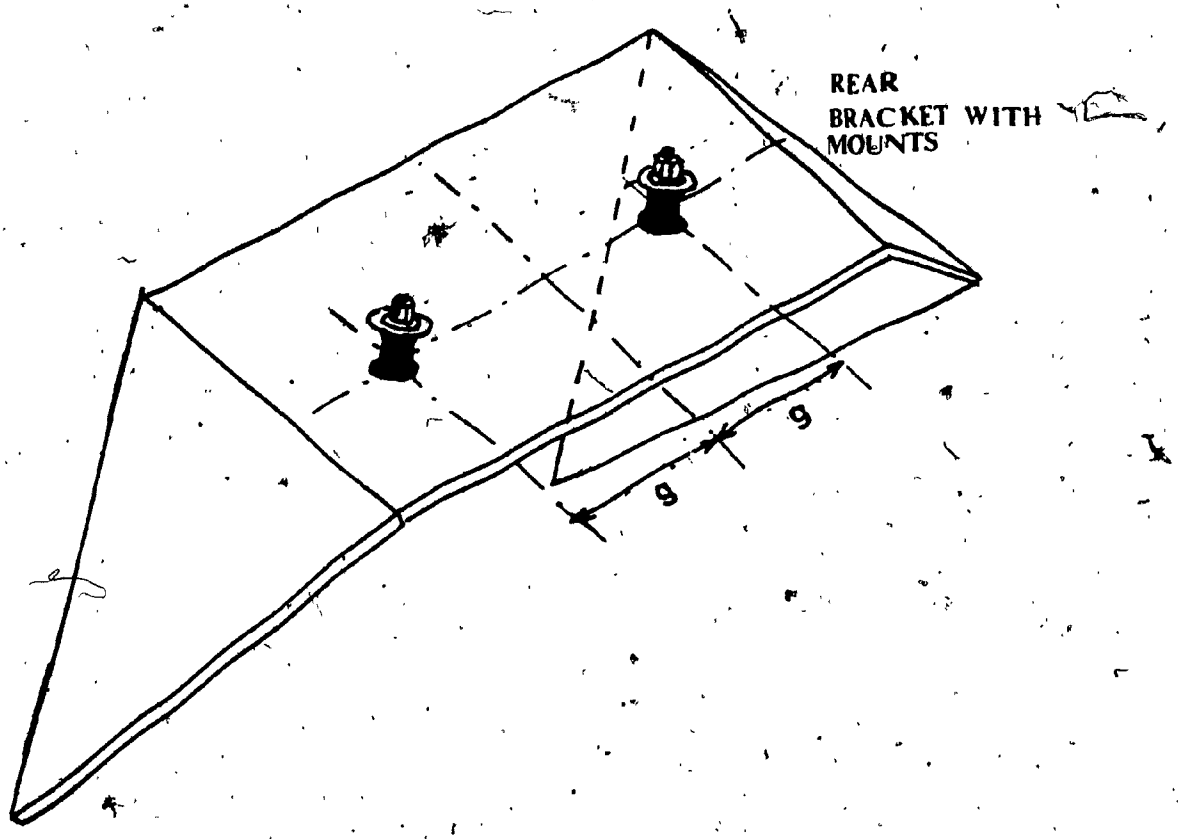

Fig 6.1: Widened Rear Bracket with Dual Mounts

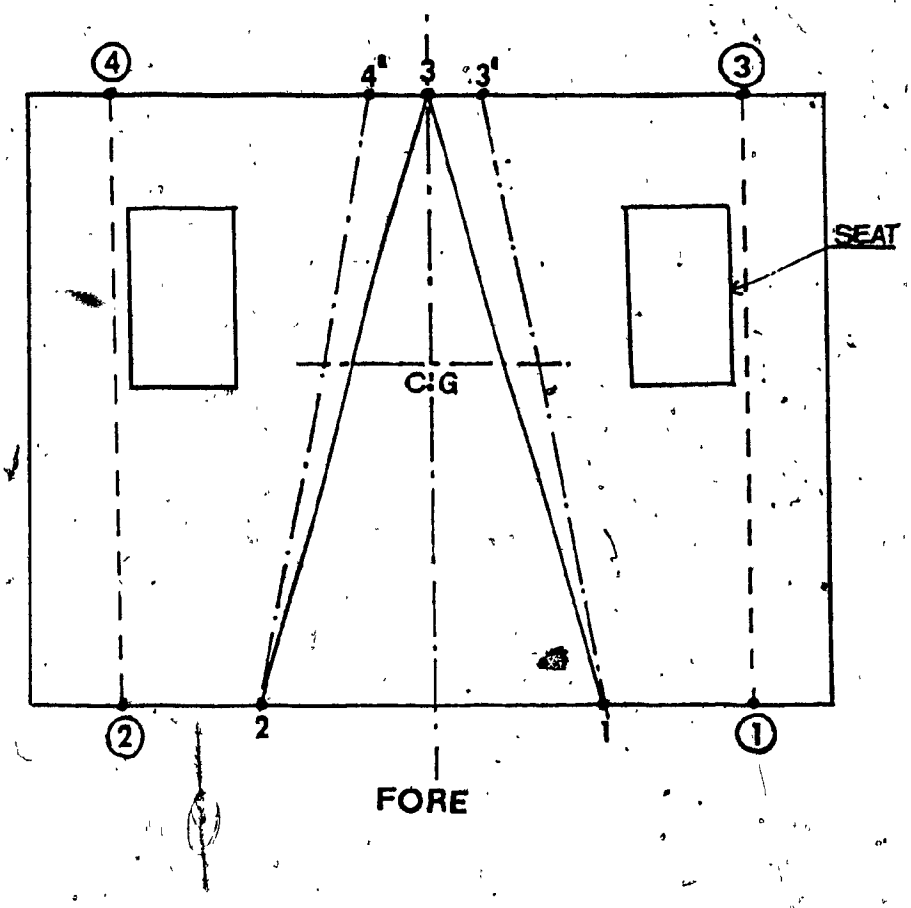

Proposed Locations of the Supports ------- ①, ②, ③ & ④

Supports at the Widened Rear Bracket ------ 3' & 4'

Existing Supports of 3 Point Layout -------- 1, 2 & 3

Fig 6.2: Proposed Four-Point Cab Layout

centre line of the cab, keeping this view of unbalanced masses, a second alternative is thought of. In this alternative, the front as well as the rear supports are located such that both the seats will be well within the area covered by the proposed supports. This ensures stability and thereby the ride comfort.

It was observed that the RMS value of response in all the modes of vibration showed improvement with the second alternative. Table 6.4 compares the results of the four point layout with that of the three-point support.

6.6 Comparison of Results

Since the "Ride Improvement" implies that the response of the cab at the driver/passenger has to reduce in comparison to the present arrangement, this section devotes to the response of the cab for various parameters at a location beneath the seat. The best alternative in each parametric study is considered for comparison of results. They are listed below:

- -Three point layout with rear mount stiffness increased to 1.25 times the present stiffness value.
- -Three point layout with frontal distance "h" increased to 0.765m, with the stiffness of the rear mount increased to 1.25 times its present value.
- -Four point layout with the frontal support distance "h" increased to 0.865m from the present 0.465m, and the rear support distance 'g' made as 0.865m. The rear mount stiffness is reduced to 0.625 times that of the present stiffness of the mount.

Table 6.4 Response of the Cab at its Centroid for a 4-Point Cab Layout

(Let K_2 represent k_{y3}, k_{x3} and k_{z3}, the units of MSP, Peak', RMS', Peak^2, and RMS^2 are the same as the previous table).

Modes of Vibration	Response Data	Existing Layout	4-Point Layout g=0.15 h=0.465, K_2	4-Point Layout g=0.865 h=0.865, K_2	4-Point Layout g=0.865, h=0.865. 0.625K_2
Bounce	MSP	8.25	11.5	11.5	9.5
	Peak'	431	67.51	67.51	41.83
	RMS'	14.6	12.56	12.56	10.18
Longi-tudinal	MSP	15	15.50	15.75	15.0
	Peak'	456	32.53	32.5	29.87
	RMS'	11.82	5.904	5.9	5.18
Pitch	MSP	26.5	26.75	26.75	26.5
	Peak^2	738	3317	3317	1398
	RMS^2	24	31.9	31.9	23.8
Roll	MSP	8.5	8.50	18.0	17.25
	Peak^2	2628	6490	605	1011
	RMS^2	32.7	43.55	17.27	18.9
Yaw	MSP	9.50	9.5	17.0	17
	Peak^2	286	718	10.24	164
	RMS^2	14.2	11.79	3.81	7.76
Lateral	MSP	2.5	3.5	3.50	3.0
	Peak'	5800	78.86	71.34	31.24
	RMS'	110	7.11	5.93	4.13

Results of the response data for each of the above cases are listed in Table 6.5.

It is observed that the four-point cab layout shows improvement in the bounce, roll and lateral modes over the other three alternatives including the original arrangerment in the candidate vehicle. Whereas the three point layout with increased frontal distance shows improvement in the longitudinal and yaw modes. RMS value of pitch mode remains the same for this alternative.

6.7 Recommendations

Based on the earlier studies and analysis the following recommendations for the improved ride are made.

The four point layout as shown in figure 6.2 with increased frontal support distance with a matching rear support distance (supports ①, ②, ③ and ④) shows improvement in the major modes of vibration. In this case the rear mount stiffness, however has to be made 0.625 times the existing stiffness value in order to get a definite improvement. Secondly, as said earlier the proposal would eliminate rocking motion due to the unbalanced masses of the driver and the passenger.

As a second alternative solution, the three point layout with "h" increased to 0.765m and the rear mount stiffness increased to 1.25 times the present value could be considered to improve the ride.

Table 6.5 Response of the Cab at a Location Beneath the Seat of the Driver

(K2 represents k_{x3}, k_{y3}, and k_{z3}, the units of MSP, Peak', RMS', Peak^2, and RMS^2, are the same as the previous table)

Modes of Vibration	Response Data	Existing Layout	3-Point Layout $1.25K_2$	3-Point Layout $h=0.765$ $1.25K_2$	4-Point Layout $g=h=0.865$ $0.625K_2$
Bounce	MSP	9.0	9.00	9.0	9.50
	Peak'	931	985	295	45.3
	RMS'	23.5	22.5	22.6	14.6
Longi-tudinal	MSP	15.0	15.25	15.0	15.0
	Peak'	448	59.65	47.8	29.6
	RMS'	14.55	14.16	9.2	11.7
Pitch	MSP	26.5	26.75	26.5	26.7
	Peak^2	738	974	974	1398
	RMS^2	24	23.6	23.57	23.80
Roll	MSP	8.5	8.5	13.75	17.25
	Peak^2	2628	2784	3107	1012
	RMS^2	32.7	32.3	32.7	18.9
Yaw	MSP	9.25	9.50	15.0	17.0
	Peak^2	46	2100	17.0	193
	RMS^2	6.06	24.3	3.52	8.4
Lateral	MSP	2.5	2.75	2.75	3.0
	Peak'	5900	6495	81	-
	RMS'	121	41.8	12	1.0

6.8 Summary

In this chapter, four types of parameters which has influence on the response of the cab are varied to study their corresponding effect. Comparison of the RMS values of the acceleration response is made by presenting the data in the form of tables. Finally, recommendations which would satisfy the ride improvement criteria are made for the specific case study chosen.

CHAPTER VII

CONCLUSIONS AND RECOMMENDATIONS FOR FUTURE WORK

CHAPTER VII

Conclusions and Recommendations for Future Work

7.1 Conclusions

Improvement in the ride quality is desired in any vehicle for a simple reason of human comfort, eventhough there are other associated factors such as reduction in vibrational stresses and noise. Considerable research was carried out in the past for the design of suspensions of highway vehicles. However, off-road vehicles, particulary tracked vehicles pose intriguing problems in their ride behaviour leaving enough scope for their study and analysis. In this thesis, a computer-aided analysis of vehicle cab suspensions supported either by three or four mounts is presented. A candidate off-road tracked vehicle manufactured by Bombardier Inc. is selected to validate the analysis and to gain insight into practial ways in improving the ride quality of this vehicle.

As a first step, a mathematical model of a three point supported cab suspension system is developed for terrain induced excitations. For carrying out the computer simulation of the mathematical model, the geometrical parameters of the cab of "BR-400", are extracted using a finite element model. Laboratory tests are also carried out to determine the stiffness and damping coefficients of the front isolator. The results obtained form the F.E analysis, particularly the centroid and the total mass of the cab compared favourably with those data furnished by Bombardier Inc.

The equations of motion are solved for natural frequencies and mode shapes based on the geometrical parameters such as the total mass, moment of intertias about the three orthogonal axes, as well as the physical parameters of the isolators such as stiffnesses and damping coefficients. Modal analysis of the F.E model is also carried out and the results are compared with that of the lumped mass analysis. A close correlation is observed between the two, thus validating the equations of motion formulated.

Field trials to record the input and response accelerations of the cab are carried out for various conditions. The recorded signals which are in the time domain are converted into frequency domain in a Fast Fourier Analyser, thus obtaining the Power Spectral Density plots for both input and response of the cab. Based on the discretized input acceleration PSDs, a computer simulation is carried out to evaluate the response acceleration PSDs. Analytical and field data are compared and the conclusions are drawn.

Finally, parametric studies by varying the stiffnesses and damping coefficients, by varying the front support distance and also by having four supports instead of three are carried out.

The following conclusions are drawn with regard to the response acceleration PSD at a location beneath the seat of the driver:

-Four Point cab layout with 'g' and 'h' made as 0.865 m and the rear mount stiffness reduced to 0.625 times the present stiffness, shows improvement in the major modes of vibration., namely in bounce, roll and lateral modes.

-Three point cab layout with 'n' made as 0.765 m and the rear mount stiffness increased by 1.25 times the present value shows improvement in longitudinal and yaw modes.

-RMS values of the pitch acceleration remains the same as the existing value in both these cases.

7.2 Recommendations for Future Work

The following paragraphs deal with the areas that could be considered for future work.

1. Laboratory tests of either the cab or its scale model could be carried out with deterministic excitations. Mathematical model could be validated by this method. In addition, this would enable the study of parametric variations experimentally.

2. The cross-spectra that was ignored in the input matrix could be taken into account in the computer simulation.

3. The constraints that could be present in the physical system may be studied more closely, so that the mathematical model can be improved to take into account the damping due to friction as well as the non-linear stiffnesses at the front supports.

4. Active and semi-active suspensions involving hydraulic/pneumatic cylinders in place of elastomers could be considered for improved ride.

5. A general purpose software to solve the eigenvalue problem as well as to determine the random response could be developed for various types of cab layouts and configurations.

REFERENCES

REFERENCES

1. Albert W. Foster., "A Heavy Truck Cab Suspension for Improved Ride", SAE prepr, N 780408, For meet Feb 27-Mar 3, 1978.
2. Wallace Flower., "Analytical and Subjective Ride Quality Comparison of Front and Rear Cab Isolation System on a COE Tractor", SAE prepr, N 780411, For meet Feb 27-Mar 3, 1978.
3. Selman, A.A. and Pixton. T.A.H., "Cab Suspension for Transcontinental Operation", SAE prepr, N 780409, For meet Feb 27-Mar 3, 1978.
4. Roley, D.G. and Burkhardt, T.H., "Performance Characteristics of Cab Suspension Models", ASAE prepr, For Annu meet, 1975.
5. Suggs C.W. and Huang B.K., "Tractor Cab Suspension Design and Scale Model Simulation", ASAE, Vol. 12, N 3, 1969, pp. 283-289.
6. Cadman, R. Keith; Nelson, Mark F.; and Chen, Francis H.K., "Structural Analysis of a Fibre-reinforced Plastic Truck Cab", Polymer-Plastic Technol.Eng., Vol. 20, N 1, 1983, pp. 79-99.
7. Young, Paul B. and Rabideau, G.F., "Development of a Model for Truck-Cab Design Based on Operator Task", SAE prepr, N 740273, Foe meet Feb 25-Mar 1, 1974.
8. Wild, R., "Practical Approach to Cab Suspension", SAE prepr, N 780407, For meet Feb 27-Mar 3, 1978.
9. Rakheja, S. and Sankar, S., "Suspension Design to Improve Tractor Ride: II. Passive Cab Suspension" SAE prepr, N 841108, 1984.
10. Simons, Wayne K., "New Concept in Cab-Over-Engine Truck Design", SAE prepr, N 751017, For meet Nov 10-13, 1975.
11. Michael J. Crosby and Rush E. Allen., "Cab Isolation and Ride Quality", SAE prepr, N 740294, 1974.

12. Miles, J.C. and Wardill, G.A., "Analysis and Design of a Fire Engine Safety Cab Using Finite Element Methods", The Institution of Mechanical Engineering, Vol. 191, N 29, 1977, pp. 187-193.

13. Rose, R.A.L., "The Evoluation of the CSV Water Tender and its Safety Cab", The Institution of Mechanical Engineering, Vol. 191, N 35, 1977, pp. 177-185.

14. Leichtle, Irvin J., "Design and Test of Pick-up Truck Box Cover", SAE prepr, N 740978, For meet Oct 21-25, 1974.

15. Emme, Joseph H., "Design Considerations for Noise Insulation of Operator Cabs", SAE prepr, N 720702, For meet Apr 27, 1972.

16. Mcafee R.E., "Interior Cab Design of the IH Transtar", SAE prepr, 720262, For meet Jan 10-14, 1972.

17. Greenwood, Donald T., Classical Dynamics. Eaglewood Cliffs, N.J: Prentice Hall, 1977.

18. ANSYS users manual Vol. I and II, Swanson Analysis Systems, Inc., Houston, Pennsylvania, U.S.A.

19. Meirovitch, L., Analytical Methods in Vibrations. Macmillan Co., N.Y. 1967.

20. Rakheja, S., "Computer Aided Dynamic Analysis and Optimal Design of Suspension System for Off-Road Tractors", Doctoral Thesis-Faculty of Engineering and Computer Science, Concordia University, 1983.

21. Julius S. Bendat and Allan F. Piersol., Random Data: Analysis and Measurement Procedures. Wiley-Interscience, 1971.

APPENDIX I

EQUATIONS OF MOTION OF A TILT-CAB WITH FOUR SUPPORTS

APPENDIX I

Equations of Motion of a Tilt-Cab with Four Supports

Figures AI.1 and AI.2 illustrate a mathematical model of a cab having four supports and the model subjected to terrain induced excitations respectively. The general equation of motion of such a Tilt-cab is formulated as follows:

$$[M](\ddot{\alpha})+[C](\dot{\alpha})+[K](\alpha)=[C'](\dot{\beta})+[K'](\beta) \qquad \text{(AI.1)}$$

where,

$$[M]=\begin{bmatrix} m & 0 & 0 & 0 & 0 & 0 \\ 0 & I_{xx} & 0 & 0 & 0 & 0 \\ 0 & 0 & I_{zz} & 0 & 0 & 0 \\ 0 & 0 & 0 & m & 0 & 0 \\ 0 & 0 & 0 & 0 & m & 0 \\ 0 & 0 & 0 & 0 & 0 & I_{yy} \end{bmatrix}$$

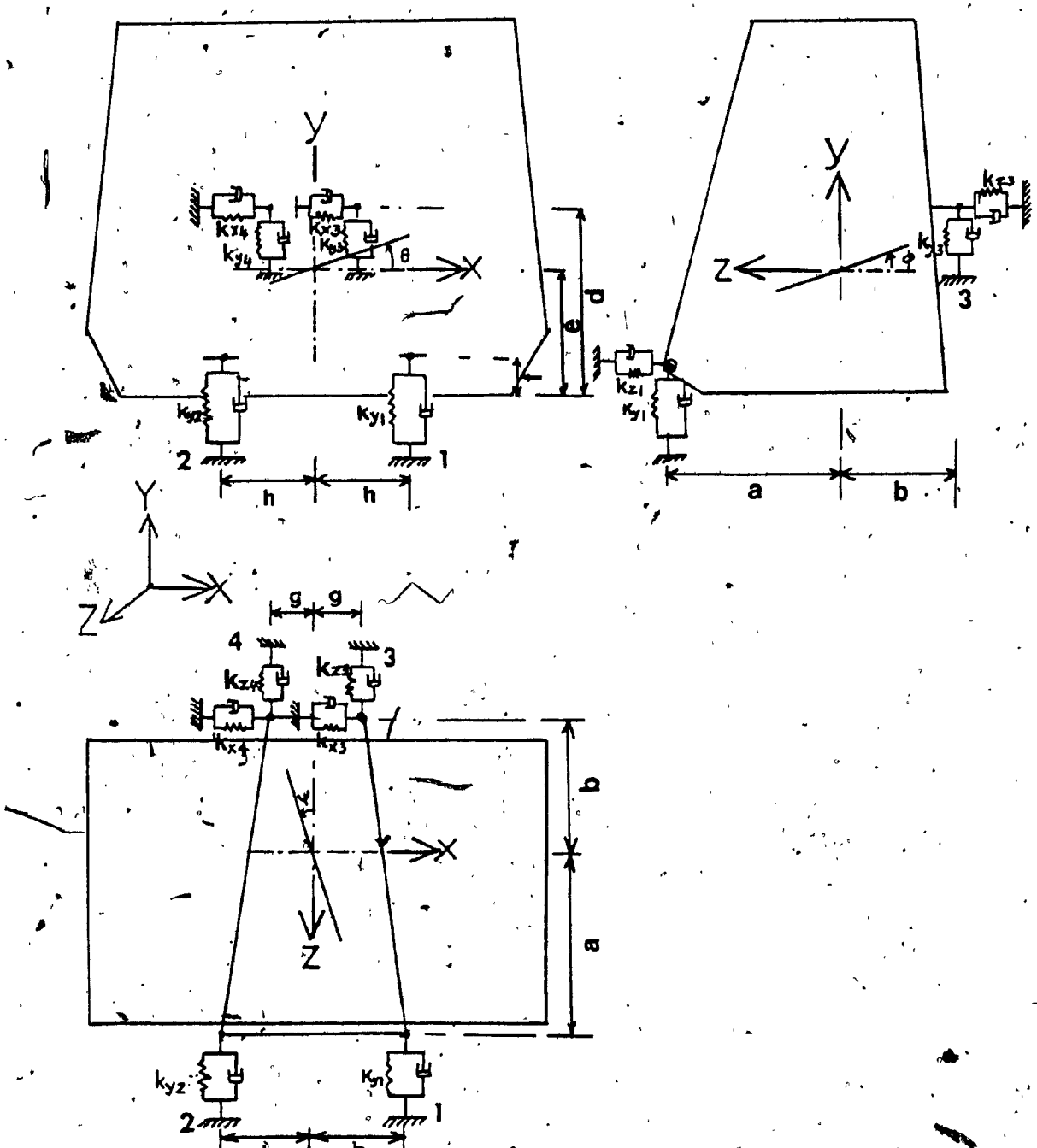

Fig AI.1: Mathematical Model of a Four-Point Cab Layout

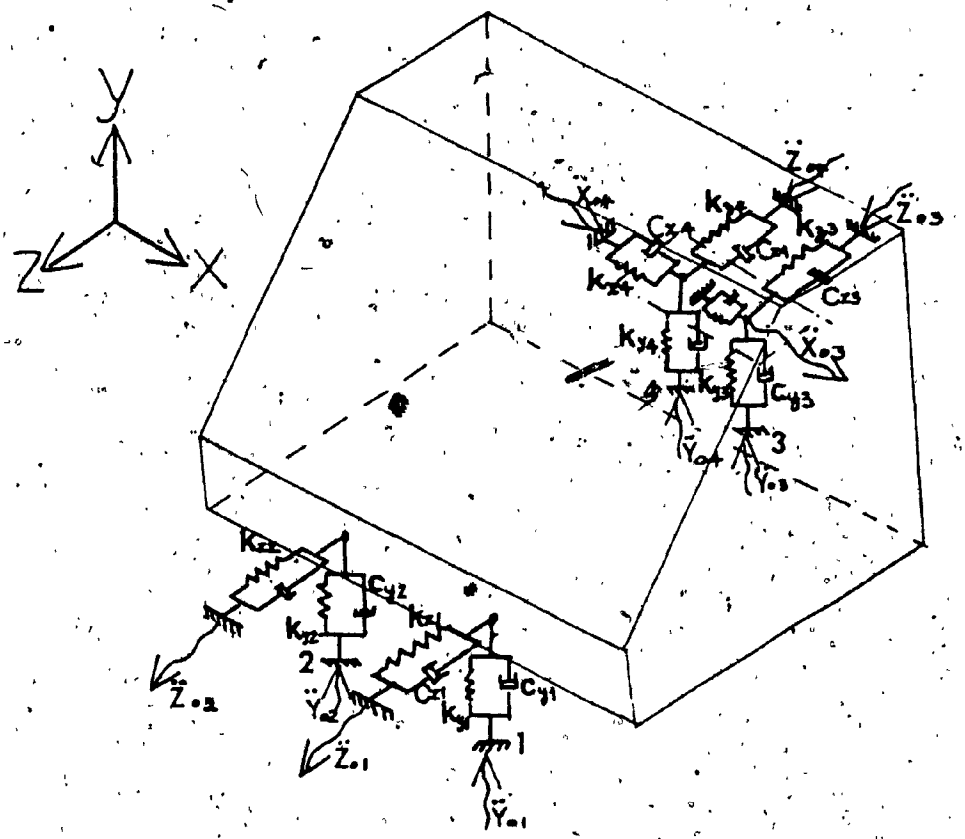

Fig AI.2: Four Point Cab Subjected to Terrain Excitations

$$[C]=\begin{bmatrix}
c_{y1}+c_{y2}+c_{y3}+c_{y4} & -a(c_{y1}+c_{y2})+b(c_{y3}+c_{y4}) & h(c_{y1}-c_{y2})+g(c_{y3}-c_{y4}) & 0 & 0 & 0 \\
-a(c_{y1}+c_{y2})+b(c_{y3}+c_{y4}) & (d-e)^2(c_{z3}+c_{z4})+b^2(c_{y3}+c_{y4})+a^2(c_{y1}+c_{y2})+(e-f)^2(c_{z1}+c_{z2}) & 0 & (d-e)(c_{z3}+c_{z4})-(e-f)(c_{z1}+c_{z2}) & 0 & 0 \\
h(c_{y1}-c_{y2})+g(c_{y3}-c_{y4}) & 0 & h^2(c_{y1}+c_{y2})+(d-e)^2(c_{z3}+c_{z4})+g^2(c_{y3}+c_{y4}) & 0 & -(d-e)(c_{x3}+c_{x4}) & b(d-e)(c_{x3}+c_{x4}) \\
0 & (d-e)(c_{z3}+c_{z4})-(e-f)(c_{z1}+c_{z2}) & 0 & c_{z1}+c_{z2}+c_{z3}+c_{z4} & 0 & 0 \\
0 & 0 & -(d-e)(c_{x3}+c_{x4}) & 0 & c_{x3}+c_{x4} & -b(c_{x3}+c_{x4}) \\
0 & 0 & b(d-e)(c_{x3}+c_{x4}) & 0 & -bc_{x3}-bc_{x4} & b^2(c_{x3}+c_{x4})+h^2(c_{z1}+c_{z2})
\end{bmatrix}$$

$$
[K]=\begin{bmatrix}
k_{y1}+k_{y2}+k_{y3}+k_{y4} & -a(k_{y1}+k_{y2})+b(k_{y3}+k_{y4}) & h(k_{y1}-k_{y2})+g(k_{y3}-k_{y4}) & 0 & 0 & 0 \\
-a(k_{y1}+k_{y2})+b(k_{y3}+k_{y4}) & (d-e)^2(k_{z3}+k_{z4})+b^2(k_{y3}+k_{y4})+a^2(k_{y1}+k_{y2})+(e-f)^2(k_{z1}+k_{z2}) & 0 & (d-e)(k_{z3}+k_{z4})-(e-f)(k_{z1}+k_{z2}) & 0 & 0 \\
h(k_{y1}-k_{y2})+g(k_{y3}-k_{y4}) & 0 & h^2(k_{y1}+k_{y2})+(d-e)^2(k_{z3}+k_{z4})+g^2(k_{y3}+k_{y4}) & 0 & -(d-e)(k_{x3}+k_{x4}) & b(d-e)(k_{x3}+k_{x4}) \\
0 & (d-e)(k_{z3}+k_{z4})-(e-f)(k_{z1}+k_{z2}) & 0 & k_{z1}+k_{z2}+k_{z3}+k_{z4} & 0 & 0 \\
0 & 0 & -(d-e)(k_{x3}+k_{x4}) & 0 & k_{x3}+k_{x4} & -b(k_{x3}+k_{x4}) \\
0 & 0 & b(d-e)(k_{x3}+k_{x4}) & 0 & -bk_{x3}-bk_{x4} & b^2(k_{x3}+k_{x4})+h^2(k_{z1}+k_{z2})
\end{bmatrix}
$$

$$[C'] = \begin{bmatrix} c_{y1} & c_{y2} & c_{y3} & c_{y4} & 0 & 0 & 0 & 0 & 0 & 0 \\ -c_{y1}a & -c_{y2}a & c_{y3}b & c_{y4}b & -(e-f)c_{z1} & -(e-f)c_{z2} & (d-e)c_{z3} & (d-e)c_{z4} & 0 & 0 \\ c_{y1}h & -c_{y2}h & c_{y3}g & -c_{y4}g & 0 & 0 & 0 & 0 & (d-e)c_{x3} & (d-e)c_{x4} \\ 0 & 0 & 0 & 0 & c_{z1} & c_{z2} & c_{z3} & c_{z4} & 0 & 0 \\ 0 & 0 & 0 & 0 & 0 & 0 & 0 & 0 & c_{x3} & c_{x4} \\ 0 & 0 & 0 & 0 & -hc_{z1} & hc_{z2} & 0 & 0 & -c_{x3}b & -c_{x4}b \end{bmatrix}$$

$$[K'] = \begin{bmatrix}
k_{y1} & k_{y2} & k_{y3} & k_{y4} & 0 & 0 & 0 & 0 & 0 & 0 \\
-k_{y1}a & -k_{y2}a & k_{y3}b & k_{y4}b & -(e-f)k_{z1} & -(e-f)k_{z2} & (d-e)k_{z3} & (d-e)k_{z4} & 0 & 0 \\
k_{y1}h & -k_{y2}h & k_{y3}g & -k_{y4}g & 0 & 0 & 0 & 0 & (d-e)k_{x3} & (d-e)k_{x4} \\
0 & 0 & 0 & 0 & k_{z1} & k_{z2} & k_{z3} & k_{z4} & 0 & 0 \\
0 & 0 & 0 & 0 & 0 & 0 & 0 & 0 & k_{x3} & k_{x4} \\
0 & 0 & 0 & 0 & -hk_{z1} & hk_{z2} & 0 & 0 & -k_{x3}b & -k_{x4}b
\end{bmatrix}$$

(α) is the state vector representing $(y, \phi, \theta, z, x, \Psi)^T$;

$(\dot{\alpha})$ and the $(\ddot{\alpha})$ representing the first and second derivative with repect to time repectively.

(β) is the excitation vector representing

$(y_{01}, y_{02}, y_{03}, y_{04}, z_{01}, z_{02}, z_{03}, z_{04}, x_{03}, x_{04})^T$ and $(\dot{\beta})$ is the first derivative with respect to time.